A Chloroplast Protein Atlas Reveals Novel Structures and Spatial Organization of Biosynthetic Pathways

Authors:

Lianyong Wang[1], Weronika Patena[1], Kelly A. Van Baalen[1], Yihua Xie[1], Emily R. Singer[1], Sophia Gavrilenko[1], Michelle Warren-Williams[1], Linqu Han[2,3], Henry R. Harrigan[1], Vivian Chen[1], Vinh T.N.P. Ton[1], Saw Kyin[1], Henry H. Shwe[1], Matthew H. Cahn[1], Alexandra T. Wilson[1], Jianping Hu[2,3], Danny J. Schnell[2], Claire D. McWhite[1], Martin Jonikas[1,4*]

[1]Department of Molecular Biology, Princeton University, Princeton, NJ 08544, USA

[2]Department of Plant Biology, Michigan State University, East Lansing, MI 48824, USA

[3]MSU-DOE Plant Research Lab, Michigan State University, East Lansing, MI 48824, USA

[4]Howard Hughes Medical Institute, Princeton University, Princeton, NJ 08544, USA

[*] Correspondence: mjonikas@princeton.edu

Graphical Abstract:

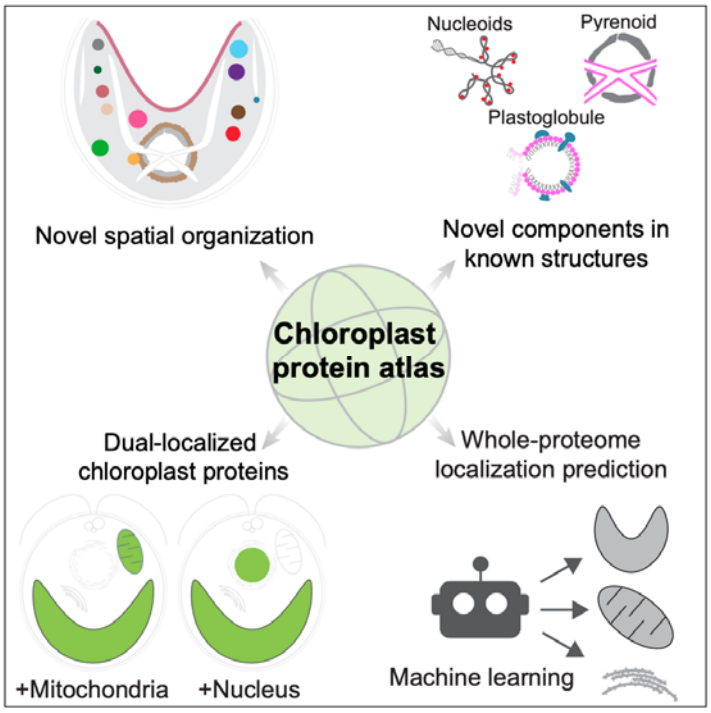

Highlights:

- 1,032 candidate chloroplast proteins localized by fluorescent tagging.
- This protein atlas reveals novel chloroplast structures, functional regions, and components.
- Prevalent dual-organelle localization suggests extensive cross-compartment coordination.
- Atlas-trained machine learning predicts localizations of all *C. reinhardtii* proteins.

Summary

Chloroplasts are eukaryotic photosynthetic organelles that drive the global carbon cycle. Despite their importance, our understanding of their protein composition, function, and spatial organization remains limited. Here, we determined the localizations of 1,032 candidate chloroplast proteins by using fluorescent protein tagging in the model alga *Chlamydomonas reinhardtii*. The localizations provide insights into the functions of hundreds of poorly-characterized proteins, including identifying novel components of nucleoids, plastoglobules, and the pyrenoid. We discovered and further characterized novel organizational features, including eleven chloroplast punctate structures, cytosolic crescent structures, and diverse unexpected spatial distributions of enzymes within the chloroplast. We observed widespread protein targeting to multiple organelles, identifying proteins that likely function in multiple compartments. We also used machine learning to predict the localizations of all *Chlamydomonas* proteins. The strains and localization atlas developed here will serve as a resource to enable studies of chloroplast architecture and functions.

Keywords:

Chloroplast, protein localization, fluorescent tagging, protein-protein interaction, affinity-purification mass spectrometry, plastoglobule, nucleoid, pyrenoid, dual targeting, protein localization prediction, *Chlamydomonas reinhardtii*

INTRODUCTION

The chloroplast is a hallmark organelle of eukaryotic photosynthetic organisms. Over 85% of global biological light energy capture, CO_2 fixation, and O_2 production happens in a chloroplast, driving the biochemistry of the biosphere (Behrenfeld et al., 2001; Rousseaux and Gregg, 2013). In addition to performing photosynthesis, the chloroplast plays essential roles in key cellular processes including amino acid synthesis (Hildebrandt et al., 2015), starch synthesis (Pfister and Zeeman, 2016), lipid metabolism (Hölzl and Dörmann, 2019), isoprenoid synthesis (Lange et al., 2000), purine/pyrimidine synthesis (Zrenner et al., 2006), and the immune response of land plants (Nomura et al., 2012). Despite the chloroplast's importance, the mechanisms of its function and regulation are still not well understood.

All chloroplasts are thought to have originated from a single primary endosymbiosis of a free-living photosynthetic cyanobacterium by a host eukaryotic cell (Keeling, 2010). Over time, the engulfed cyanobacterium lost its autonomy and transferred most of its genes to the nucleus. In parallel, sophisticated communication evolved between the chloroplast and other organelles. This endosymbiosis event is thought to have given rise to the *Archaeplastidia* eukaryotic supergroup, which includes land plants, red algae, and green algae. Secondary endosymbiosis of members of *Archaeplastidia* then produced the more complex chloroplasts found in other eukaryotic supergroups including the coccolithophores and diatoms. Hereafter, we focus on the chloroplast of *Archaeplastidia*, which remain dominant on a global scale, with land plants performing the vast majority of photosynthesis on land and green algae contributing a significant portion of photosynthesis in the oceans (Behrenfeld et al., 2001; Rousseaux and Gregg, 2013).

To understand the function and regulation of the chloroplast, we need to study its proteins and its sub-organellar organization. While the chloroplast has retained a minimal genome, the vast majority of its proteins are now encoded in the nucleus and are imported into the chloroplast (Leister, 2003). Although hundreds of nuclear-encoded proteins have recently been associated with the chloroplast through proteomics (Ferro et al., 2010; Terashima et al.,

2010), phylogenetics (Karpowicz et al., 2011), and bioinformatics studies (Emanuelsson et al., 1999; Tardif et al., 2012), the protein composition of the chloroplast remains poorly defined. Moreover, most chloroplast-associated proteins remain functionally uncharacterized (Hooper et al., 2017; Leister, 2003; Leister and Kleine, 2008).

One promising starting point for understanding the functions of chloroplast-associated proteins is the systematic determination of their cellular and sub-chloroplast localizations (Huh et al., 2003; Thul et al., 2017). Existing knowledge of the chloroplast indicates that its functions are highly spatially organized into distinct regions within the organelle (Engel et al., 2015). For example, sub-chloroplast regions called nucleoids contain the chloroplast's DNA (Kobayashi et al., 2002), chloroplast-traversing thylakoid membranes specialize in the photosynthetic capture of light energy (Wise and Hoober, 2006), and thylakoid membrane-associated lipid droplets called plastoglobules play roles in lipid metabolism (Ytterberg et al., 2006). Localizing a protein of unknown function to such a functionally-specialized region would immediately suggest a corresponding function for the protein.

Of the various approaches for determining subcellular protein localization, fluorescent protein tagging provides significant advantages for the present application. Fluorescent protein tagging is more accurate and has higher spatial resolution than proteome analysis of purified organelles or bioinformatics-based localization predictions, and can also reveal localizations and sub-organellar organization that were not previously known to exist (Mackinder et al., 2017). Furthermore, tagged strains can be affinity-purified and subjected to mass spectrometry-based proteomics to identify associating proteins that are other components of novel cellular structures.

To date, only a small subset of chloroplast proteins have been localized using fluorescent tagging or immunofluorescence. A recent comprehensive survey (Hooper et al., 2017) found that altogether only 582 of the ~3,000 bioinformatically-predicted chloroplast proteins (Emanuelsson et al., 1999; Tardif et al., 2012) (~19%) have been experimentally localized in the leading model land plant Arabidopsis. These numbers suggest that many

opportunities lie ahead for the discovery of novel chloroplast structures and protein functions through systematic localization of fluorescently-tagged proteins.

The green alga *Chlamydomonas reinhardtii* (Chlamydomonas hereafter, Figure 1A) is a powerful model system for studying the cell biology of photosynthetic eukaryotes. Its unicellular nature and microbial lifestyle allow for higher throughput than land plant model systems, enabling systematic large-scale analysis of gene and protein function (Fauser et al., 2022). As an evolutionary relative of land plants (Gutman and Niyogi, 2004; Merchant et al., 2007), Chlamydomonas has been a critical model system that has revealed conserved pathways and key principles of chloroplast biology including electron transport (Iwai et al., 2010), photosynthetic regulation (Depège et al., 2003), assembly of photosynthetic complexes (Minai et al., 2006), and chloroplast genome segregation (Kobayashi et al., 2017). Thus, further study of the Chlamydomonas chloroplast is likely to continue to shed light on the chloroplast biology of land plants, including agriculturally important crop species.

In this study, we establish a comprehensive atlas of the subcellular localizations of 1,032 chloroplast candidate proteins in Chlamydomonas (Figure 1). Our results reveal novel chloroplast structures and spatial organization, new components of known cellular structures, and widespread dual localization of proteins. We also use this dataset to train a more accurate Chlamydomonas protein localization predictor. These insights and the associated plasmid, strain, and protein localization prediction resources open doors to the characterization of novel proteins and spatial organization of the chloroplast in green algae and land plants.

RESULTS

Establishing a Framework for Mapping Chloroplast Protein Localization

In order to maximize the total number of proteins localized in or associated with the chloroplast, we selected target proteins for fluorescent tagging from seven sources (Figure 1C and S1A; Table S1): 1) proteins homologous to those identified in the *Arabidopsis thaliana*

chloroplast mass-spectrometry-based proteome (Ferro et al., 2010); 2) the Chlamydomonas mass-spectrometry-based chloroplast proteome (Terashima et al., 2010); 3) the Chlamydomonas mass-spectrometry-based pyrenoid proteome (Zhan et al., 2018); 4) proteins predicted to localize to the chloroplast by the bioinformatics software PredAlgo (Tardif et al., 2012); 5) GreenCut2 proteins (Karpowicz et al., 2011), which are a set of proteins conserved exclusively in the green lineage; 6) proteins identified to be required for photosynthesis based on Chlamydomonas mutant phenotypes (Li et al., 2019); and 7) other proteins we identified as potentially associated with chloroplast functions based on protein domains or annotations (see STAR Methods). To facilitate the classification of localizations, we included 29 proteins with known localization to the chloroplast or to other organelles in Chlamydomonas (Figure S1B).

To determine protein localizations, we used a previously established system (Mackinder et al., 2017) for expressing proteins tagged with the fluorescent protein Venus (see STAR Methods). Specifically, we cloned the open reading frame of each gene into a vector that drives expression from a constitutive promoter and appends a C-terminal fluorescent Venus tag (Nagai et al., 2002) for localization and three copies of the FLAG epitope (Hopp et al., 1988) for affinity purification of the tagged protein. We electroporated each construct into wild-type Chlamydomonas cells, which produced stable insertions at random sites within the genome (Zhang et al., 2014). We imaged the protein localizations in photoheterotrophically-grown live cells by using confocal fluorescence microscopy. While localizations can be affected by protein tags and non-native expression, we previously showed that such artifacts are rare with this pipeline (Mackinder et al., 2017).

Localization Dataset Validation

We were successful in mapping the localization of 1,032 tagged proteins to 141 distinct localization patterns across 17 major organelles/cellular sites (Figure 1D; Table S2 and S3). To minimize experimenter bias in classifying the localization patterns, each localization image was

148 independently analyzed by two researchers. The organelles/cellular site with the most localized
149 proteins were the chloroplast (580 proteins), followed by the cytosol (238 proteins) (Figure 1D).
150 These numbers include dual-localized proteins, which we will discuss later.

151 Next we evaluated the reliability of our data. Given that fluorescent tagging could lead to
152 inaccurate protein localization due to either protein complex disruption or alteration of native
153 regulation, we first investigated the reproducibility and agreement of our results with protein
154 localizations from previous studies. Of the localized proteins, 62% were represented by at least
155 two independent strains (Figure 1E). The localizations observed in the independent strains for a
156 given protein agreed in >99% of the cases (Figure S1C and S1D). Furthermore, our
157 localizations matched previously published localizations for 27 of the 28 Chlamydomonas
158 proteins (96%) (Figure 1F; Table S4). The only exception was EZY1 (Cre06.g255750), which is
159 normally expressed exclusively in early diploid zygotes and participates in the uniparental
160 inheritance of the chloroplast genome (Armbrust et al., 1993). Since cells imaged in this study
161 were haploid cells, the mis-localization of EZY1 to mitochondria in our data (Table S2), could be
162 attributed to expression under non-native conditions, where the appropriate chloroplast targeting
163 machinery may not be available.

164 We also analyzed the localization enrichment of a set of previously well-characterized
165 proteins. All 32 known photosynthetic complex proteins and all 23 plastid ribosome proteins
166 represented in our dataset were enriched in the chloroplast (Figure S1E). Taken together, the
167 excellent agreement of our localization data with previous studies suggests that our dataset
168 provides reliable localizations for uncharacterized proteins.

169 Our fluorescence images are particularly effective in validating reported organelle
170 proteomics data and identifying potential contaminant proteins in those datasets (Figure 1G;
171 Table S2). Our localization data suggest that 26 out of the 233 proteins from the published
172 Chlamydomonas chloroplast proteome (Terashima et al., 2010) that are also represented in our
173 dataset are actually not in the chloroplast under our experimental conditions. Similarly, 10 out of

the 41 proteins previously detected in the pyrenoid proteome (Zhan et al., 2018), 56 out of the 81 proteins previously detected in the Chlamydomonas mitochondrial proteome (Atteia et al., 2009), and 21 out of the 25 reported high confidence flagellar proteome proteins (Pazour et al., 2005) do not match our localization data. We note that these numbers should not be interpreted as reflecting the overall accuracy of the mitochondrial or flagellar proteomes: we only tagged the subsets of these proteomes for which other omics evidence suggested a possible chloroplast localization, which enriches our dataset for mitochondrial or flagellar proteome false-positives.

To validate our data in these cases, we investigated the localizations of three proteins using antibodies to the native proteins by indirect immunofluorescence. The conserved histone-arginine N-methyltransferase (PRM1/PRMT: Cre03.172550) (Scebba et al., 2007), which had been previously detected in the chloroplast proteome (Terashima et al., 2010), was localized to the ER/nucleus in our data (Figure 1H). Prohibitin 2 (PHB2: Cre12.g519350) (Wang et al., 2010), which had been found in the mitochondrial proteome (Atteia et al., 2009), was localized to the cytosol (Figure 1H). A GreenCut2 protein (SNE1: Cre01.g019250) (Major et al., 2005), which had been previously detected in the flagellar proteome (Pazour et al., 2005), was localized to nucleoplasm (Figure 1H). Consistent with our localization dataset, we detected the native PRM1, PHB2, and SNE1 mainly in the ER/nucleus, cytosol, and nucleoplasm, respectively, by immunofluorescence (Figure 1I).

Protein Localization Reveals Eleven Novel Chloroplast Punctate Structures Suggestive of Compartmentalized Biosynthetic Reactions

We assigned the 580 chloroplast proteins we characterized to one or more of 30 sub-chloroplast locations (Figure 1J). Among the most striking were 11 unique punctate localization patterns that we could not associate with previously described structures within the chloroplast (Figure 2 and S2; Table S2). The localization patterns differed in the number, diameter, and position of puncta within the chloroplast, suggesting that they correspond to distinct structures

(Figure 2A, 2B, and 2C). We named the 7 previously-unnamed punctate-localized proteins chloroplast punctate proteins (CPP1-7).

To further explore these 11 novel structures and to identify additional components of each one, we performed immunoprecipitation-mass spectrometry on the tagged proteins. We identified on average 5 high-confidence protein interactors per structure, for a total of 59 proteins associated with these novel chloroplast punctate structures (Figure 2E, 2H, 2K, and 2N; Table S5). Many of the constituent proteins are conserved in land plants, suggesting the possibility that at least some of these structures are broadly conserved.

A number of the tagged proteins or their interactors correspond to metabolic enzymes, suggesting that these punctate structures may play functional roles in the spatial organization of biosynthetic reactions. Two themes emerge from the data: 1) Typically, only some of the enzymes of a pathway are localized to puncta, suggesting that the puncta enhance or regulate a subset of the reactions. 2) In some cases, punctate localization of an enzyme may allow it to perform its reaction at a location where its substrate is most available. These observations are consistent with previous observations of metabolism associated with cellular condensates (Castellana et al., 2014; Küken et al., 2018; O'Connell et al., 2012; Pareek et al., 2021). Below, we illustrate what we have been able to glean about the composition and potential functions of some of these novel structures:

L-serine Biosynthesis: The conserved predicted 3-phosphoglycerate dehydrogenase Cre07.g344550 (Figure S3A), which catalyzes the commitment step of L-serine biosynthesis, localized to puncta, most of which were directly adjacent to the pyrenoid (Figure 2D). Since the pyrenoid is the site of production of 3-phosphoglycerate (3-PGA) by ribulose 1,5-bisphosphate carboxylase/oxygenase (Rubisco), the localization of 3-phosphoglycerate dehydrogenase to puncta next to the pyrenoid may enhance its activity through metabolic channeling. The pyrenoid is surrounded by presumably impermeable starch plates that are only punctured in a few places by thylakoid membranes (Engel et al., 2015); we speculate that the 3-

phosphoglycerate dehydrogenase puncta localize to these openings to capture exiting 3-phosphoglycerate (Figure 2F). Cre07.g344550 co-precipitated with another predicted 3-phosphoglycerate dehydrogenase encoded adjacent to it in the genome, Cre07.g344400 (Figure 2E), suggesting that both enzymes may function in these puncta. Based on these observations, we propose to name these enzymes Pyrenoid-associated 3-Phosphoglycerate Dehydrogenase PPGD1 and PPGD2, respectively, and the puncta glydehydrosomes.

Chlorophyll Biosynthesis: CHLP1 (Cre01.g050950), a conserved predicted geranylgeranyl diphosphate reductase (Figure S3B) that catalyzes a series of reductions during the last step of the biogenesis of the key photosynthetic pigment chlorophyll (Tanaka et al., 1999), formed the most numerous puncta of all the novel structures we observed (Figure 2G). We did not observe a punctate localization for any of the 8 other enzymes in the chlorophyll biosynthesis pathway that we tagged and examined in our dataset (Table S2), suggesting that this is the only step of chlorophyll biosynthesis that benefits from being performed in puncta. Since CHLP1 needs to perform three separate reductions on its substrate (Figure 2I), we speculate that localization of CHLP1 to puncta increases the enzyme's local concentration, allowing released product to more efficiently re-bind a CHLP1 active site during these sequential reductions.

CHLP1 physically interacted with Cre03.g199535, a conserved early light-induced protein with a chlorophyll *a*/*b* binding protein domain (Tanaka et al., 2010), and with the conserved but poorly-characterized protein CGLD10 (Cre06.g273050) (Figure 2H). These observations suggest that Cre03.g199535 and CGLD10 also play roles in chlorophyll biosynthesis, possibly by enhancing CHLP1's function.

Metabolic Regulation: The punctate-localized conserved protein Cre06.g278195, which we named CPP1 (Figure S3C), co-precipitated with two subunits of acetyl-CoA carboxylase, ACX1 (Cre12.g519100) and BCX1 (Cre12.g484000), and with the chloroplastic isocitrate dehydrogenase IDH3 (Cre04.g214500) (Figure 2J and 2K). Both of these enzymes perform essentially irreversible reactions downstream of citrate/acetyl-CoA. Thus, we hypothesize that

the puncta formed by CPP1 regulate the branching of metabolism between fatty acid synthesis, which is downstream of acetyl-CoA carboxylase (Sasaki and Nagano, 2004), and the production of glutamate, which is downstream of isocitrate dehydrogenase (Elias and Givan, 1977) (Figure 2L).

Glyoxylate Cycle: The conserved punctate-localized protein RBD3 (Cre24.g755197) (Figure 2M) contains a predicted Rubredoxin-like domain (Figure S3D), suggesting that it plays a role in electron transfer. RBD3 physically interacted with the predicted isocitrate lyase ICL2 (Cre03.g149250) (Figure 2N), a key enzyme in the glyoxylate cycle, which allows cells to metabolize two-carbon compounds such as acetate when simple sugars are not available (Figure 2O). Intriguingly, the glyoxylate cycle is thought to occur in peroxisomes (Kong et al., 2017) and was not previously thought to occur in the chloroplast. However, from our data and the literature, there is evidence suggesting that the enzymes necessary for the cycle are also present in the chloroplast. Specifically, we observed chloroplast localization of a malate dehydrogenase MDH1 (Cre03.194850) and a citrate synthase (Cre13.g579050) (Table S2). In addition, succinate dehydrogenase activity has been observed in spinach chloroplasts (Willeford et al., 1989), and bioinformatics (Table S7) (Tardif et al., 2012) predicts the chloroplast targeting of aconitases (Cre06.g252650 and Cre01.g004500), succinate dehydrogenase (Cre12.g528450), and fumarase (Cre06.g272500). Our observations therefore help support the possibility that chloroplasts are able to operate a glyoxylate cycle, which could increase the cell's metabolic flexibility, and suggest that a portion of this cycle occurs in punctate structures.

Punctate Structures Differ in their Exchange and Movement Dynamics

Intriguingly, the novel punctate structures we observe exhibit different dynamics in terms of the exchange of components with the chloroplast stroma and the movement of the structures within the chloroplast. Puncta of the predicted muramyl amino acid ligase CPP2 (Cre12.g519900) demonstrated rapid exchange of components with the stroma similar to the behavior of puncta

of the chloroplast DNA-binding nucleoid component HLP1, as examined by fluorescence recovery after photobleaching (Figure 2V and 2W). In contrast, the punctate structure formed by CPP1, which we associated with branching of metabolism between fatty acid synthesis and the production of glutamate (Figure 2W), did not exhibit such rapid exchange. Moreover, whereas most structures did not move significantly during a 10-minute image acquisition, puncta that contained CPP7 (Cre15.g640650) showed rapid movement on the timescale of minutes (Figure 2X and Movie S1). We speculate that the rapid exchange of CPP2 and nucleoid components with stroma, and the rapid movement of CPP7 are important to the function of these compartments.

Localization Data Reveals Novel Components of Chloroplast Substructures

In addition to discovering novel structures, we identified novel components across different known substructures within the chloroplast.

Novel Nucleoid Components: One of two previously known punctate structures in our dataset were nucleoids (Figure 3A) (Kobayashi et al., 2017). Our dataset revealed two novel nucleoid proteins (Figure 3B), both of which co-precipitated and colocalized with the previously-characterized nucleoid protein HLP1 (Cre06.g285401) (Karcher et al., 2009) (Figure 3C and 3D). One of these novel proteins, Cre16.g672300, which we called Nucleoid protein 1 (NUC1), is conserved in land plants and contains two predicted high mobility group protein domains (Figure S3E) that bind DNA (Mallik et al., 2018). The other protein, SND1B (Cre06.g256850), contains a predicted histone-lysine N-methyltransferase and a SAND DNA-binding domain (Bottomley et al., 2001). We hypothesize that these proteins mediate nucleoid function.

***Novel Plastoglobule Components*:** The other previously-known site of protein localization corresponded to plastoglobules, which are thylakoid membrane-associated lipid droplets containing triacylglycerols, plastoquinone, phylloquinone, carotenoids, and proteins related to their biosynthesis (Figure 3E) (Ytterberg et al., 2006). Our data revealed two novel

plastoglobule-localized proteins, Cre03.g197650 and Cre03.g145507, which we named plastoglobule component 1 and 2 (PGC1 and PGC2). PGC1 contains a PAP fibrilin domain found in structural proteins of plastoglobules (Deruere et al., 1994), which led us to hypothesize that the puncta it formed (Figure 3F) corresponded to plastoglobules. PGC2 showed very similar localization pattern to PGC1 (Figure 3F), co-localized with it (Figure 3G), and coprecipitated with it (Figure 3H), suggesting that they are part of the same structure. Immunoprecipitation of these two proteins pulled down six proteins whose homologs were previously found in the *Arabidopsis* plastoglobule proteome (Figure 3H) (Lundquist et al., 2012; Ytterberg et al., 2006). These proteins included the electron transport protein NAD5 (Cre16.g671000), the SOUL heme-binding protein SOUL3 (Cre16.g666550) (Shanmugabalaji et al., 2020), two phylloquinone biosynthesis related proteins UMM6 (Cre06.g286350) and COQ5 (Cre06.g286300) (Gross et al., 2006; Lee et al., 1997), and the plastid lipid-associated protein PLPA9, which we computationally predict forms a complex with COQ5 (Figure 3I). Based on this, we conclude that PGC1 and PGC2 are novel plastoglobule proteins.

Interestingly, our immunoprecipitation experiments also identified enzyme involved in processes not previously thought to occur at the plastoglobules. Specifically, we found DXS1 (Cre07.g356350), a conserved protein predicted to be a synthase for 1-deoxy-D-xylulose 5-phosphate (Figure S3F), which generates a precursor for isoprenoid and vitamin B_1 and B_6 synthesis (Lois et al., 1998). We also found in the immunoprecipitation AOF8 (Cre13.g587500) and AOF9 (Cre17.g719500), two conserved predicted flavin-containing amine oxidases that catalyze the oxidative cleavage of alkylamines into aldehydes and ammonia. These findings suggest that plastoglobules perform previously unappreciated functions in the metabolism of 1-deoxy-D-xylulose 5-phosphate and alkylamines.

***Novel Pyrenoid Components*:** The pyrenoid is a non-membrane-bound proteinaceous sub-organelle of the chloroplast in which the rate of CO_2 fixation into organic carbon is enhanced by supplying the CO_2-fixing enzyme Rubisco with a high concentration of CO_2 (Figure 4A) (Osafune

et al., 1990; Wunder et al., 2019). Within our dataset, we observed the localization of 18 novel proteins localized to the pyrenoid periphery, matrix, tubules, or pyrenoid center (Table S2). Two of the pyrenoid matrix-localized proteins, the predicted histone deacetylase HDA5 (Cre06.g290400) and uncharacterized protein Cre16.g648400, harbor predicted Rubisco-binding motifs (Meyer et al., 2020), suggesting that they bind directly to Rubisco (Figure 4B).

MIND1 (Cre12.g522950), the Chlamydomonas homolog of the Arabidopsis chloroplast division site regulator MinD1 (Fujiwara et al., 2017), was enriched at the pyrenoid periphery (Figure 4C). MIND1 co-precipitated with plastid chaperonin 60 beta 1 subunit CPN60B1 (Cre17.g741450) (Figure 4D), whose Arabidopsis homolog has also been implicated in plastid division (Suzuki et al., 2009), suggesting the conservation of this interaction in plastid division in algae. Considering that the pyrenoid typically divides by fission during chloroplast division (Freeman Rosenzweig et al., 2017), we hypothesize that MIND1's localization to the pyrenoid periphery plays a role in coordinating pyrenoid fission with chloroplast division.

The predicted phosphoglycolate phosphatase CPLD2 (Cre03.g206550) (Schwarte and Bauwe, 2007) was enriched in the pyrenoid matrix (Figure 4B). Phosphoglycolate phosphatase consumes 2-phosphoglycolate, a competitive inhibitor of the Calvin-Benson cycle enzymes triose phosphate isomerase (Wolfenden, 1969) and sedoheptulose 1,7-bisphosphate phosphatase (Flügel et al., 2017). The localization of CPLD2 to the pyrenoid likely allows the cell to consume 2-phosphoglycolate at its source near Rubisco before it can exit the pyrenoid and inhibit the activity of key enzymes in the surrounding chloroplast stroma.

The pyrenoid tubules are modified thylakoid membranes that traverse the pyrenoid and are thought to supply it with concentrated CO_2. We observed 9 proteins localizing to the pyrenoid tubules, including two predicted peptidyl-prolyl cis-trans isomerases (CYN20: Cre12.g544114 and CYN7: Cre12.g544150) (Figure 4B) and the predicted DegP-type protease DEG8 (Cre01.g028350) (Figure 4E), which co-precipitated with another DegP-type protease,

355 DEG5 (Figure 4F). These observations suggest that tubules may have a role in protein folding,
356 degradation, and/or import of new proteins into the pyrenoid.

357 Finally, our data support a role for the pyrenoid in nucleic acid degradation in algae. The
358 bifunctional nuclease domain-containing protein Cre03.g183550, which we named pyrenoid
359 nuclease 1 (PNU1), localized to the pyrenoid center (Figure 4B). In plants, bifunctional
360 nucleases are responsible for the degradation of RNA and single-stranded DNA in several
361 biological processes (Pérez-Amador et al., 2000). Considering that oxidized RNA localizes to
362 the pyrenoid in Chlamydomonas (Zhan et al., 2015), we speculate that the pyrenoid may be a
363 site of degradation of oxidized RNA. Localizing RNA-degrading enzymes to the pyrenoid could
364 allow for increased specificity of degradation for damaged RNA.

365

366 **Calvin Cycle Enzymes are Enriched in the Stroma Surrounding the Pyrenoid**

367 The Calvin Cycle is the metabolic cycle that enables the assimilation of CO_2. It consists of the
368 CO_2-fixing enzyme Rubisco and 11 other enzymes that convert Rubisco's product,
369 phosphoglycerate, into its substrate, ribulose-1,5-bisphosphate, allowing the cycle to continue.
370 In Chlamydomonas and likely in all pyrenoid-containing algae, Rubisco is the only Calvin Cycle
371 enzyme present in the pyrenoid, while the other enzymes are all in the stroma (Figure 4G)
372 (Küken et al., 2018).

373 From our dataset, we observed that the Calvin Cycle enzyme sedoheptulose-1,7-
374 bisphosphatase SEBP1 and the Calvin Cycle regulatory protein CP12 were both enriched in a
375 region of the stroma immediately surrounding the pyrenoid (Figure 4H). This enrichment around
376 the pyrenoid had not been noticed in our previous study (Küken et al., 2018) because of the lack
377 of other stromal-localized proteins for comparison. Revisiting those data and reexamining the
378 localization of the proteins again under the current growth conditions, it is now apparent that the
379 Calvin Cycle enzymes phosphoglycerate kinase (PGK1), glyceraldehyde 3-phosphate
380 dehydrogenase (GAP1 and GAP3), fructose-1,6-bisphosphate aldolase (FBA3), sedoheptulose-

1,7-bisphosphatase (SEBP1), ribulose phosphate-3-epimerase (RPE1), and phosphoribulokinase (PRK1) are all enriched in the region of the stroma immediately surrounding the pyrenoid (Figure 4I and S4). The enrichment of these enzymes in the periphery of the pyrenoid may enhance the activity of the Calvin Cycle, considering that Rubisco is resident inside the pyrenoid and its substrates and products must therefore diffuse in and out of the periphery of the pyrenoid. These observations motivate questions for future research, including: how are these enzymes localized to the periphery of the pyrenoid and how does their localization change under high CO_2, where some of the Rubisco dissolves into the stroma?

Data Reveal Unexpected Thylakoid Associations and Protein Distributions

Our data suggest the unexpected thylakoid association of several proteins, as well as reveal an intriguing gradient distribution for one thylakoid protein. The thylakoid membranes are the site where light energy is captured by chlorophyll pigments used to generate ATP and NADPH for the cell. Of the proteins with non-homogeneous chloroplast localization in our dataset, 40 exhibited high localization overlap with chlorophyll (Figure 5A and 5B), while 31 exhibited low overlap (Figure 5C). We interpret high localization overlap with chlorophyll as indicative of thylakoid membrane association. Indeed, of the 71 proteins with non-homogeneous localization patterns, all 11 proteins with transmembrane domains showed high chlorophyll overlap ($p=0.001$, Fisher's exact test). Below, we illustrate how our observation of thylakoid membrane association advances our understanding of protein functions.

In photosynthetic eukaryotes, fatty acids are made by fatty acid synthase in the chloroplast stroma (Walker and Harwood, 1985), but the localization of the enzymes that process the nascent fatty acids has not been completely defined. Interestingly, our data suggest that the only predicted chloroplastic acyl-ACP thioesterase FAT1 (Cre06.g256750), which releases fatty acids from fatty acid synthase (Hölzl and Dörmann, 2019), is associated with

thylakoid membranes (Figure 5D). This observation suggests that nascent fatty acids are released in the proximity of thylakoid membranes, into which they may initially partition.

Our data also suggest that riboflavin kinase RFK2 (Cre01.g025250) is associated with the thylakoid membrane (Figure 5E). Riboflavin kinase phosphorylates riboflavin to produce flavin mononucleotide, an essential cofactor for a variety of enzymes including the thylakoid-localized NADH dehydrogenase (Tsibris et al., 1966). However, the localization of riboflavin kinase within the chloroplast was not previously known. The localization of RFK2 to the thylakoid membrane suggests that flavin mononucleotide is produced in proximity to where it is needed for assembly into NADH dehydrogenase.

In addition to the new proteins associated with the thylakoid, we also uncovered an intriguing distribution of a known thylakoid-associated protein, PETO (Cre12.g558900). PETO has been proposed to be important for photosynthetic cyclic electron flow, a poorly-understood pathway of photosynthesis that pumps additional protons across the thylakoid membrane without producing net reducing equivalents (Takahashi et al., 2016). In our dataset, PETO stood out as the only protein that showed a gradient localization pattern across the chloroplast, with a two-fold enrichment at the base of the chloroplast (Figure 5F, 5G, and S5A). While the specific function of PETO in cyclic electron flow remains unknown, our observation that it is localized in a gradient suggests the possibility that cyclic electron flow may be more active at the base of the chloroplast. This activity could result in pumping of additional protons into the thylakoid lumen in the proximity of the pyrenoid, where they are needed to drive the conversion of HCO_3^- to CO_2 by carbonic anhydrase (Pronina and Semenenko, 1990; Raven, 1997).

Our immunoprecipitation and mass spectrometry data examining interactors confirm the previously observed physical interaction of PETO with the cyclic electron flow regulator ANR1 (Cre03.g164000) (Takahashi et al., 2016) (Figure 5H). However, unlike PETO, ANR1 did not show a gradient localization (Figure 5F) and affinity purification of ANR1 did not yield detectable amounts of PETO (Figure 5H, Table S5), suggesting that only a fraction of ANR1 is associated

with PETO. In addition, ANR1 co-precipitated with Cytochrome b_6f subunit IV (PetD) and with the cyclic electron flow regulator PGRL1 (Cre07.g340200) (Terashima et al., 2012) (Figure 5H), supporting a possible direct role of ANR1 in the regulation of cyclic electron flow. The highest-confidence interactor of ANR1 was the predicted NADH-dependent glutamate synthase GSN1 (Cre13.g592200), suggesting the possibility that ANR1 could be downregulating cyclic electron flow in response to increased needs for NADPH by glutamate synthase.

Chloroplast Envelope Localization Patterns Suggest Functionally Specialized Regions

The chloroplast envelope, as the interface between the chloroplast and surrounding cytosol, controls the exchange of ions, metabolites, proteins, and signals (Figure 5I). Surprisingly, out of the 20 chloroplast envelope-localized proteins, only five showed a homogeneous localization throughout the envelope (Figure 5J, 5K, and S5B), whereas all of the other 15 showed one of at least three distinct heterogeneous localization patterns: patches (12 proteins), nucleus-facing patches (2 proteins), and puncta (1 protein) (Figures 5K-M, 5O, and S5C-S5E; Table S2). It is possible that the patches represent multiple distinct structures, as the proteins with these localization patterns did not share any high-confidence protein interactions (Table S5). These observations suggest that most proteins operate in specialized regions at the chloroplast envelope. Below, we discuss protein functions associated with each localization pattern.

Proteins localized to patches along the chloroplast envelope included LMR1 (Cre09.g393765), which contains two predicted peptidoglycan-binding LysM domains (Mesnage et al., 2014) (Figure 5L). While some chloroplasts are surrounded by peptidoglycan, as in the moss *Physcomitrella patens* (Hirano et al., 2016), the apparent absence of most of the peptidoglycan biosynthesis genes in the Chlamydomonas genome suggest that LMR1 instead binds other glycans at the chloroplast envelope.

Proteins localized to nucleus-facing patches included the conserved protein Cre03.g177350 (Figure 5M and S3G). This protein physically interacted with the cytosolic 80S

ribosomal protein L11 (Figure 5N), suggesting that Cre03.g177350 could be involved in the cytosolic translation of chloroplast proteins prior to their import into the chloroplast.

The protein that localizes to puncta along the chloroplast envelope (Figure 5O) is the conserved protein RRM16 (Cre03.g175800) (Figure S3H), which bears two ribosomal RNA (rRNA) methyltransferase domains. This localization suggests that the chloroplast envelope could also be a site where rRNA modification takes place. Consistent with this hypothesis, our mass spectrometry data showed high-confidence interactions between RRM16 and several chloroplast ribosome small subunit components, including rps4, PRPS17, rps2-1, rps14, and PSRP3 (Figure 5P). The presence of a predicted chloroplast targeting sequence in RRM16 (Tardif et al., 2012) and its physical interactions with chloroplast-encoded ribosome subunits suggest that RRM16 is acting on chloroplast rRNA rather than cytosolic rRNA. The localization of chloroplast rRNA modification to the chloroplast envelope could provide an opportunity for cytosolic signals to regulate the chloroplast ribosome.

Many Proteins Have Unexpected Localizations to Multiple Compartments

Localization of a single gene's protein products to multiple cellular compartments is a widespread phenomenon (Carrie and Whelan, 2013; Krupinska et al., 2020; Thul et al., 2017), which can enable signaling between organelles (Isemer et al., 2012a, 2012b) or increase the number of coding products within a restricted genome size (Carrie et al., 2009).

We identified 341 proteins with multiple compartment localization (Figure 6A), substantially more than the approximately 250 that have been identified across all previous studies in plants to date (Carrie and Whelan, 2013). We observed multiple targeting in 87 distinct localization patterns (Figure 6B and Table S3), six times more distinct patterns than seen previously in plants. Four proteins were multiply localized to 4 compartments (Figure 6A and 6C).

Because of how we selected our proteins for localization, our dataset is particularly enriched in proteins where one of the multiple sites of localizations is the chloroplast. Of the 341 multiple-localized proteins, 214 proteins were dual targeted to the chloroplast and one of 13 other regions, including the cytosol, mitochondria, endosome, lysosome, puncta/vesicles in the cytoplasm, patches in the cytoplasm, crescent structures in the cytoplasm, uncategorized shapes in the cytoplasm, the nuclear envelope, the nucleoplasm, the nucleolus, the plasma membrane/cell wall, and the flagella (Figure 6B and S6A-S6U; Table S2).

Chloroplast and Cytosol: We observed 16 proteins with clear dual localizations to the chloroplast and cytosol (Figure 6D, 6E, and S6A). Many of these proteins contained predicted enzymatic domains (Figure 6D), suggesting that they are enzymes that function in both compartments. In some cases, our observed dual localizations identify candidate enzymes for activities that have been observed biochemically in those compartments. For example, the activity of ribose-phosphate pyrophosphokinase, which catalyzes a key step in purine nucleotide synthesis, has been detected in both the chloroplast and cytosol in spinach (Krath and Hove-Jensen, 1999), but the protein responsible for the activity in the chloroplast has not previously been identified. Our observation that the conserved ribose-phosphate pyrophosphokinase RPPK2 (Cre09.g394550) (Figure S3I) shows dual localization to both the cytosol and chloroplast suggests that this enzyme mediates the synthesis of phosphoribosyl diphosphate in both compartments (Figure 6F).

We also observed 31 proteins with a primary fluorescence signal in the chloroplast and relatively weak signal in the cytosol (Figure S6B). Some of these proteins are likely to be functional only in the chloroplast, as they are components of the photosynthetic apparatus or of the plastid ribosome (Table S2). The observation of these proteins in the cytosol may reflect a longer cytosolic residence time before their import into chloroplast (Jarvis and Robinson, 2004), or this could be an overexpression artifact of our system.

***Chloroplast and Nucleus*:** Our dual localization data suggest that the chloroplast and nucleus share nucleic acid processing and repair factors. We identified five proteins showing exclusively chloroplast and nucleus localizations (Figure 6G, 6H, and S6E). These proteins all had predicted functions related to nucleic acids. Of these five, the conserved predicted RNA helicase CGLD3 (Cre03.g166650) and putative RNA splicing factor Cre06.g280700 both localized to the nucleus and throughout the chloroplast (Figure 6H), suggesting that both proteins act on RNA in both compartments. The conserved DNA repair exonuclease APEX1 (Cre03.g175850) (Figure S3J) localized to both the nucleus and chloroplast nucleoids (Figure 6H), and co-localized and co-precipitated with the nucleoid component HLP1 (Figure 6I and 6J), suggesting that it contributes to the repair of both genomes.

***Chloroplast and Endosome or Lysosome*:** We observed 6 proteins localized to the chloroplast and either the endosome or the lysosome (Figure 6K, and S6K-S6M). For some of these proteins, this dual localization likely reflects a functional role of the protein in both compartments. For example, the conserved peptidyl-prolyl cis-trans isomerase CYN20-3 (Cre12.g495951) (Figure S3K) could isomerize prolines in both the chloroplast and in the endosome (Figure 6K). However, other proteins showing dual chloroplast and endosome localization, such as the light-harvesting protein LHCBM8 (Cre06.g284250) (Figure 6K), are likely proteins that function in the chloroplast and are degraded in the lysosome by chlorophagy (Ishida et al., 2008; Wolfe et al., 1997).

Chloroplast and Crescent Structures in the Cytoplasm: Among the most striking dual localizations were proteins that localized to the chloroplast and crescent structures in the cytoplasm, a localization pattern that has not been described previously to our knowledge (Figure 6M). Depending on the localized protein, the crescent structures were either small (~1 μm) or medium-sized (~2 μm); these two sizes could represent either distinct structures or different stages of development of the same structure. The structures did not appear to be Golgi

(Figure 6L), endosomes (Figure S1B and S6L), or lysosomes (Figure S6M), as the latter organelles showed different localizations and morphologies.

The predicted domains of 9 out of 20 proteins that localize to these crescent structures suggest that the crescent structures play roles in nucleotide and phosphate metabolism (Table S2). These proteins included the predicted polynucleotide phosphatase/kinase Cre11.g467709 (Figure 6V), the predicted purine biosynthesis enzyme Cre17.g734100 (Figure S6N), and the predicted phosphate transporter Cre07.g325740 (Figure S6V). Since cellular phosphate is primarily used for nucleotide biosynthesis, it makes sense that these two functions would be spatially co-localized.

The predicted functions, localization patterns, and size of the structures together suggest that the crescent localizations correspond to the matrix of acidocalcisomes, poorly-characterized vesicular structures that store phosphate as a single large spherical granule of polyphosphate (Aksoy et al., 2014; Docampo et al., 2005; Komine et al., 2000; Ruiz et al., 2001). Fluorescently-tagged proteins localizing to the matrix of acidocalcisomes would show a crescent structure due to their exclusion from the spherical polyphosphate granule (Figure 6M, S6N, and S6V). Indeed, the matrix of acidocalcisomes observed by electron microscopy (Aksoy et al., 2014) appeared as crescents of similar size to the structures we observed by microscopy.

Acidocalcisomes are possibly the only organelle conserved from bacteria to plants and humans (Docampo et al., 2005). They are essential for cellular survival under nutrient deprivation, but we are only beginning to understand their protein composition in any organism (Huang et al., 2014). Our identification of 20 candidate acidocalcisome proteins advances the molecular characterization of these fascinating structures. Moreover, the relatively large number (12) of proteins dual-localized to the chloroplast and these structures suggests that there could be extensive interactions between chloroplasts and acidocalcisomes, with potential for cycling of phosphate between the two compartments.

***Chloroplast and Other Structures*:** We observed 27 proteins dual-localized to the chloroplast and cytoplasmic puncta of one of three different diameters: small (~1 μm), medium (~2 μm), or large (~3 μm) (Figure 6N-6P and S6O-S6Q). All three classes of puncta contained proteins with predicted enzymatic domains (Table S2), but contained no homologs of well-characterized proteins, precluding us from conclusively assigning these localizations to known structures. We also observed 12 proteins dual-localized to the chloroplast and small (~2 μm diameter), medium (~3.5 μm), or large (~5 μm) cytoplasmic patches (Figure 6Q-6S and S6R-S6T), or to one of many other uncategorized shapes in the cytoplasm (Figure S6U). Future characterization of the functions and spatial dynamics of these proteins is likely to provide novel insights into the cell biology of plants and algae.

Machine Learning Enables Proteome-Wide Protein Localization Predictions

Machine learning provides an opportunity to expand the scope of the protein localization findings of the present study to the genome-wide scale. The current state-of-the-art predictor for Chlamydomonas protein localization, PredAlgo (Tardif et al., 2012), has been a tremendously useful resource for the scientific community. However, it was trained on a relatively small dataset of 152 proteins. The much larger number of protein localizations resulting from this present work combined with advances in machine learning classification of protein sequences allowed us to train a more accurate protein localization predictor.

We built our new predictor, PB-Chlamy, based on ProtBertBFD (Elnaggar et al., 2021), a natural language processing model of protein features pre-trained on the BFD database (Steinegger et al., 2019) containing 2.5 billion protein sequences from diverse organisms. We trained three separate ProtBertBFD protein sequence classifiers on Chlamydomonas protein localization data (Figure 7A): one each to recognize chloroplast, mitochondrial, and secretory proteins. For each localization category we generated a combined dataset using the data in the present work, our previous protein localization study (Mackinder et al., 2017), and the training

584 dataset assembled for PredAlgo (Tardif et al., 2012). Each dataset is composed of a set of
585 positives, i.e. proteins known to localize to a particular subcellular location, and negatives, i.e.
586 proteins found to not localize to the location. We split each dataset into training, validation, and
587 testing subsets with a 3:1:1 ratio (Table S7). We used the training set to train a linear classifier
588 to distinguish proteins that do or do not localize to a compartment, evaluating against the
589 validation set of proteins during training.

590 We evaluated the performance of PB-Chlamy in comparison to PredAlgo. To ensure that
591 neither of the predictors being compared had been trained on any of the proteins in the test sets,
592 we used testing datasets with proteins used to train PredAlgo excluded. PB-Chlamy reliably
593 performs better than PredAlgo on our test sets for proteins localized to the chloroplast,
594 mitochondria, and secretory pathway (Figure 7B and S7).

595 We proceeded to use PB-Chlamy to predict protein localizations for the entire
596 Chlamydomonas proteome (Figure 7C; Table S7), finding 2,245 putative chloroplast proteins,
597 725 putative mitochondrial proteins, and 2,755 putative secretory proteins. These numbers
598 include 70 proteins with predicted dual localizations, mostly chloroplast+mitochondria (Table
599 S7). Notably, we predict only two-thirds as many chloroplast proteins and one-quarter as many
600 mitochondrial proteins as PredAlgo (which predicts 3,375 chloroplast and 2,843 mitochondrial
601 proteins), providing a sharper view of the predicted proteome of these organelles.

602

603 **DISCUSSION**

604

605 **Insights into the Functions of Poorly-Characterized Proteins**

606 Our localization information is the first compendium of this kind in any photosynthetic organism.
607 The data are particularly useful for advancing the understanding of the molecular functions of
608 poorly-characterized proteins. The molecular functions of 702 (68%) of our localized proteins
609 are unknown and 459 (45%) of the localized proteins were previously unnamed (Figure S1F).

We provided examples of how our localization data give insights into the functions of such poorly-characterized proteins, like the predicted DNA-binding protein SND1B, which we localized to chloroplast nucleoids. We also illustrated of how the function of poorly-characterized proteins can be elucidated by immunoprecipitation and mass spectrometry of our tagged strains, as in the case of the poorly-characterized proteins PGC1 and PGC2 where our data allowed us to assign them to plastoglobules. For proteins where we could not obtain experimental localization data, our new PB-Chlamy classifier accurately predicts their localization. Together, our localization data, protein-protein interactions, and computational predictions greatly narrow down the possible functions of poorly-characterized proteins and facilitate generation of specific hypotheses for their further characterization, accelerating the elucidation of chloroplast organization and function.

The images and protein-protein interactions from this study can be browsed and searched at https://www.chlamylibrary.org/. This site also provides links for ordering the corresponding strains and plasmids from the Chlamydomonas Resource Center.

Novel Organizational Features of the Chloroplast

Our systematic survey of protein localizations revealed extensive spatial organization of the chloroplast. This organization includes 11 novel punctate structures, which appear to be metabolic hubs that enhance or regulate specific reactions such as the commitment step of L-serine biosynthesis or the final step of chlorophyll biosynthesis. We observed the enrichment of Calvin-Benson cycle enzymes in the proximity of the pyrenoid, which may enhance the cycle's overall activity by localizing each enzyme to the site where its substrate is produced. We observed extensive spatial organization of the thylakoid membrane and chloroplast envelope, including distinct chloroplast envelope regions that appear to be specialized for interactions with cytosolic ribosomes, and other regions that appear to be specialized for interactions with

635 chloroplast ribosomes. These discoveries open doors to characterizing the functions of these
636 organizational features and of the molecular bases that underlie their organization.
637
638 **Insights Into Dual Targeting**
639 Our study provides the largest-scale survey to date of proteins with multiple compartment
640 localization in any photosynthetic eukaryote, making it a resource for studying the biological
641 functions of this phenomenon, the mechanisms that underlie it, and its evolution. Whereas the
642 vast majority of previously-known dual-localized plant proteins were dual-localized to the
643 chloroplast and mitochondria (Carrie and Whelan, 2013), only two of our proteins showed this
644 localization and the vast majority of our dual-localized chloroplast proteins had a second
645 localization in a compartment other than mitochondria (Figure 6B and 6C; Table S2), making
646 our dataset a complementary resource. We observed dual localization to the chloroplast and a
647 broad range of other organelles, including previously un-described dual localizations to
648 crescent-shaped structures that we propose based on corroborating data to correspond to
649 acidocalcisomes. These observations suggest widespread sharing of functions between the
650 chloroplast and cytosolic organelles, and/or extensive cytosolic degradation of chloroplast
651 proteins. Our identification of these dual-localized proteins provides a starting point for future
652 characterization of the functional and regulatory interactions between the corresponding
653 organelles.
654
655 **Evolution of Chloroplast-Associated Protein Localizations and Interactions.**
656 Our study provides insights into both genes specific to the Chlorophyte green algal lineage and
657 genes conserved across the eukaryotic supergroup *Archaeplastidia*: 933 of the
658 Chlamydomonas proteins we localized are conserved in the green alga *Volvox carteri*, 696 are
659 conserved in the green alga *Coccomyxa subellipsoidea*, and 618 are conserved in the land
660 plant *Arabidopsis thaliana* (Figure S1G; Table S2). We observed similarities and differences in

661 protein localizations between Chlamydomonas and land plants for proteins that show single and
662 multiple localizations (Table S2). For example, the Chlamydomonas protein Cre12.g494250
663 localized to the chloroplast, cytosol, nucleus, and mitochondrion; and its Arabidopsis homolog
664 AT4G16060 showed a similar multiple localization to the chloroplast, cytosol, and mitochondrion
665 when expressed in tobacco leaves (Figure 6T, S6W, and S6X). These observations suggest
666 that our dataset provides a rich resource that will allow the study of the evolutionary principles of
667 protein localization and of dual targeting.
668
669 **Perspective**
670 Climate change and the rising global population drive a pressing need to understand the basic
671 biology of photosynthetic organisms and to advance our ability to engineer them. Our study lays
672 the groundwork for understanding remaining mysteries of the chloroplast, the organelle at the
673 heart of photosynthetic organisms. Importantly, the systematic and comprehensive nature of the
674 present study allowed us to reach deep into the unknown, revealing organizational features that
675 would not have been readily accessible with traditional hypothesis-driven research. We hope
676 that further characterization by the research community of these data and strains will help
677 advance the understanding of the evolution of protein localization, the roles of poorly-
678 characterized chloroplast proteins, and the spatial organization of chloroplast functions.

SUPPLEMENTAL INFORMATION

Supplemental Information includes 7 figures, 8 tables, and 1 movie.

AUTHOR CONTRIBUTIONS

L.W. and M.C.J. conceived the project. L.W., K.A.V.B., Y.X., S.G., and H.H. performed the gene cloning, generating fluorescently tagged strains, and confocal microscopy. M.W. prepared materials for this large-scale work. L.W. and E.R.S. performed immunoprecipitation and prepared the samples for analysis by mass spectrometry. S.K. and H.H.S conducted the mass spectrometry. W.P. conducted bioinformatic prediction of protein localizations. C.D.M., V.C., and V.T. conducted the prediction of protein structure. L.W. performed indirect immunofluorescence assay. L.H., D.J.S., C.B., and J.H. performed the protein localization in Tobacco. M.H.C., W.P., L.W., and M.C.J. built the website to share the data and materials. All authors analyzed the data. L.W., A.T.W., and M.C.J. wrote the manuscript with input from all authors.

ACKNOWLEDGMENTS

We thank the Princeton University Confocal Microscopy manager Gary Laevsky for instrumentation support; Princeton Institute for Computational Science and Engineering for providing research computing resources; Laurent Cournac, Ben Engel, Ursula Goodenough, Olivier Vallon, Christoph Benning, Ned Wingreen, Xiaobo Li, Silvia Ramundo, Luke C.M. Mackinder, Moritz T. Meyer, Shan He, Alice Lunardon, Jessica H. Hennacy, Sabrina Ergun, Yuliya Zubak, Moshe A. Kafri, Eric Franklin for discussions and feedback on the manuscript; Marie Bao, as part of Life Science Editors, for help with editing the manuscript. The project was funded by DOE grant DE-SC0020195, HHMI/Simons Foundation grant 55108535, and the Lewis-Sigler Scholars Fund. Martin Jonikas is a Howard Hughes Medical Institute Investigator.

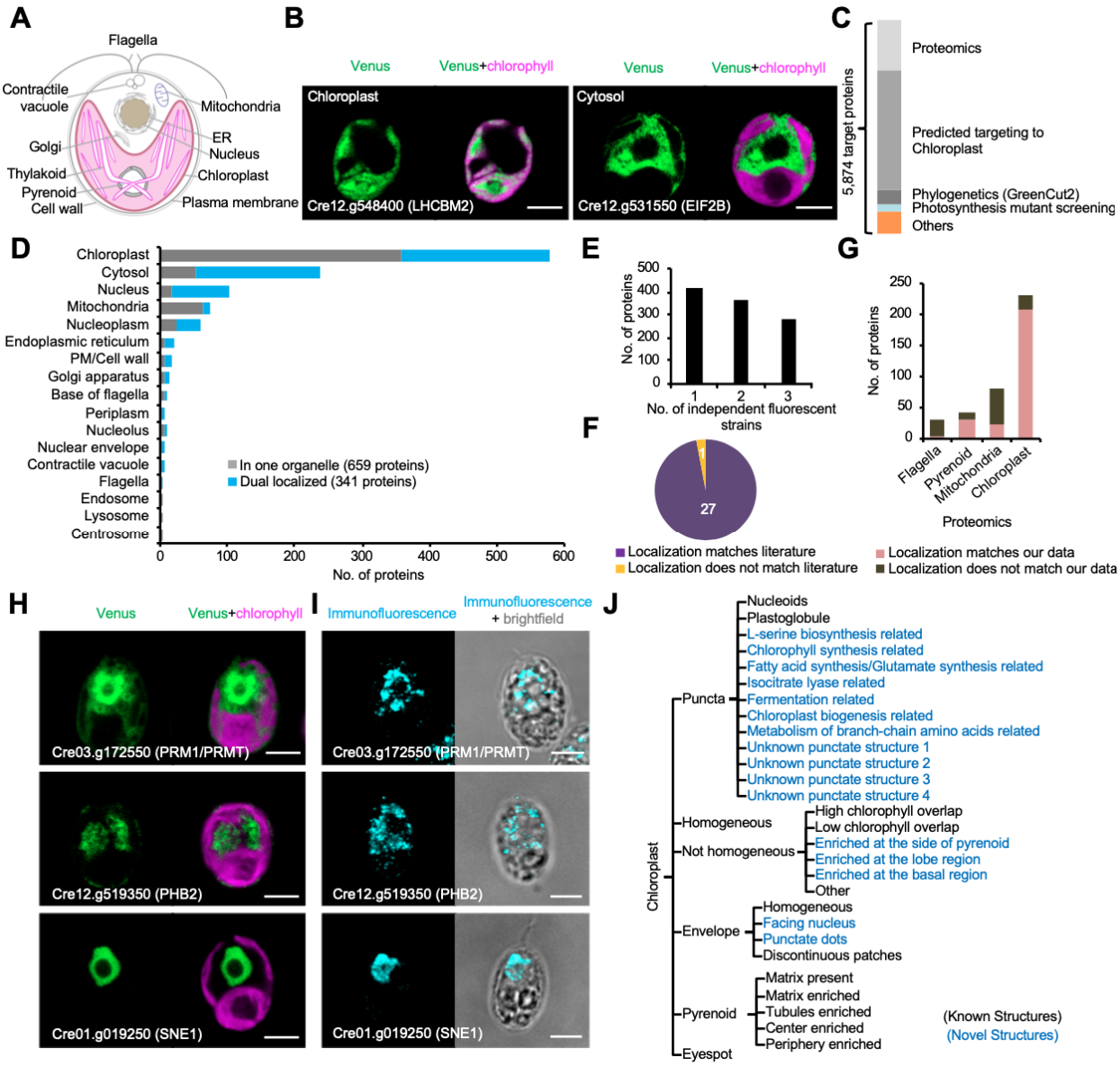

Figure 1. We assigned 1,032 tagged proteins to diverse localization patterns in 17 major compartments.

(A) A diagram shows the cell structure of *Chlamydomonas reinhardtii.*

(B) Representative images of the Venus-tagged chloroplast protein Cre12.g548400 (LHCBM2) and cytosol protein Cre12.g531550 (EIF2B).

(C) A summary of target genes from various sources.

(D) The number of proteins per subcellular location is shown, including proteins observed in one organelle (grey) and proteins observed in multiple organelles (blue).

(E) The number of independent strains imaged for determining the localization patterns.

(F) Agreement of our data with localizations identified in previous literature.

(G) Comparison of our localizations with several proteomes in Chlamydomonas.

(H) Our data are shown for proteins whose localizations disagree with proteomics-based localizations in Chlamydomonas. Cre03.g172550 (PRM/PRMT1) was previously found in the chloroplast proteome, Cre12.g519350 (PHB2) was previously found in the mitochondria proteome, and Cre01.g019250 (SNE1) was previously found in the flagella proteome.

(I) Localizations of PRM1/PRMT, PHB2, and SNE1 in wild-type were assessed using immunofluorescence.

(J) A decision tree for assigning chloroplast proteins to specific subcellular locations. Novel structures are labeled in blue.

All scale bars are 5 μm.

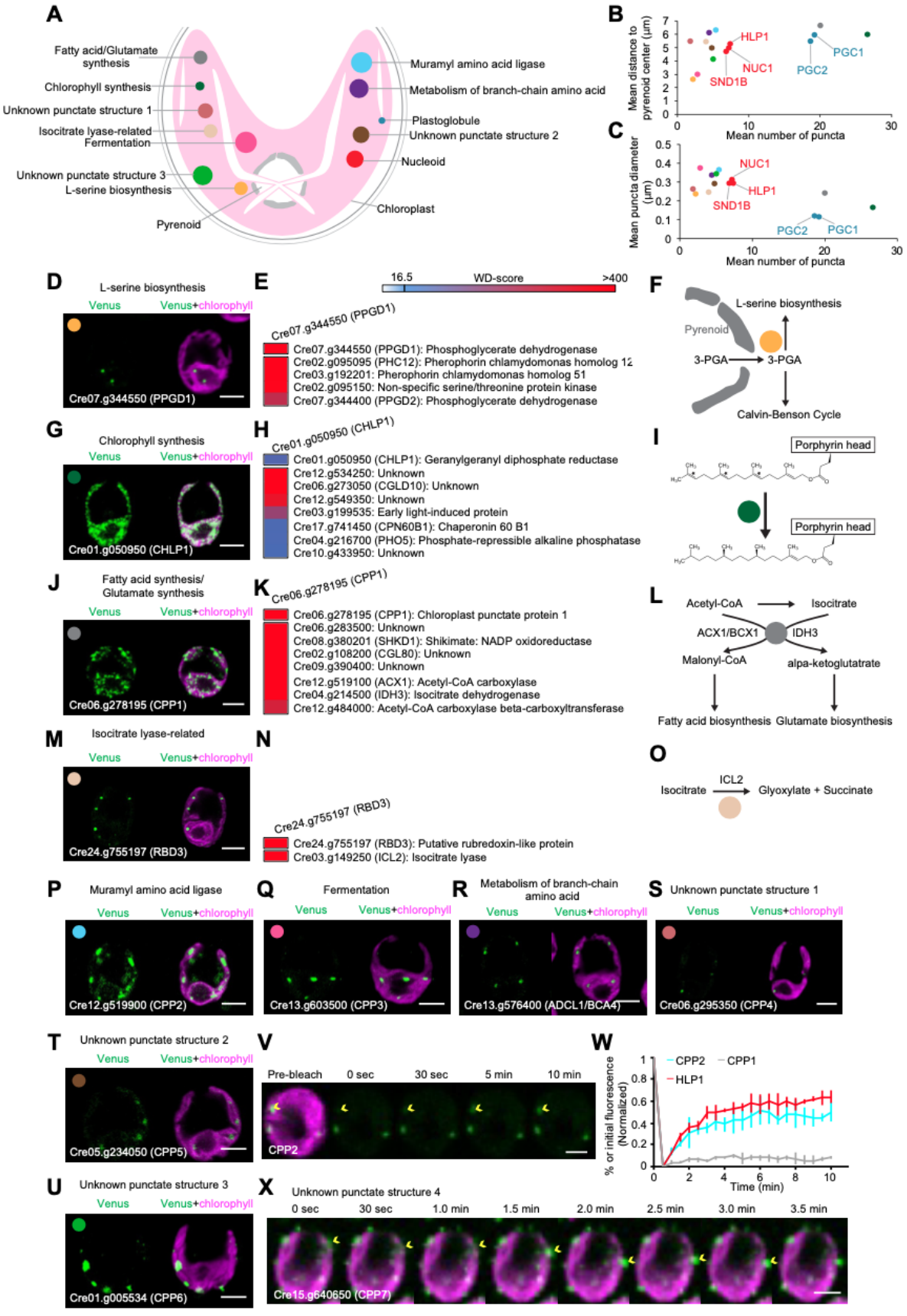

731

Figure 2. The data revealed novel punctate structures in the chloroplast.

(A) A diagram illustrates the 12 chloroplast puncta structures we observed, 10 of which are novel. The relative size and approximate distance from the center of the pyrenoid are represented; for simplicity, only one of each structure is shown. Each structure is assigned a unique color that is used throughout this figure and Figure S2.

(B-C) Novel punctate structures showed differences in the average position, number, and size of puncta. For each punctate structure, its mean distance to the pyrenoid center, the average number of puncta, and the mean punctum size are shown. Mean values ± SD from five independent cells are shown in Figure S2.

(D) Representative images of Cre07.g344550 (PPGD1).

(E) High-confidence interacting proteins of PPGD1. WD-scores represent our confidence in the interactions; scores greater than 16.5 correspond to the 3.7% highest-confidence interactions (see STAR Methods).

(F) A diagram illustrates how the 3-phosphoglycerate dehydrogenase PPGD1 enhance its activity by localizing adjacent to the pyrenoid

(G) Representative images of Cre01.g050950 (CHLP1).

(H) High-confidence interacting proteins of CHLP1.

(I) A diagram illustrates how the geranylgeranyl diphosphate reductase CHLP1 catalyzes the last step of the biogenesis of chlorophyll.

(J) Representative images of Cre06.g278195 (CPP1).

(K) High-confidence interacting proteins of CPP1.

(L) A diagram illustrates how the CPP1 regulates the branching of metabolism between fatty acid synthesis and production of glutamate.

(M) Representative images of Cre24.g755197 (RBD3).

(N) High-confidence interacting proteins of RBD3.

(O) A diagram shows how the RBD3 supports the isocitrate lyase ICL2.

(P-U) Representative images of Cre12.g519900 (CPP2) (P), Cre13.g603500 (CPP3) (Q), Cre13.g576400 (ADCL1/BCA4) (R), Cre06.g295350 (CPP4) (S), Cre05.g234050 (CPP5) (T), Cre01.g005534 (CPP6) (U).

(V) Fluorescence recovery of an CPP2-Venus punctum during 10 minutes after photobleaching of the whole punctum. The yellow arrow indicates the bleached punctum.

(W) Fluorescence recovery profile of puncta of CPP2, Cre06.g285401 (HLP1), , and CPP1. Shown are the mean ± SD of 3 different puncta for each protein.

(X) Representative images of Cre15.g640650 (CPP7) showing rapid movement of puncta. The yellow arrows indicate one of the puncta rapidly moving along the lobe of chloroplast.

All scale bars are 5 μm.

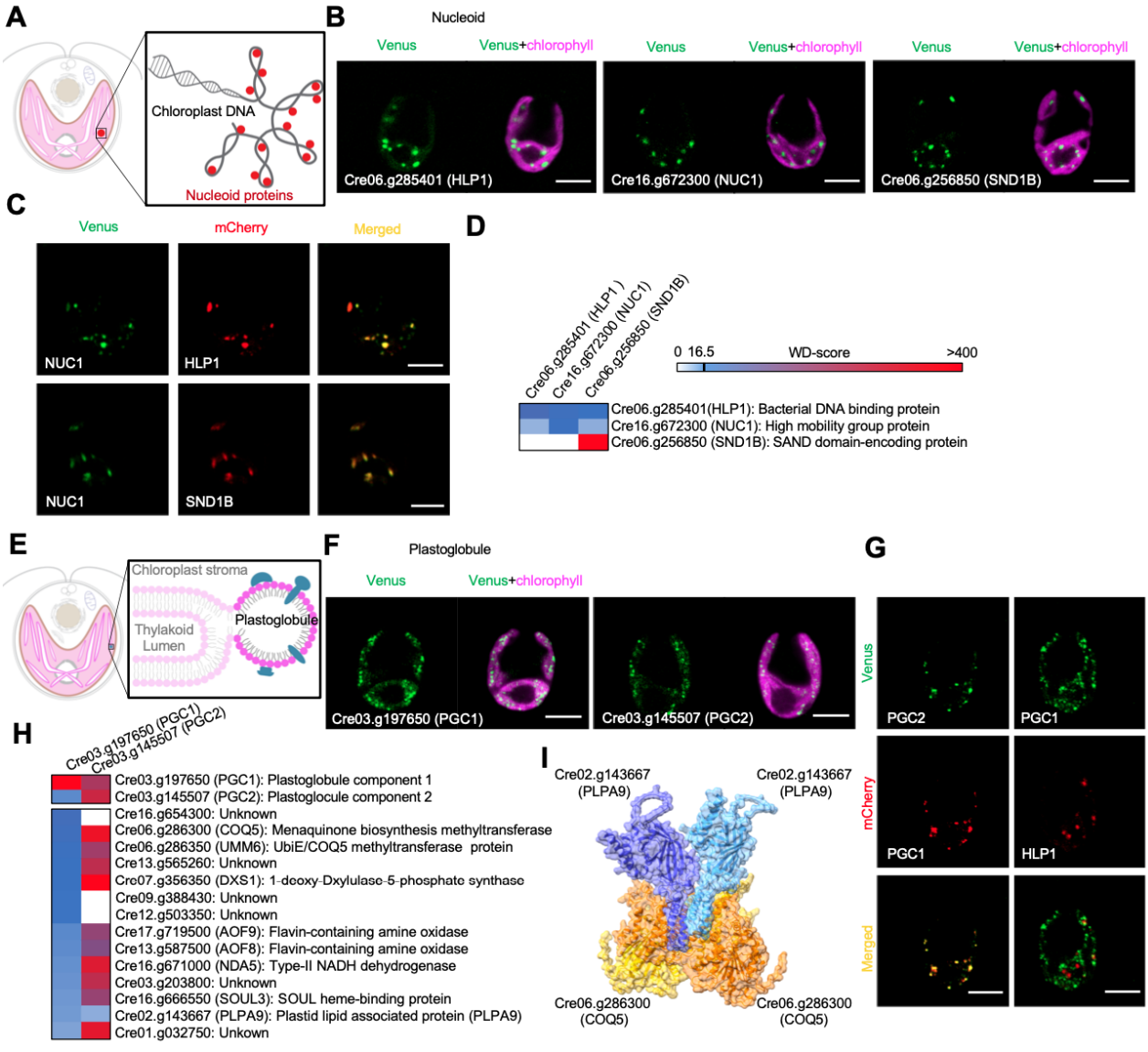

Figure 3. The data revealed novel components of nucleoids and plastoglobules in the chloroplast.

(A) A diagram of the chloroplast nucleoid, in which the chloroplast DNA is organized into DNA-protein conglomerates.

(B) Representative images of fluorescently-tagged Cre06.g285401 (HLP1), Cre16.g672300 (NUC1), and Cre06.g256850 (SND1B).

(C) Dual tagging indicates the co-localization of HLP1, NUC1, and SND1B.

(D) Protein-protein interactions among HLP1, NUC1, and SND1B.

(E) Diagram of a plastoglobule, a thylakoid membrane-associated lipid droplet.

(F) Representative images of fluorescently-tagged Cre03.g197650 (PGC1) and Cre03.g145507 (PGC2).

(G) Dual tagging indicates the co-localization of PGC1 and PGC2. PGC1 was not co-localized with HLP1, indicating that they localize to distinct structures.

(H) High-confidence interacting proteins of PGC1 and PGC2.

(I) Structure modeling of Cre02.g143667 (PLPA9) and Cre06.g286300 (COQ5) by Alphafold suggests a direct interaction between these two proteins.

All scale bars are 5 μm.

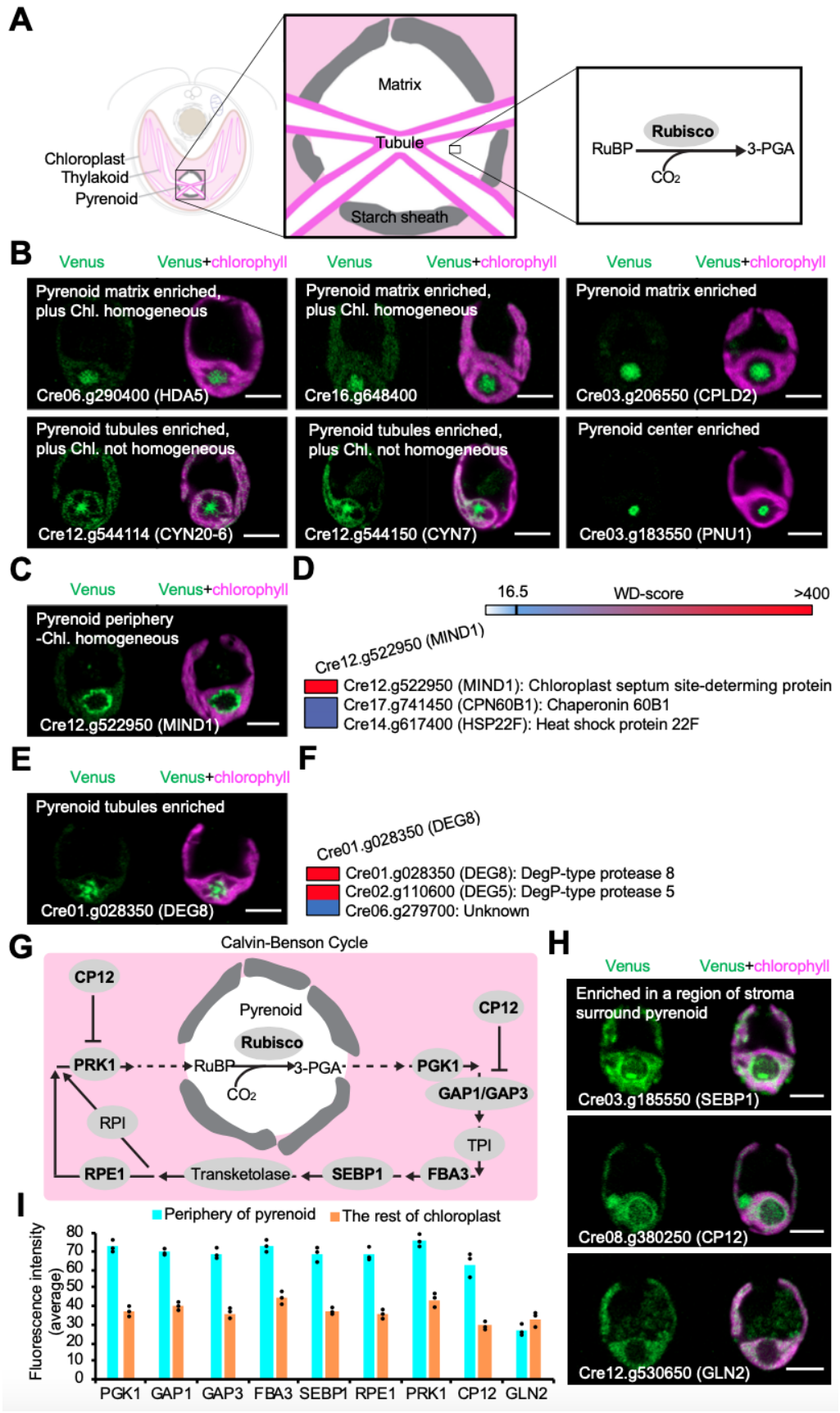

791

Figure 4. Our data revealed novel pyrenoid components and the enrichment of Calvin-Benson cycle enzymes in the stroma around the pyrenoid.

(A) A diagram of the pyrenoid highlights the starch sheath, pyrenoid tubules, and pyrenoid matrix where most of the carbon-fixing enzyme Rubisco is located.

(B) Representative images of Cre06.g290400, Cre16.g648400, and Cre03.g206550 (CPLD2), enriched at the pyrenoid matrix; Cre12.g544114 (CYN20-6) and Cre12.g544150 (CYN7) enriched in the pyrenoid tubules; and Cre03.g183550 (PNU1) localized to the pyrenoid center.

(C) Representative images of Cre12.g522950 (MIND1) enriched at the pyrenoid periphery.

(D) High-confidence interacting proteins of MIND1.

(E) Representative images of Cre01.g028350 (DEG8) enriched in the pyrenoid tubules.

(F) High-confidence interacting proteins of DEG8.

(G) Simplified model of the Calvin-Benson cycle in Chlamydomonas.

(H) Representative images of Cre03.g185550 (SEBP1) and Cre08.g380250 (CP12) enriched in a region of the stroma immediately surrounding the pyrenoid. For comparison, Cre12.g530650 (GLN2, Glutamine synthetase), homogeneously localized throughout the stroma.

(I) Calvin-Benson cycle enzymes showed 1.85-fold enrichment in the stroma around pyrenoid. The measurement of fluorescence intensity was conducted with Fiji (ImageJ). The measured value and mean from three independent cells are shown.

All scale bars are 5 μm.

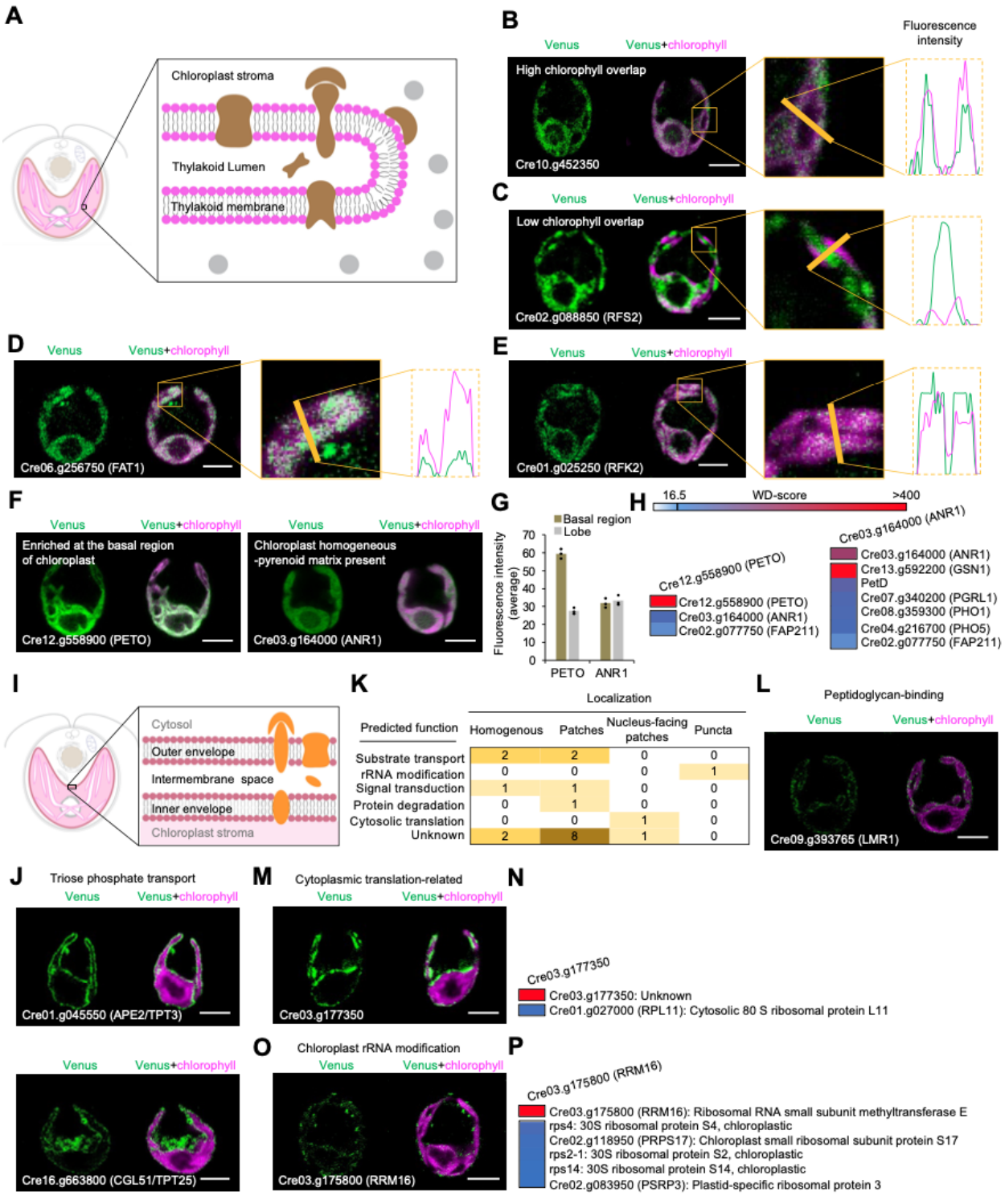

Figure 5. Our data revealed thylakoid-associated enzymes, the enrichment of PETO at the base of the chloroplast, and regions of the chloroplast envelope specialized for different functions.

(A) A diagram shows the thylakoid membrane, thylakoid-associated enzymes (brown), and non-thylakoid-associated enzymes (grey).

(B) Representative images and line intensity profile of fluorescently-tagged Cre10.g452350, which showed high overlap with chlorophyll. The measurement of fluorescence intensity was conducted with Fiji (ImageJ).

(C) Representative images and line intensity profile of Cre02.g088850 (RFS2), which showed low overlap with chlorophyll.

(D) Representative images and line intensity profile of Cre06.g256750 (FAT1), which showed high chlorophyll overlap.

(E) Representative images and line intensity profile of Cre01.g025250 (RFK2), which showed high chlorophyll overlap.

(F) Representative images of Cre12.g558900 (PETO), which was enriched in the base of the chloroplast. ANR1 (Cre03.g164000) homogeneously localized throughout the chloroplast.

(G) PETO showed a 2-fold enrichment of average fluorescence intensity in basal region. The average fluorescence intensity in the basal or lobe region are shown for three independent cells; bars represent mean values.

(H) High-confidence interacting proteins of PETO and ANR1. GSN1, glutamate synthase; PetD, cytochrome b6f subunit IV; PGRL1, proton-gradient related-like; PHO1 and PHO5, alkaline phosphatases.

(I) A diagram of the chloroplast envelope highlights the outer membrane, intermembrane space, inner membrane, and chloroplast envelope-associated proteins.

(J) Representative images of Cre01.g045550 (APE2/TPT3) and Cre16.g663800 (CGL51/TPT25), homogeneously localized throughout the chloroplast envelope.

(K) A heat map shows the observed localization and predicted function of 20 chloroplast envelope proteins.

(L) Representative images of Cre09.g393765 (LMR1), which localized to patches along the chloroplast envelope.

(M) Representative images of Cre03.g177350, which localized to the nucleus-facing portion of the chloroplast envelope.

(N) High-confidence interacting proteins of Cre03.g177350.

(O) Representative images of Cre03.g175800 (RRM16), which localized as punctate dots along the chloroplast envelope.

(P) High-confidence interacting proteins of Cre03.g175800 (RRM16).

All scale bars, 5 μm.

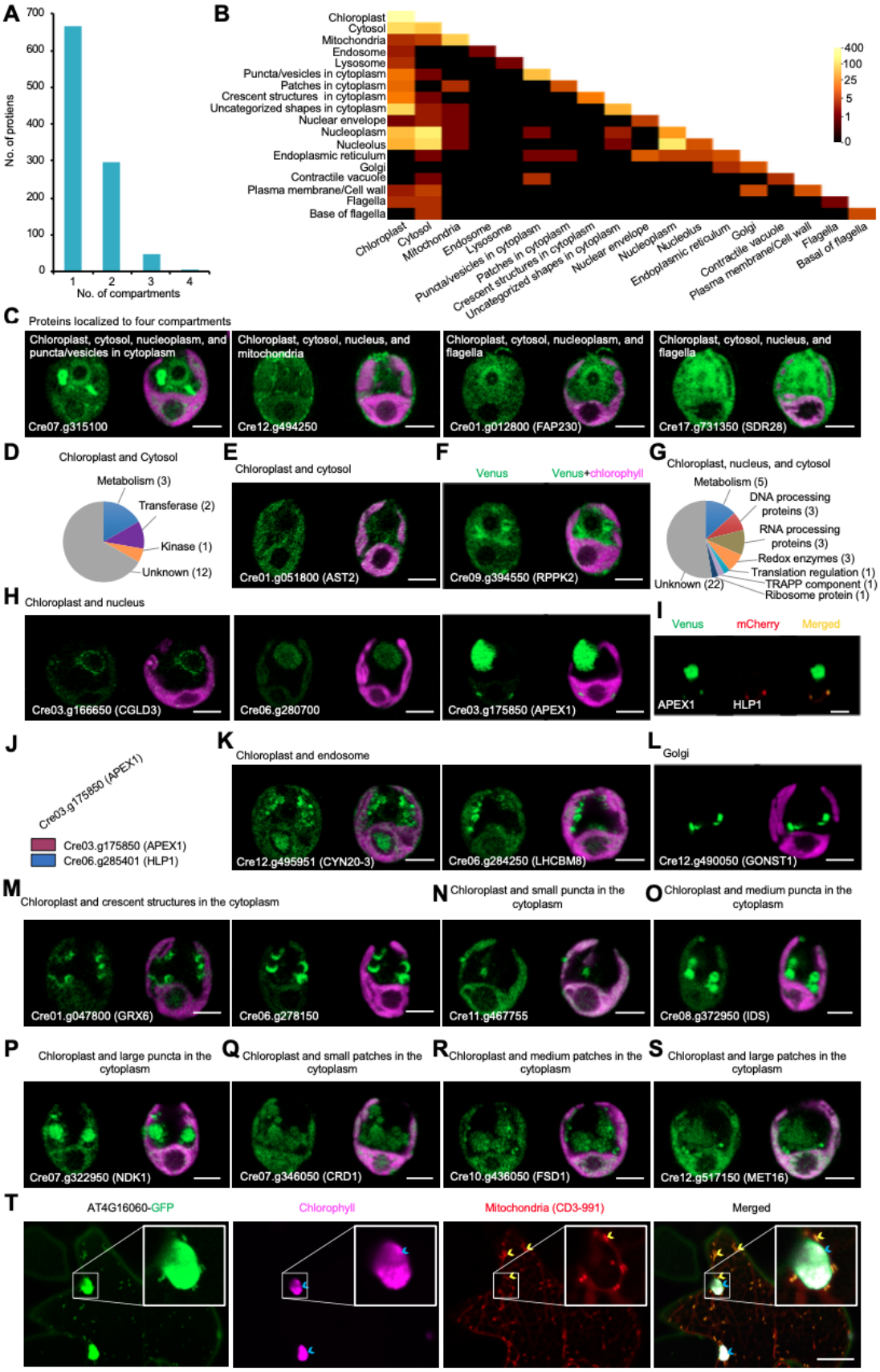

854

Figure 6. Many proteins localized to multiple compartments.

(A) The number of proteins localized to 1, 2, 3, or 4 compartments is shown.

(B) A heat map shows observed dual localizations.

(C) Representative images of proteins localized to four compartments.

(D) Functional classification of 18 proteins dual-localized to the chloroplast and cytosol.

(E) Representative images of Cre01.g051800 (AST2), dual-localized to the chloroplast and cytosol.

(F) Representative images of Cre09.g394550 (RPPK2), which localized to the chloroplast, cytosol, and nucleoplasm.

(G) Functional classification of 39 proteins dual-localized to the chloroplast, nucleus, and cytosol.

(H) Representative images of proteins dual-localized to the chloroplast and nucleus.

(I) Dual tagging revealed the co-localization of Cre03.g175850 (APEX1, a putative exodeoxyribonuclease III), and HLP1 in the chloroplast.

(J) The IP-MS data revealed a high-confidence interaction between APEX1 and HLP1.

(K) Representative images of Cre12.g495951 (CYN20-3) and Cre06.g284250 (LHCBM8), dual-localized to the chloroplast and endosome.

(L) Representative images of Cre12.g490050 (GONST1) whose homolog in Arabidopsis (AT2G13650) is localized to the Golgi apparatus.

(M) Representative images of Cre01.g047800 (GRX6) and Cre06.g278150, dual-localized to the chloroplast and crescent structures in the cytoplasm.

(N) Representative images of Cre11.g467755, dual-localized to the chloroplast and small puncta in the cytoplasm.

(O) Representative images of Cre08.g372950 (IDS1), dual-localized to the chloroplast and medium puncta in the cytoplasm.

(P) Representative images of Cre07.g322950 (NDK1), dual-localized to the chloroplast and large puncta in the cytoplasm.

(Q) Representative images of Cre07.g346050 (CRD1), dual-localized to the chloroplast and small patches in cytoplasm.

(R) Representative images of Cre10.g436050 (FSD1), dual-localized to the chloroplast and medium patches in cytoplasm.

(S) Representative images of Cre12.g517150 (MET16), dual-localized to the chloroplast and large patches in cytoplasm.

(T) Representative images of AT4G16060, the Arabidopsis homolog of Cre12.g494250, in tobacco leaf cells. AT4G16060 was observed in the chloroplast, cytosol, and mitochondria. The yellow arrows indicate mitochondria labeled by mitochondria mCherry marker CD3-991. The blue arrows indicate chloroplasts.

All scale bars are 5 μm.

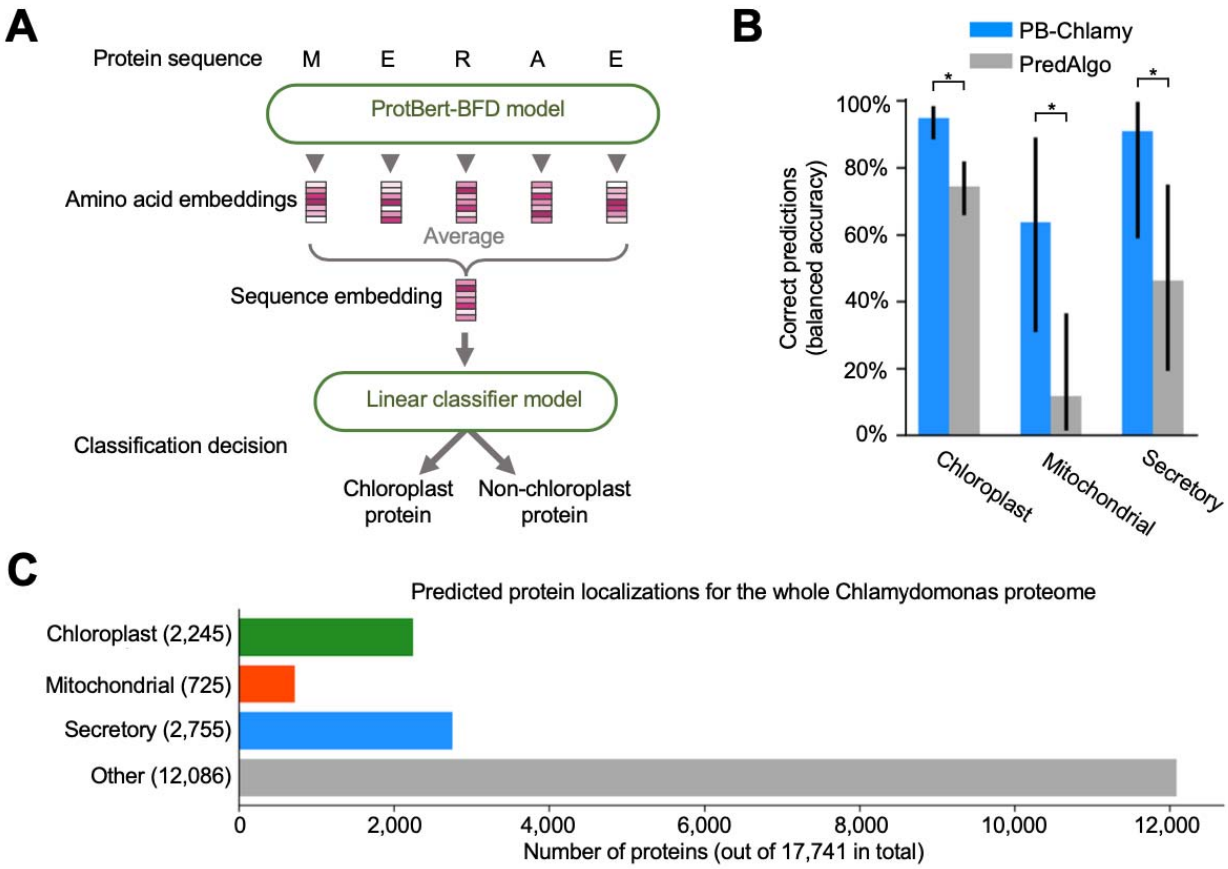

Figure 7. We predicted localizations of all proteins in *Chlamydomonas reinhardtii*.

(A) The PB-Chlamy set of predictors was created based on a pre-trained ProtBertBFD instance with second-stage supervised training using our protein localization dataset.

(B) PB-Chlamy displays improved accuracy compared to PredAlgo, the previous state-of-the-art localization predictor for Chlamydomonas, on a test set randomly chosen from our localized proteins and not used for training. The measure displayed is balanced accuracy, an average of sensitivity (the % of real positives correctly classified) and specificity (the % of real negatives correctly classified). Each separate localization predictor had its own test set, with sizes as follows: 111 chloroplast and 97 non-chloroplast proteins, 12 mitochondrial and 194 non-mitochondrial, 18 secretory and 149 non-secretory. The asterisk * indicates $p<0.05$.

906 (C) PB-Chlamy was used to predict localizations for the whole Chlamydomonas proteome

907 (v5.6, primary transcripts only).

908

STAR★METHODS

KEY RESOURCES TABLE

REAGENT or RESOURCE	SOURCE	IDENTIFIER
Antibodies		
Goat anti-Rabbit IgG(H+L) Highly Cross-Adsorbed Secondary Antibody, Alexa Fluor 488	Invitrogen	Cat# A11034
Rabbit polyclonal anti-Cre01.g028150	This paper	N/A
Rabbit polyclonal anti-Cre01.g013150	This paper	N/A
Rabbit polyclonal anti-Cre12.g519350	This paper	N/A
Rabbit polyclonal anti-Cre03.g172550	This paper	N/A
Rabbit polyclonal anti-Cre01.g019250	This paper	N/A
Chemicals, Peptides, and Recombinant proteins		
Digitonin, Water soluble	Research Products International	Cat# 11024-24-1
cOmplete, EDTA-free Protease inhibitor	Roche	Cat# 5056489001
Anti-FLAG M2 Magnetic Beads	Sigma-Aldrich	Cat# M8823
3×FLAG peptide	Sigma-Aldrich	Cat# F4799
4×Laemmli sample buffer	Bio-Rad	Cat# 1610747
Dimethyl sulfoxide	Sigma-Aldrich	Cat# 67-68-5
Betaine	Sigma-Aldrich	Cat# 107-43-7
Formaldehyde solution 4 %, pH6.9	Sigma-Aldrich	Cat# 1004960700
Bovine Serum Albumin	Sigma-Aldrich	Cat# A3059
VECTASHIELD Mounting Medium	Vector Laboratories	Cat# H-1300
UltraPure Low-Melting Point Agarose	Invitrogen	Cat# 16500100
4-15 % Criterion TGX Precast Midi Protein Gel	Bio-Rad	Cat# 5671084
MAX efficiency transformation Reagent for Algae	Invitrogen	Cat# A24229
DL-Dithiothreitol	Sigma-Aldrich	Cat# D0632
Trypsin Gold, Mass Spectrometry Grade	Promega	Cat# V5280
Critical Commercial Assays		
Phusion High-Fidelity DNA polymerase	New England BioLabs	Cat# M0530L
MinElute Gel Extraction Kit	QIAGEN	Cat# 28606
Gibson Assembly Master Mix	New England BioLabs	Cat# E2611L
Invitrogen Gateway Clonase II	Invitrogen	Cat#11791020
QIAprep Spin Miniprep Kit	QIAGEN	Cat# 27106
Experimental Models: Organisms/Strains		
C.reinhardtii: wild-type CC-4453	Chlamydomonas Resource Center	CC-4533 cw15
E. coli Stellar Competent Cells	Takara	Cat# 636763
Chlamydomonas strains expressing tagged proteins listed in Table S6	This paper, Chlamydomonas Resource Center	https://www.chlamycollection.org/
Oligonucleotides and Recombinant DNA		
pLM005	(Mackinder et al., 2016); GenBank	KX077945.1
pLM006	(Mackinder et al., 2016); GenBank	KX077949.1
pENTR223	ABRC	https://www.arabidopsis.org/
pEarleyGate 103	ABRC	https://www.arabidopsis.org/
Mitochondria marker (CD3-991)	ABRC	https://www.arabidopsis.org/
Plasmid constructs generated and listed in Table S1	This paper, Chlamydomonas Resource	https://www.chlamycollection.org/

Software and Algorithms		
Fiji	(Schindelin et al., 2012)	https://imagej.net/software/fiji/downloads
Thermo Proteome Discoverer 2.5	Thermo Scientific	Cat# OPTON-30945
Continued		
REAGENT or RESOURCE	SOURCE	IDENTIFIER
Scaffold 5	Proteome Software	https://www.proteomesoftware.com/products/scaffold-5
Others		
Electroporation Cuvette, 2mm gap	Bulldog Bio.	Cat# 12358-346
Ibidi USA µ–Slide 8 well, Glass bottom	Ibidi	Cat# NC0704855
Poly-L-lysine coated glass slides	Sigma-Aldrich	Cat# P0425
Kontes Duall #22 homogenizer	Kimble	Cat# KT885450-0022
Avanti J-26X with 8.1000 rotor	Beckman Coulter	N/A
Cryomill	Retsch	Part NO. 20.749.0001
Electroporator	NEPA GENE	NEPA21 type II
SP5 Confocal Microscope	Leica	TCS SP5
Singer Rotor HAD	Singer Instruments	Cat# ROT-001
Typhoon FLA9500 fluorescence scanner	GE Healthare	N/A
Colony picker	Norgren Systems	Part NO.12461
Nikon Confocal laser scanning microscope	Nikon	A1Rsi
Nikon Confocal microscope	Nikon	A1R-STED

CONTACT FOR REAGENT AND RESOURCE SHARING

Further information and requests for resources and reagents should be directed to and will be fulfilled by the Lead Contact, Martin C. Jonikas (mjonikas@princeton.edu)

EXPERIMENTAL MODEL AND SUBJECT DETAILS

Strains and culture conditions

The *Chlamydomonas reinhardtii* strain CC-4533 (cMJ030) was used for wild-type (hereafter WT) in all experiments. All strains were maintained on Tris-acetate-phosphate (TAP) solid medium with 1.5 % agar at 22 °C under dim light (<10 µmol photons m^{-2} s^{-1}). All media used revised trace element solution (Kropat et al., 2011).

METHOD DETAILS

Target genes selection

Target genes were selected from seven sources (Figure S1A), including 1,093 genes encoding proteins identified in Arabidopsis chloroplast proteomics (Ferro et al., 2010), 644 genes

encoding proteins identified in Chlamydomonas chloroplast proteomics (Terashima et al., 2010), 154 genes encoding proteins identified in Chlamydomonas pyrenoid proteomics (Zhan et al., 2018), 3,317 genes encoding PredAlgo predicted chloroplast proteins and 858 genes encoding proteins with low PredAlgo score in non-chloroplast organelles (Tardif et al., 2012), 510 genes encoding GreenCut2 proteins (Karpowicz et al., 2011), and 303 genes encoding candidate proteins required for photosynthesis suggested in mutant screening (Li et al., 2019). In addition, we also selected 777 genes because of their potential association with chloroplast function suggested either in their Phytozome annotation (https://phytozome-next.jgi.doe.gov/) or in related reports, such as the TEF proteins present in thylakoid enriched fraction (Allmer et al., 2006) and FTT proteins interacting with well-known chloroplast proteins (Mackinder et al., 2017). To avoid duplicating effort, we removed the overlapping genes across the seven sources above and genes encoding proteins which had been localized in Mackinder et al., 2017. Altogether, we obtained 5,874 target genes.

Plasmid Construction and Cloning

We designed our primers according to gene sequences present in the v5.5 *Chlamydomonas reinhardtii* genome. Cross et al. (Cross, 2016) identified upstream ATGs in many of these gene sequences, and supplementary data in Mackinder et al. 2017 indicate that for genes that include such upstream ATGs, using the original ATG leads to lower localization success rates, suggesting that the Cross et al. 2016 upstream ATGs more frequently correspond to the native translation start site. Therefore, wherever an upstream ATG had been identified by Cross et al., we used this ATG instead of the one annotated in the genome, leading to our usage of a corrected upstream ATG in 1,213 of our target genes (Table S1).

The cloning pipeline was based on that used in Mackinder et al. 2017, with some modifications. The open reading fames were amplified from Chlamydomonas WT genomic DNA by PCR using Phusion High-Fidelity DNA polymerase (New England BioLabs) with additives of

6 % DMSO (v/v) (Sigma-Aldrich) and 1 M Betaine (Sigma-Aldrich). The PCR products were gel purified using MinElute Gel Extraction Kit (QIAGEN) and then cloned in-frame with a C-terminal Venus-3×FLAG in pLM005 by Gibson assembly (New England BioLabs). Primers were designed to amplify the open reading frame until but excluding the stop codon, and with adaptors to allow efficient assembly into *HpaI*-cut pLM005. Considering the PCR limitations to amplification of large genes, we mainly focused on genes smaller than 8 kb in this study. For genes larger than 6 kb, we split them into multiple fragments (< 3 kb) for PCR amplification and then reassembled the fragments together during the final Gibson assembly step. The fragment size was verified by restriction enzyme digestion. A pilot study showed that 334/334 (100 %) of genes had correct junctions as verified by Sanger sequencing.

Cloning of Chlamydomonas genes is known to be challenging due to high GC content, repetitive sequences, and gene length (Mackinder et al., 2017). In total, we successfully cloned 3,116 genes (53 %) (Figure S1A), a similar fraction to the 48 % in Mackinder et al. 2017. Interestingly, the cloning success of genes smaller than 500 bp is 66.2 %, which is lower than 86.5 % of genes with size between 1,000~2,000 bp (Figure S1H).

Chlamydomonas transformation

Constructs were linearized by *EcoRV*, *DraI*, *AflII*, or *BsaI* prior to the electroporation into WT Chlamydomonas strain CC-4533. WT cells were pre-cultured in TAP liquid medium at 22 °C under light with a photon flux density of 150 µmol photons m^{-2} s^{-1} until the cell density reached to ~2 $\times 10^6$ cells mL-1.For each transformation, 150 ng of cut plasmid was mixed with 60 µL of 2×10^8 cells mL^{-1} suspended in MAX Efficiency Transformation reagent (Invitrogen) in an ice-cold 0.2 cm gap electroporation cuvette (Bulldog Bio.) and transformed into WT strains by electroporation using a NEPA21 electroporator (NEPA GENE) (Yamano et al., 2013). The settings were: Poring Pulse: 250.0 Volts, 8.0 ms pulse length, 50.0 ms pulse interval, 2 pulses, 10 % decay rate, + polarity; Transfer Pulse: 20.0 Volts, 50.0 ms pulse length), 50.0 ms pulse

interval), 10 pulses, 40 % decay rate), +/- polarity. For recovery, cells were transferred to 10 mL TAP liquid medium plus 40 mM sucrose and incubated with gentle shaking under dim light (<10 µmol photons m^{-2} s^{-1}) overnight. The transformants were plated on TAP agar medium supplied with 20 µg mL^{-1} paromomycin under light (150 µmol photons m^{-2} s^{-1}.). After 7 days incubation under dim light (<10 µmol photons m^{-2} s^{-1}), 48 transformants from each plate were arrayed on a new rectangular TAP agar PlusPlate (Singer Instruments) using a colony Picker (Norgren Systems). The transformants were replicated manually onto a fresh TAP agar PlusPlate using a 96-Long pin pad (Singer Instruments). The TAP plates with arrayed transformants were screened for fluorescence using a Typhoon FLA9500 fluorescence scanner (GE Healthcare) with the following settings: Venus, 532 nm excitation with 555/20 nm emission. The colonies with positive fluorescence signals were isolated and maintained in 96 arrays using a Singer Rotor propagation robot (Singer Instruments).

Transformation of constructs and localization of proteins in Chlamydomonas are known to be inefficient (Mackinder et al., 2017), possibly due to several mechanisms that fight foreign DNA (Neupert et al., 2009; Zhang et al., 2014). Our transformation and localization success rate (34 %) was lower than that in Mackinder et al. 2017 (49 %), possibly because the genes targeted in the present study were overall expressed at lower levels. To generate dual-tag lines, pLM006 harboring an mCherry-6×HIS tag was used as the backbone, and TAP agar medium supplied with 20 µg mL^{-1} hygromycin was used for selection.

Confocal Microscopy

For confocal imaging, colonies were transferred to a 96-well microtiter plate with 100 µL TP liquid medium and 5 µg mL^{-1} antibiotics in each well and then pre-cultured in air under 150 µmol photons m^{-2} s^{-1} on an orbital shaker with gentle agitation of 600 RPM. After ~16 hr of growth, 10 µL cells were transferred onto an µ-Slide 8-well glass-bottom plate (Ibidi) and 200 µL of 1 % TP low-melting-point agarose at ~35 °C was overlaid to restrict cell movement. All imaging except

for Fluorescence Recovery After Photobleaching (FRAP) assays was conducted using a Leica SP5 confocal microscope with the following settings: Venus, 514 nm excitation with 530/10 nm emission; mCherry, 561 nm excitation with 610/30 nm emission; and chlorophyll, 514 nm excitation with 685/40 nm emission. All confocal microscopy images were analyzed using Fiji (Schindelin et al., 2012). For each strain, a confocal section through a cell showing the predominant localization pattern was captured and analyzed. To minimize the bias in determining the localization patterns, each localization image was independently analyzed by two researchers. Localization patterns for 31 proteins where there was clear disagreement or insufficient signal were categorized as Ambiguous.

FRAP assays were performed using a Nikon A1R-STED confocal microscope with the following setting: Venus 514 nm excitation with 530/10 nm emission; and chlorophyll, 514 excitation with 685/40 nm emission. One baseline image was acquired before FRAP was performed. The selected puncta were bleached by a high-intensity laser beam (514 nm wavelength). The recovery of fluorescence at the bleached puncta was imaged every 30 s for 10 min.

Indirect Immunofluorescence Assay

Indirect immunofluorescence was performed as described previously (Wang et al., 2016). Briefly, Cells were harvested by centrifugation and rinsed with PBS buffer twice. Then 100 µL of cells was spotted onto Poly-L-lysine coated glass slides (Sigma-Aldrich). Cells were fixed with 4 % (w/v) formaldehyde (Sigma-Aldrich) in PBS for 20 min and then incubated with 100 % ice-cold methanol for 20 min to remove chlorophyll. Purified antibodies (Yenzyme) against Cre01.g028150, Cre01.g013150, Cre12.g519350, Cre03.g172550, and Cre01.g019250, were used at a dilution of 1:200. The purified antibodies were generated using the following peptides: C-Ahx-PDQPPRILTTRRE-amide (Cre01.g028150), C-Ahx-TWDVKAPINKHYNFH-cooh (Cre01.g013150), C-Ahx-YLPNTGNMLMQVNPNQ-cooh (Cre12.g519350), C-Ahx-

RGQVKNTQQYRMR-cooh (Cre03.g172550), and C-Ahx-KGVDATKYSHSTIVQT-amide (Cre01.g019250). After washing the slides 4 times, each with 50 mL PBS-T (supplied with 0.1% Tween 20 (v/v)) in Coplin jar, Alexa Fluor 488 goat anti-rabbit IgG (H+L) Cross-Adsorbed Secondary Antibody (Invitrogen) was used at a dilution of 1:500. Then, washing the slides 4 times, each with 50 mL PBS-T. Fluorescence and bright-field images were acquired using a confocal microscope (Leica, SP5).

Protein Structure Modeling

Alphafold2.1 (Jumper et al., 2021) was used to screen for candidate multimeric structures of proteins identified in pull-down experiments of plastoglobule complex, using one NVIDIA A100 GPU. Pairs of protein sequences were concatenated in silico with a 50-U linker sequence (Moriwaki, 2021), and structures were predicted with Alphafold-monomer model. Proteins found to dimerize were again compared to other proteins in the same pull-down experiment. ChimeraX (Pettersen et al., 2021) was used to visualize structures. The Alphafold2 predicted complex of Cre02.g143667 and Cre06.g286300 was deposited in Modelarchive (https://www.modelarchive.org/).

Protein localization prediction

For each subcellular localization, we trained a protein language model to predict protein localization from protein sequence. Protein language models are first trained on large numbers of sequences, and then these pretrained models can be retrained for a specific prediction task, in this case subcellular location prediction (Figure 7A). For our pretrained model, we used ProtBertBFD, a protein language model pre-trained on billions of protein sequences (Elnaggar et al., 2021; https://huggingface.co/Rostlab/prot_bert_bfd). Given a protein sequence, ProtBertBFD outputs numeric vectors, or embeddings, that capture features of each amino acid in that sequence. These amino acid embeddings contain information on biochemical and

structural properties (Elnaggar et al., 2021). To represent a protein sequence, we take an average of the embeddings of all of its amino acids, and use this representation as an input to a linear classifier to distinguish if a protein is localized to a particular cellular compartment or not. Specifically, we use the model architecture BertForSequenceClassification from the huggingface python package (Wolf et al., 2020). Our script for running training and evaluation is https://github.com/clairemcwhite/transformer_infrastructure/hf_classification.py. For each compartment (chloroplast, mitochondrial and secretory) we used proteins found to localize to the compartment as positive cases, and proteins not found to localize to the compartment as negative cases. We used a random 60% of these positive and negative cases to train the model, 20% for performance validation during training, and 20% as a fully withheld test set to evaluate model performance on unseen examples. These sets are listed in Table S7.

The raw score distributions, PR and ROC curves and summary measures compared to PredAlgo are shown in Figure S11; for the purpose of comparisons with PredAlgo, we used the testing sets minus any proteins that were included in PredAlgo training data. We then used the trained models to predict protein localizations for the entire Chlamydomonas proteome (Table S7).

We downloaded Chlamydomonas protein sequences from Phytozome (https://phytozome-next.jgi.doe.gov/info/Creinhardtii_v5_6, genome version 5.6); we only used primary transcripts for training and for localization prediction. We adjusted the protein sequences to use the new start codons described by Frederick Cross (Cross, 2016) - they are included in Table S7.

The training command and environment setup for the chloroplast were as follows, with analogous commands for the other localizations:

```
module load cudatoolkit
bash make_hf-transformers_conda_env.sh
conda activate hf-transformers
```

python hf_classification.py -m prot_bert_bfd/ -tr chloro_train.csv -v chloro_val.csv -te chloro_test.csv -o results_chloro -maxl 1150 -n chloro -e 10 -tbsize 1 -vbsize 1 -s 3

The input files containing the training/validation/test sets were plaintext, formatted as follows:

Entry_name,sequence,label

Cre03.g155400,M H K T P C L H G G S S L S A G R A P L A R L C C A S Q R V R G P A P A Q A F W K Q S G A S A G K S G K A R P G A K A Q Q P K Q K A G G G K Q G G G G G G G L M D S E V P V Y A E A F D I N K C V D L Y L R F F K W V S S P V T G G S G K K,Chloroplast

The trained model files are available (https://huggingface.co/wpatena/PB-Chlamy/tree/main).

Affinity Purification and Mass Spectrometry

Each affinity purification-mass spectrometry (AP-MS) experiment was performed twice from independently grown samples of the same strain. Cells expressing Venus-3×FLAG-tagged proteins were pre-cultured in 50 mL TAP medium with 5 μg mL^{-1} paromomycin until the cell density reach to ~2-4 $\times 10^6$ cells mL^{-1}. Then, cells were harvested by centrifugation at 1,000 g for 5 min and the pellets were suspended in 1,000 mL TP liquid medium. Cells were grown with air bubbling and constant stirring of 210 RPM under 150 μmol photons m^{-2} s^{-1} light until the cell density reached ~2-4 $\times 10^6$ cells mL^{-1}. Cells were collected by centrifugation at 3,000 g for 4 min in an Avanti J-26X centrifuge with an 8.1000 rotor (Beckman) at 4 °C. The pellets were washed in 35 mL ice-cold washing buffer (25 mM HEPES, 25 mM KOAc, 1 mM $Mg(OAc)_2$, 0.5 mM $CaCl_2$, 100 mM Sorbitol, 1mM NaF, 0.3 mM Na_3VO_4, and cOmplete EDTA-free protease inhibitor (1 tablet/500 mL)) and then resuspended in a 1:1 (v/w) ratio of ice-cold 2×IP buffer (50 mM HEPES, 50 mM KOAc, 2 mM $Mg(OAc)_2$, 1 mM $Cacl_2$, 200 mM Sorbitol, 1mM NaF, 0.3 mM Na_3VO_4, and cOmplete EDTA-free protease inhibitor (1 tablet/50 mL)). 3 mL cell slurry was immediately added to liquid nitrogen to form small popcorn pellets which were stored at -80 °C

until needed. Cells were lysed by cryogenic grinding using a Cryomill (Retsch) at frequency of 25 oscillations per second for 20 min. The ground powder was defrosted on ice for 45 min and dounced 25 times on ice with a Kontes Duall #22 homogenizer (Kimble). 1mL homogenized cells of each sample was used for the following processes. Membrane proteins were solubilized by incrementally adding an equal volume of ice-cold 1×IP buffer plus 2 % digitonin (RPI) followed by an incubation of 45 min with nutation at 4 °C. The cell debris were removed by spinning at 12,700 g for 30 min at 4°C. The supernatant was then mixed with 50 µL anti 3×FLAG magnetic beads (Sigma) which had been previously washed sequentially with 1×IP buffer 3 times and 1×IP buffer plus 0.1 % digitonin 2 times. The mixture was incubated with nutation at 4 °C for 1.5 hr, followed by the removal of supernatant. The beads were washed 4 times with 1×IP buffer plus 0.1 % digitonin followed by a 30 min competitive elution with 45 µL of 1×IP buffer plus 0.25 % digitonin and 2 µg/µL 3×FLAG peptide (Sigma-Aldrich). After elution, 30 µL protein samples were mixed with 9.75 µL 4×SDS-PAGE buffer (Bio-Rad) containing 100 mM DTT (Sigma-Aldrich) followed by denaturation by heating at 70 °C for 10 min. Then, 30 µL denatured protein sample was loaded into a well of a 4-15 % Criterion TGX Precast Midi Protein Gel (BioRad) for electrophoresis at 50 V for 40 min until the protein front moved ~2.5 cm. ~2.0 cm gel slice containing target proteins with molecular weight >= 10 kDa (to exclude the 3xFLAG peptide) were excised and stored at 4 °C until processing for in-gel digestion. To decrease cross-contamination from samples in neighboring wells, samples were loaded in every other well. To further avoid carry-over contamination of mass spectrometry and contamination from sequential samples, we performed two biological repeats of AP-MS and changed the order of samples in the two biological repeats.

In-gel digestion of protein bands using trypsin was performed as previously (Shevchenko et al., 2006). Trypsin digested samples were dried completely in a SpeedVac and resuspended with 20 µL of 0.1 % formic acid pH 3 in water. 2 µL (~ 360 ng) was injected per run using an Easy-nLC 1,200 UPLC system. Samples were loaded directly onto a 15 cm long, 75 µm inner

diameter nanocapillary column packed with 1.9 µm C18-AQ resin (Dr. Maisch, Germany) mated to a metal emitter in-line with an Orbitrap Fusion Lumos (Thermo Scientific, USA). The column temperature was set at 45 °C and a half-hour gradient method with 300 nL per minute flow was used. The mass spectrometer was operated in data dependent mode with a 120,000 resolution MS1 scan (positive mode, profile data type, AGC gain of 4e5, maximum injection time of 54 s and mass range of 375-1,500 m/z) in the Orbitrap followed by HCD fragmentation in ion trap with 35 % collision energy. A dynamic exclusion list was invoked to exclude previously sequenced peptides for 60s and a maximum cycle time of 3 s was used. Peptides were isolated for fragmentation using the quadrupole (1.2 m/z isolation window). The ion trap was operated in Rapid mode.

Transient expression of Arabidopsis gene in Tobacco leaf

We first cloned the full-length cDNA of AT4g16060 into pENTR223 (ABRC). Then the AT4G16060 was cloned in-frame with a C-terminal GFP in pEarleyGate 103 by LR recombination reaction (Invitrogen Gateway Clonase II). The construct of AT4G16060-GFP and mitochondria mCherry marker CD3-991 (ABRC) were then separately transformed into Agrobacterium tumefaciens by heat shock. A mixture (OD600 = 0.125) of the Agrobacterium tumefaciens harboring At4G16060-GFP, the Agrobacterium tumefaciens carrying CD3-991, and the p19 protein of tomato bushy stunt virus (TBSV) in a 2:1:2 ratio co-infiltrated into 4-weeks old tobacco plants (*Nicotiana tabacum*) (Sainsbury et al., 2009). Three days after infiltration, the abaxial epidermis of the leaves were imaged using Nikon A1Rsi confocal laser scanning microscopy (CLSM) with Nikon 60x Apo (NA1.40) objective. The imaging was performed with the following setting: GFP, 488 nm excitation with 525/25 nm emission; mCherry, 561 nm excitation with 595/25 nm emission; and Chlorophyll, 647 nm excitation with 699/37 nm emission. Image acquisition and analysis were performed using the Nikon NIS Elements software (version 5.21.03).

QUANTIFICATION AND STATISTICAL ANALYSIS

Peptide identification

Raw files were searched using MSAmanda 2.0 (Dorfer et al., 2021) and Sequest HT algorithms (Eng et al., 1994) within the Proteome Discoverer 2.5.0 suite (Thermo Scientific, USA). 10 ppm MS1 and 0.4 Da MS2 mass tolerances were specified. Carbamidomethylation of cysteine was used as fixed modification, oxidation of methionine, deamidation of asparagine and glutamine were specified as dynamic modifications. Pyro glutamate conversion from glutamic acid and glutamine are set as dynamic modifications at peptide N-terminus. Acetylation was specified as dynamic modification at protein N-terminus. Trypsin digestion was selected with a maximum of 2 missed cleavages allowed. Files were searched against the UP000006906 Chlamydomonas database downloaded from Uniprot.org (https://www.uniprot.org/).

Scaffold (version Scaffold 5.1.0, Proteome Software Inc., Portland, OR) was used to validate MS/MS based peptide and protein identifications. Peptide identifications were accepted if they could be established at greater than 95.0 % probability by the Scaffold Local FDR algorithm. Protein identifications were accepted if they could be established at greater than 99.9 % probability and contained at least 2 identified peptides. Protein probabilities were assigned by the Protein Prophet algorithm (Nesvizhskii et al., 2003).

Calculating WD-scores

The WD-scores of MS data were calculated using the ComPASS method, which analyzes spectral counts based on the specificity of the prey, spectral count number and reproducibility (Sowa et al., 2009). Instead of using the spectral counts from two technical repeats, we used the spectral counts from two biological replicas with different neighbors for each sample. First, we generate a Stats table containing all the bait proteins and interactors as below,

Stats Table

	Bait 1	Bait2	Bait3	Bait4	Bait *k*	
Interactor 1	$X_{1,1}$	$X_{2,1}$	$X_{3,1}$	$X_{4,1}$	$X_{k,1}$	$\bar{X}_1$
Interactor 2	$X_{1,2}$	$X_{2,2}$	$X_{3,2}$	$X_{4,2}$	$X_{k,2}$	$\bar{X}_2$
Interactor 3	$X_{1,3}$	$X_{2,3}$	$X_{3,3}$	$X_{4,3}$	$X_{k,3}$	
Interactor 4	$X_{1,4}$	$X_{2,4}$	$X_{3,4}$	$X_{4,4}$	$X_{k,4}$	
Interactor *m*	$X_{1,m}$	$X_{2,m}$	$X_{3,m}$	$X_{4,m}$	$X_{k,m}$	$\bar{X}_m$

$X_{i,j}$ is the average spectral counts from two biological replicas for interactor *j* from bait *i*.

m is the total number of unique prey proteins identified (8,067).

k is the total number of unique bait (41).

We calculated the WD-scores using the equations ((Sowa et al., 2009)) below,

$$WD_{i,j}=\sqrt{\left(\frac{k}{\sum_{j=1}^{i=k} f_{i,j}}\omega_j\right)^p X_{i,j}} \qquad \text{(Equation S1)}$$

$$\omega_j=\left(\frac{\sigma_j}{\bar{X}_j}\right),\ \bar{X}_j=\frac{\sum_{i=1,j=n}^{i=k} X_{i,j}}{k},\ n=1,2,\ldots m,\ \begin{array}{l}\text{if } \omega_j \le 1 \Rightarrow \omega_j=1\\ \text{if } \omega_j > 1 \Rightarrow \omega_j=\omega_j\end{array}$$

$$f_{i,j}=\begin{cases} 1;\ X_{i,j}>0 \\ X_{i,j}\end{cases}$$

p is the number of replicates runs in which the interactor is present $f_{i,j}$.

The minimum WD score values for high-confidence interactions will be different for each study because the WD score depends on the specific proteins and methods used in each study. In Mackinder et al., 2017, we set the high-confidence WD cut-off based on WD-scores of prey

proteins that localized to a different compartment than the bait. Because all the baits in the present study localized to the same compartment (the chloroplast) we could not use the same approach to set the WD cut-off. We therefore set our WD cutoff at 3.7 % of all interactions based on the corresponding value in Mackinder et al., 2017 of 3.78 %. This rationale led to a WD cut-off for the present study of 16.567, with 297 of the 8,067 interactions above this threshold (Table S5). We defined high-confidence protein-protein interactions as those having a WD score above the cutoff of 16.567 and where the prey was detected in both biological repeats, which resulted in ~187 high-confidence protein-protein interactions (Table S5).

Data visualization

The calculation of WD-score and assembly of bait-prey matrix were performed in Microsoft Exel. The alignment of amino acid sequence was conducted using Clustal Omega with default settings (https://www.ebi.ac.uk/Tools/msa/clustalo/). The protein structures were visualized using ChimeraX (https://www.cgl.ucsf.edu/chimerax/).

Transmembrane prediction and Protein homology prediction

Protein transmembrane domains were predicted using TMHMM2.0 (https://services.healthtech.dtu.dk/service.php?TMHMM-2.0). Protein homologies were predicted using Phyre2 (http://www.sbg.bio.ic.ac.uk/phyre2/html/page.cgi?id=index)

Statistical tests

Statistical tests comparing PredAlgo and PB-Chlamy were performed in Python using scipy.stats and rpy2. All other statistical tests were performed in Microsoft Excel.

ADDITIONAL RESOURCES

Protein localization images are available at https://www.chlamylibrary.org/.

Fluorescently tagged strains and plasmid constructs are available at https://www.chlamycollection.org/.

Supplemental Information

A

Order	Sources of candidate	Number of candidates	Number of cloned candidates	Number of localized candidates	References
(1)	Chloroplast proteomics in *Arabidopsis thaliana*	1,093	516	295	Ferro *et al.*, 2010
(2)	Chloroplast proteomics in *Chlamydomonas reinhardtii*	644	384	235	Terashima *et al.*, 2011
(3)	Pyrenoid proteomics	154	80	44	Zhan *et al.*, 2018
(4)	PredAlgo predicted chloroplast proteins	4,175	2,142	696	Tardif *et al.*, 2012
(5)	GreenCut2 proteins	510	329	155	Karpowicz *et al.*, 2011
(6)	Candidate proteins required for photosynthesis	303	132	47	Li *et al.*, 2019
(7)	Others	777	554	200	-
	In total	5,874	3,116	1,032	-

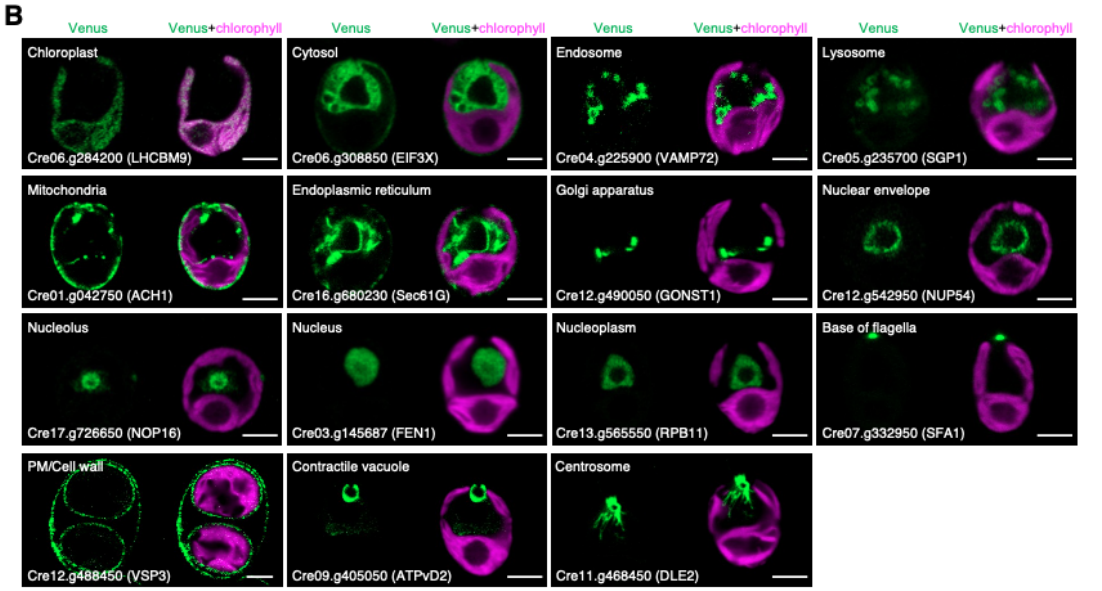

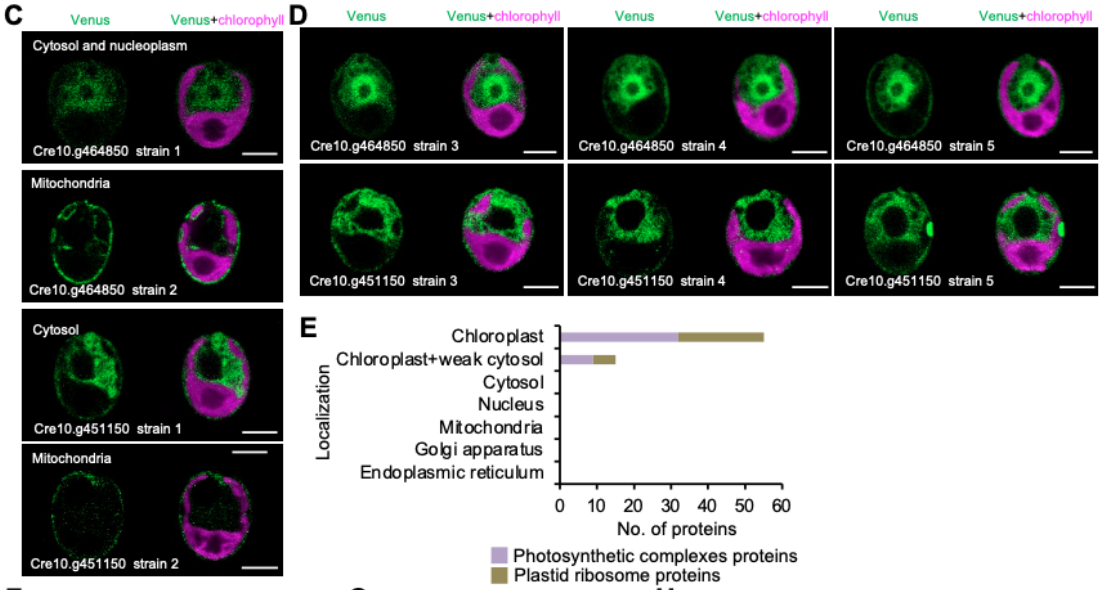

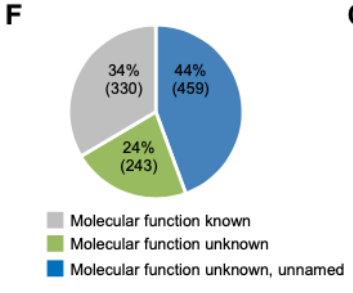

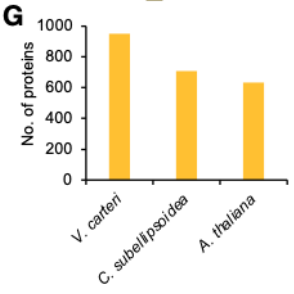

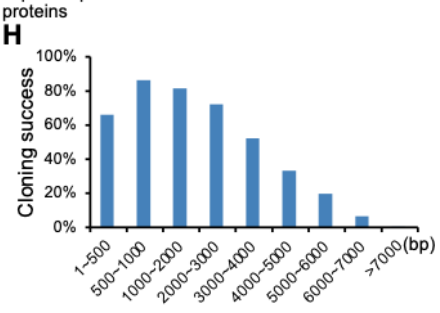

1234

Figure S1. We localized 1,032 proteins from 5,874 target proteins.

Related to Figure 1

(A) A summary of seven sources from which target genes were selected. The number of target genes, number of cloned genes, and number of successfully localized proteins are shown.

(B) Representative images of organelle marker proteins that localized to different cellular locations.

(C) Our localization data showed high reproducibility and chloroplast enrichment of photosynthetic complex proteins and plastid ribosome proteins. Out of 654 proteins for which we obtained two or more independent transformants, the localizations in the independent transformants disagreed for two proteins (<1%), Cre10.g464850 and Cre10.g451150. For each of these two proteins, representative images of the two independent transformants are shown.

(D) Representative images of the localization of Cre10.g464850 and Cre10.g451150 in additional transformants, indicating that Cre10.g464850 is localized to cytosol and nucleoplasm; Cre10.g451150 is localized to cytosol. All scale bars are 5 μm.

(E) The localization enrichment of plastid ribosome proteins and photosynthetic complexes proteins in chloroplast.

(F) Characterization status of our localized proteins.

(G) Number of localized proteins conserved in *Volvox carteri*, *Coccomyxa subellipsoidea*, or *Arabidopsis thaliana*.

(H) Correlation of cloning success with open reading frame size.

Venus-tagged protein	Average number of puncta	Average distance to pyrenoid center (μm)	Average puncta size (μm, diameter)
Cre13.g576400	4.4 ± 0.5	6.11 ± 0.74	0.337 ± 0.10
Cre12.g519900	5.4 ± 0.9	6.33 ± 1.14	0.367 ± 0.10
Cre05.g234050	4.8 ± 0.8	5.00 ± 1.52	0.292 ± 0.06
Cre24.g755197	4.0 ± 0.7	5.44 ±1.63	0.246 ± 0.06
Cre13.g603500	2.8 ± 0.8	2.99 ± 0.59	0.375 ± 0.07
Cre07.g344550	2.2 ± 0.4	2.63 ± 0.70	0.237 ± 0.07
Cre01.g005534	5.0 ± 1.0	4.13 ± 0.81	0.344 ± 0.13
Cre01.g050950	26.6 ± 3.2	5.99 ± 0.83	0.166 ± 0.06
Cre03.g145507	18.6 ± 0.9	5.48 ± 0.24	0.120 ± 0.03
Cre03.g197650	19.2 ± 3.4	5.95 ± 0.52	0.115 ± 0.09
Cre06.g256850	7.4 ± 1.7	5.30 ± 0.37	0.293 ± 0.09
Cre16.g672300	7.2 ± 1.5	4.98 ± 0.90	0.313 ± 0.06
Cre06.g285401	6.8 ± 1.6	4.73 ± 0.77	0.295 ± 0.05
Cre06.g295350	1.8 ± 0.4	5.50 ± 1.94	0.264 ± 0.11
Cre06.g278195	20.0 ± 4.0	6.68 ± 2.00	0.243 ± 0.08

Figure S2. Novel chloroplast punctate structures showed difference in the number of puncta, puncta position, and puncta size.

Related to Figure 2

Novel punctate structures showed differences in the average position, number, and size of puncta. For each punctate structure, its mean distance to the pyrenoid center, the average number of puncta, and the mean punctus size are shown. Mean values ± SD from five independent cells are shown. Each structure is assigned a unique color that is used in Figure 2**.**

A

```
Cre07.g344550.t1.2|C.reinhardtii  ----------MMLSTKLPVSMAKVAAPGQSARPVACPTPRVAGAGSARRL  40
AT4G34200.1|A.thaliana            MSATAAASSSIAVATNSLRNVTLSSRSPLP---------SAISVAFPS--RGRNTLQRRL  49

Cre07.g344550.t1.2|C.reinhardtii  PVARATSTEGDEIALLEKALSIAKERAAKAKTAAAAPAAAAGGYSGPAFAIKTFNAISPV  100
AT4G34200.1|A.thaliana            VLVSCSTGDGS-------------------------------KPTILV--AEKLGDA  73

Cre07.g344550.t1.2|C.reinhardtii  GLERFP-----AGKYVVSGDDAKLPASPM-AIMLRSHQ-L---KQEEVPPTVRCIVRCGA  150
AT4G34200.1|A.thaliana            GIKLLEDVANVDCSYNMTPEELNIKISLCDALIVRSGTKVGREVFESSHGRLKVVGRAGV  133

Cre07.g344550.t1.2|C.reinhardtii  GVNNIPVPKMTELGIPVFNTPGANANAVKELVICGLLLASRGILEGNKYTEEVIYKEENM  210
AT4G34200.1|A.thaliana            GIDNVDLSAATEFGCLVVNAPTANTIAAAEHGIALMAAMARNV----------------A  177

Cre07.g344550.t1.2|C.reinhardtii  DYDKVAKRIEKDKAKFVGCEIEGKTLGVVGLGAIGGRVVNAALALGMKVVGYDPVLSLDA  270
AT4G34200.1|A.thaliana            QADASVKAGEWKRNKYVGVSLVGKTLAVLGFGKVGTEVARRAKGLGMRVIAHDPYAPADR  237

Cre07.g344550.t1.2|C.reinhardtii  AWKLPGDRMGRAESLEELLKVSDYVTVHVPYIKNATHHMINGANLKLCKPNVSFLNFSRG  330
AT4G34200.1|A.thaliana            AHAIGVDL----VSFDEALATADFISLHMPLTPTT-SKILNDETFAKMKKGVRIVNVARG  292

Cre07.g344550.t1.2|C.reinhardtii  EIIDGEALLDMYKSGRMTGKYVSDFA------DPFLSGHPKHLVIPHLGASTEEAEDNSA  384
AT4G34200.1|A.thaliana            GVIDEDALVRALDAGIVAQAALDVFTKEPPAKDSKLVQHERVTVTPHLGASTMEAQEGVA  352

Cre07.g344550.t1.2|C.reinhardtii  AMAADTVKDFLETGTIRNSVNFPQ-----------TVLPPKPGHVGGRLCIVNKNEAGV  432
AT4G34200.1|A.thaliana            IEIAEAVVGALNGELAATAVNAPMVSAEVLTELKPYVVLAEKLGRLAVQLV---AGGSGV  409

Cre07.g344550.t1.2|C.reinhardtii  LGQITTFLGTQKVNIEQQINTSRGDIAYTVLDLSKIDDPAGLQDGLAKACPGVISSRFIG  492
AT4G34200.1|A.thaliana            KNA--------------------KITYASARA----------------TDDLDTRLLR  431

Cre07.g344550.t1.2|C.reinhardtii  NMFDDEMGKPGTFFYVKWASS*-----------------------------------  513
AT4G34200.1|A.thaliana            AMITKGIIEPISDVYVNLVNADFTAKQRGLRLSEERVLLDGSPESPLETITVQLSNVESK  491

Cre07.g344550.t1.2|C.reinhardtii  ------------------------------------------------------------  513
AT4G34200.1|A.thaliana            FASSLSESGEVKVEGKVKDGVPHLTKVGSFEVDVTLEGSIILCRQVDQPGMIGTVGSILG  551

Cre07.g344550.t1.2|C.reinhardtii  ----------------------------------------------------  513
AT4G34200.1|A.thaliana            ESNVNVNFMSVGRIAPRKQAIMAIGVDDIPSKETLKKIGEIPAVEEFVFLKL*  603
```

B

```
Cre01.g050950.t1.2|C.reinhardtii  MAATMQMNKQATRQAAQQGRVAPFKATGVVRK---VAQLPSSTFSGVTVPQRQFAVSGAR  57
AT1G74470.1|A.thaliana            MATTVTLK--------------SF--TGLRQSSTEQTNFVSHVPSSLSLPQRR-------  37

Cre01.g050950.t1.2|C.reinhardtii  SVSRAVQSVFAVKDGAALEGRKLRVAVIGGGPSGACAAETLAKGGVETFLLERKLDNCKP  117
AT1G74470.1|A.thaliana            ----TSLRVTAARATPKLSNRKLRVAVIGGGPAGGAAAETLAQGGIETILIERKMDNCKP  93

Cre01.g050950.t1.2|C.reinhardtii  CGGAIPLCMVEEFDLPMEIIDRRVTKMKMISPSNREVDVGKTLSETEWIGMCRREVFDDY  177
AT1G74470.1|A.thaliana            CGGAIPLCMVGEFNLPLDIIDRRVTKMKMISPSNIAVDIGRTLKEHEYIGMVRREVLDAY  153

Cre01.g050950.t1.2|C.reinhardtii  LRNRAQKLGANIVNGLFMRSEQ-QSAEGPFTIHYNSYEDGS-KMGKPATLEVDMIIGADG  235
AT1G74470.1|A.thaliana            LRERAEKSGATVINGLFLKMDHPENWDSPYTLHYTEYDGKTGATGTKKTMEVDAVIGADG  213

Cre01.g050950.t1.2|C.reinhardtii  ANSRIAKEIDAGEYDYAIAFQERIRIPDDKMKYYENLAEMYVGDDVSPDFYGWVFPKYDH  295
AT1G74470.1|A.thaliana            ANSRVAKSIDAGDYDYAIAFQERIRIPDEKMTYYEDLAEMYVGDDVSPDFYGWVFPKCDH  273

Cre01.g050950.t1.2|C.reinhardtii  VAVGTGTVVNKTAIKQYQQATRDRSKVKTEGGKIIRVEAHPIPEHPRPRRCKGRVALVGD  355
AT1G74470.1|A.thaliana            VAVGTGTVTHKGDIKKFQLATRNRAKDKILGGKIIRVEAHPIPEHPRPRRLSKRVALVGD  333

Cre01.g050950.t1.2|C.reinhardtii  AAGYVTKCSGEGIYFAAKSGRMAAEAIVEGSANGTKMCGEDAIRVYLDKWDRKYWTTYKV  415
AT1G74470.1|A.thaliana            AAGYVTKCSGEGIYFAAKSGRMCAEAIVEGSQNGKKMIDEGDLRKYLEKWDKTYLPTYRV  393

Cre01.g050950.t1.2|C.reinhardtii  LDILQKVFYRSNPAREAFVELCEDSYVQKMTFDSYLYKTVVPGNPLDDVKLLVRTVSSIL  475
AT1G74470.1|A.thaliana            LDVLQKVFYRSNPAREAFVEMCNDEYVQKMTFDSYLYKRVAPGSPLEDIKLAVNTIGSLV  453

Cre01.g050950.t1.2|C.reinhardtii  RSNALRSVNSK-SVNVSFGSKANEERVMAA*  504
AT1G74470.1|A.thaliana            RANALRREIEKLSV*----------------  467
```

1269

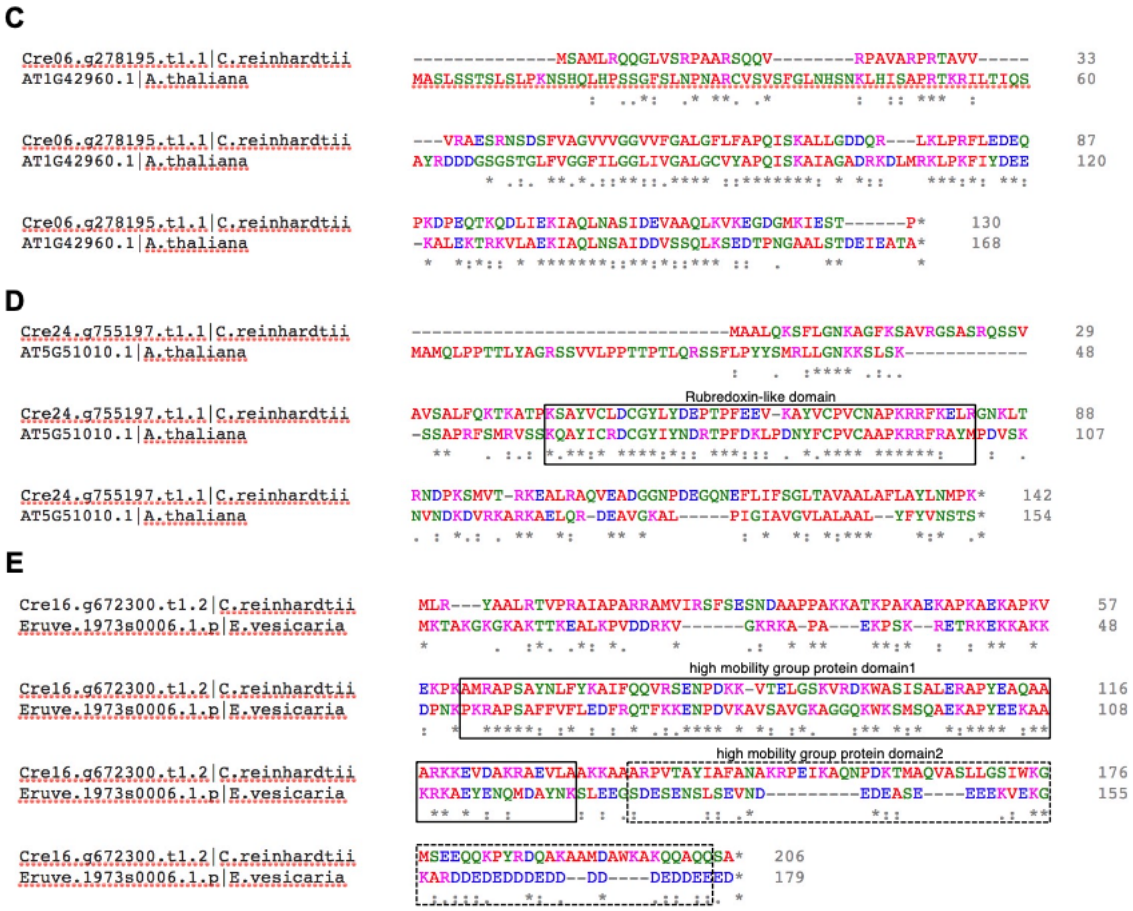

F

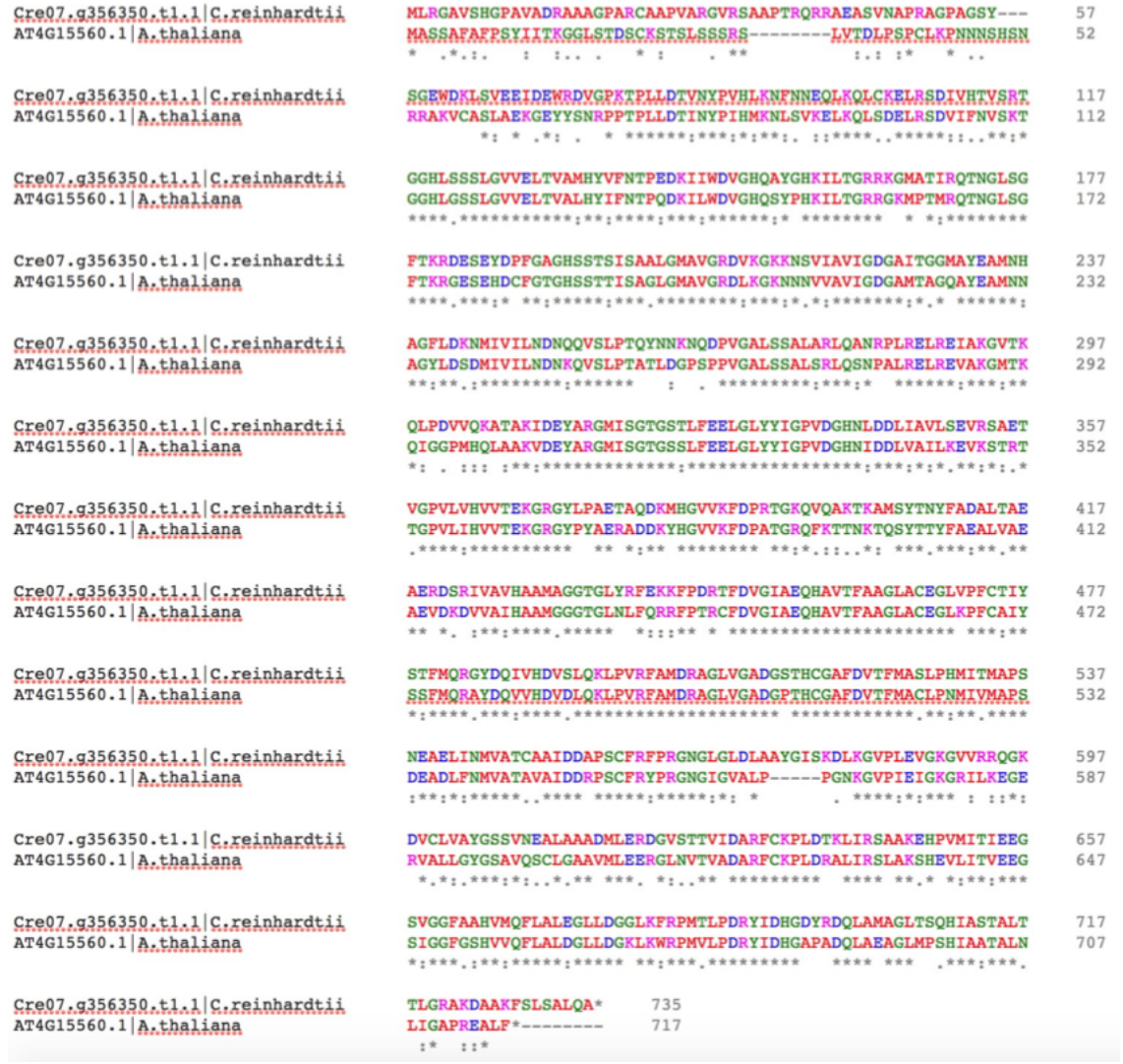

1272

1273

G

```
Cre03.g177350.t1.1|C.reinhardtii   MQSL-TARGLPSAAPIAPSARLHVPVLASRGLGCQRVPLKVCRVATGS-AGAAEGVKEDV   58
AT5G12470.1|A.thaliana             MAIASCFFCVPTPNTAISESNLTWPHIASFP-----RL--SSSSSFNGVISAKSISFN---   51
                                   *        :*:      .:.*  * :**       *:  . .   .*  :. : ..:

Cre03.g177350.t1.1|C.reinhardtii   PAVPVVPQLGGSDGNGVGKNNGGGGGGGG----GGGNNGDGKEP-----MDPKIVALLAA  109
AT5G12470.1|A.thaliana             RRVPITPVLSASSGNGGSDNNGGGLSGGGGGGDGGKNDGDGHGDEDRDRNRNEAMLLLKE  111
                                     **:.* *..*.*** ..***** .***     ** *:***:          : : **

Cre03.g177350.t1.1|C.reinhardtii   AGRSVDSFPADFKYGLLANKVTPEILQRYFSFEANFIAKLVWGIDGFRERLLADPSFFVK  169
AT5G12470.1|A.thaliana             SGIELESLPKDLAAAIEAGRIPGSVITRFLELQKSAVMRWLMQFGGFRERLLADDLFMAK  171
                                   :* .::*:* *:  .: *.::  .:: *::.:: . : : :  :.*********  *:.*

Cre03.g177350.t1.1|C.reinhardtii   LGIEIGIGVVMKITAEYTKRQENFAKEADFVFANTLMAIIADFMLTWLPAPTLSYRPRAT  229
AT5G12470.1|A.thaliana             LAMECGVGIFTKTAAEYERRRENFFNELEVVFADVAMAIIADFMLVYLPAPTVSLRPPLA  231
                                   *.:* *:*:. * :*** :*:*** :* :.***:. *********.:*****:* **  :

Cre03.g177350.t1.1|C.reinhardtii   ASGNALVNFFASCPDNAFQKVPPGMEPFSLSQRLGAILRNGSKLLGVGFCASLIGVGVTN  289
AT5G12470.1|A.thaliana             LTAGGISKFFHNCPDNAFQVALSG-TSYTLLQRLGAITRNGAKLFAVGTTSSLVGTAITN  290
                                    :...: :** .******* .  *   ::* ****** ***:**:.**  :**:*..:**

Cre03.g177350.t1.1|C.reinhardtii   SLLFVRQQLDPTMAPPNAPQNVLATSAAYGVYMSVSSNLRYQIIAGIVEERGIEVLFKGN  349
AT5G12470.1|A.thaliana             AFIKARKAVDQNSEGEVETVPIVSTSVAYGVYMAVSSNLRYQIVAGVIEQRLLEPMLHQH  350
                                   ::: .*: :* .          :::**.******:*********:**::*:* :* ::: :

Cre03.g177350.t1.1|C.reinhardtii   HQLCHLLSFVARTGNTFLGSLLWVDFVRLCGMQKASAKPAEAH*392
AT5G12470.1|A.thaliana             KLALSALCFAVRTGNTFLGSLLWVDYARLIGIQKSH*-------386
```

H

```
Cre03.g175800.t1.1|C.reinhardtii   MPAFHVAWRAARSLASRRHDANSLITIGRRRSHLQLCSHTSAAAPGSATAAPATDASEAA   60
AT1G50000.1|A.thaliana             ------------------------------------------------------------   0

Cre03.g175800.t1.1|C.reinhardtii   SNAAWGEQAFSALQKKATSRLHRFYVPQPLGPTPEPATLEALLGVAPSTTSTSAASTSTR  120
AT1G50000.1|A.thaliana             -------------------------MMRALAAASRP-----LFSDLPSLVRSWLPTSSFK   30
                                                           : : *. : .*     *:.  ** . :   ::* :

Cre03.g175800.t1.1|C.reinhardtii   SGSSGSSSSGGGSGSQAAGPAADAAPGKRRKAGSSTAAAAAASATADAATAAWAGSVAAG  180
AT1G50000.1|A.thaliana             SFA-----------TVSSSPPSDLNLRNQSRG---------------GLPRFFSDDLPSR   64
                                   * :           : ::.* :*    :: :.               .    ::..: :

Cre03.g175800.t1.1|C.reinhardtii   VPATLVLEGEEARHAARALRLAAGDRVELCDGRGNVAVGVVTGTDKQRVWVSTEGAASHQ  240
AT1G50000.1|A.thaliana             KGGVVRVQGSEFWHMAKVLRLKQEDRVELFNGKGGLVEGCIQSIDKTGVDFIAQEDQKVI  124
                                     ..: ::*.*  * *:.***    ***** :*:*.:. * : . **  * . ::   .

Cre03.g175800.t1.1|C.reinhardtii   RWSGPRWVLAVACTTLKGGRAEWLVEKATELGAFMLVPLVTERSQAGGKAKFRTSRSGGG  300
AT1G50000.1|A.thaliana             LPQGMQWQVFAAFGTLKGGRADWLIEKCTELGASSVTPLLTERSPIISE-----------  173
                                     .* :* : .*  *******:**:**.*****  :.**:****   .:

Cre03.g175800.t1.1|C.reinhardtii   GGGGGSDLDWGSDGGGGDDYQPGRLERVAIAATKQSLRPHALALVPPTPLADLLPLVRRA  360
AT1G50000.1|A.thaliana             -------------------NRVDRLERVSFAAAKQCQRLHQMVLNPPIKFGTLLDHILK-  213
                                                     : .*****::**:**. * * :.* **  :. **  : :

Cre03.g175800.t1.1|C.reinhardtii   AAGEGGEAAAASRAAGGAGGGGEGSVVGGVTQPGFSLVAVAGAPPLMSVLQQLRSGSGVG  420
AT1G50000.1|A.thaliana             --------------------------------SKLCLVATAEAKPLLNAV----------  231
                                                                   :.***.* * **:..:

Cre03.g175800.t1.1|C.reinhardtii   ASTDPGGCADSNPVAEAPPSASSPAGQGGAAAAASAAAAAAAAAAAVASNSPVRVLFVGP  480
AT1G50000.1|A.thaliana             ------------------------------------------NSSAKESSGLLIVGP  246
                                                                               :::.   :*:***

Cre03.g175800.t1.1|C.reinhardtii   EGDFTPAELAALVEAGAQPVGLGVNRLRTETAAIGLLSACLFSD*------   524
AT1G50000.1|A.thaliana             EGDFTKKEVEMMLEAGGTAVGLGPHRLRVETATIALLATLVMWSDSQEMI*   296
                                   *****  *:  ::***.  **** :***.***:*.**:: :: .
```

I

```
Cre09.g394550.t1.2|C.reinhardtii  ------------------------------------------------------MAA   3
AT1G10700.1|A.thaliana            MAAISPANATTAASLSLPQFSSTSSSLSSSSSPSFLNFKTASVSNRCIKCGVRSLENHSG  60
                                                                                          :.

Cre09.g394550.t1.2|C.reinhardtii  QNLAPALSTGEDFRIT---------TNIEATQIPAALRKDCVLFYTPDTEELAQKVAQQA  54
AT1G10700.1|A.thaliana            HRSLDFLSNGDPISLINPNSSSPITMAAATSESGSKSSKRVCLFHSDETRDLAERIV-AK  119
                                  :.    **.*: : :               :::  :   *   **:: :*.:**:::.

Cre09.g394550.t1.2|C.reinhardtii  GGAITLGRIKWKKFADGFPDLFVENATSIRNRHVAFLASFTNPTVIFEQISVIYALPRLF  114
AT1G10700.1|A.thaliana            SDCIELRSINWKKFDDGFPNLFIQNAQGIRGQHVAFLASFSSPAVIFEQLSVIYALPKLF  179
                                  ...* *  *:**** ****:**::** .**.:********:.*:*****:*******:**

Cre09.g394550.t1.2|C.reinhardtii  VSSFTLVLPFFPTGTMERVETEGDIATANTLARLLSNVPPSRGGPTSLVIFDIHALQERF  174
AT1G10700.1|A.thaliana            VSSFTLVLPFFPTGTSERMEDEGDVATAFTLARILSNIPTSRGGPTSLVTFDIHALQERF  239
                                  *************** **:* ***:*** ****:***:* ********* **********

Cre09.g394550.t1.2|C.reinhardtii  YFGDAVLPLFESGVPLLLERLRQLPDRDSITIAYPDEGAWKRFHYQFKSEGYPEVICTKV  234
AT1G10700.1|A.thaliana            YFGDTILPCFESGIPLLKSRLQSLPDSDNISIAFPDDGAWKRFHKQL--QHYPTIVCNKV  297
                                  ****::** ****:*** .**:.*** *.*:**:**:******* *:  : ** ::*.**

Cre09.g394550.t1.2|C.reinhardtii  RDGSKRIVRLKEGEPKDRHVVIVDDLVQSGGTLIECHALLASLGAKHVSAFVTHGVFPNM  294
AT1G10700.1|A.thaliana            RMGDKRIVRIKEGDAEGRHVVIVDDLVQSGGTLIECQKVLAAHGAAKISAYVTHGIFPRS  357
                                  * *.*****:***: :.******************: :**: ** ::**:****:**.

Cre09.g394550.t1.2|C.reinhardtii  SWVKFRADLGNGAQDGFRYFWLSDSCPQTVRDVRSKAPFEVLSLAGPIAAALQI*    348
AT1G10700.1|A.thaliana            SWKRFKLDTKGDPAEGLSYFWITDSCGMTVKEVMNKPPFEVLSLAGSIASALQV*    411
                                  ** :*: *  ..  :*: ***::***  **::* .* ********* **:***:*
```

J

```
Cre03.g175850.t1.1|C.reinhardtii  MLANLRSLPYCRRCVLLQSAAAFVQAAATKGHIEAGGQVLRLAHNSSRSGSGLAGFGGS-  59
AT2G41460.1|A.thaliana            -MNNVLQFG-------LQSSAIYVA------------KFLVVPLRSLRVGSSFVGVGVGT  40
                                   : *: .:         ***:* :*             :.* :  .* * **.:.*.* .

Cre03.g175850.t1.1|C.reinhardtii  -------------WGVSAA----CDQPRRSSTLTARALGSASMKDDGTSAAK---EEQAV  99
AT2G41460.1|A.thaliana            RSFNKRLMSNATAFSINNSKRKELKIPGAAIDQNCHQMGSDTDRDEMGTLQDDRKEIEAM  100
                                              :.:. :     . *  :   ..: :** : :*:  :  .   * :*:

Cre03.g175850.t1.1|C.reinhardtii  AAEPAA-------AAPRGRGRKTPAGA--GAEGAAATAKKSPAKGRG-----KKAAAAKEP  146
AT2G41460.1|A.thaliana            TVQELRSTLRKLGVPVKGRKQELISTLRLHMDSNLPDQKETSSSTRSDSVTIKRKISNRE  160
                                  :.:          .  :** ::  :       :.     *:: :. *.     *   ::.

Cre03.g175850.t1.1|C.reinhardtii  EPESEEAAASEGTAEGASEEAAPKRAAK--RAKTGAK-----TKTDAAGGEEEAQPKPAR  199
AT2G41460.1|A.thaliana            EPTEDECTNSEAYDIEHGEKRVKQSTEKNLKAKVSAKAIAKEQKSLMRTGKQQIQSKEET  220
                                  ** .:*.: **.     .*: . : : *  :**..**      *:    *::: * *

Cre03.g175850.t1.1|C.reinhardtii  KARA--TPAAKEAGAEAGAQAKPKAKRGAKEPAADLVQYTA-ALRKPAPPAGSTPLNILS  256
AT2G41460.1|A.thaliana            SSTISSELLKTEEIISSPSQSEPWTVLAHKKPQKDWKAYNPKTMRPPPLPEGTKCVKVMT  280
                                  .:        .*   .: :*::* :  . *:*  *   *.  ::* *  * *:. :::::

Cre03.g175850.t1.1|C.reinhardtii  WNVAGLRALLKKTPDAVSSLVSREAAEVVCLQEHKLQANHQKEVEELLGLQGWHHAWAFS  316
AT2G41460.1|A.thaliana            WNVNGLRGLLKFESFSALQLAQRENFDILCLQETKLQVKDVEEIKKTLIDGYDHSFWSCS  340
                                  *** ***.***    :. .*..**  :::**** ***.:. :*::: *     *  *: *

Cre03.g175850.t1.1|C.reinhardtii  TAKLGYSGVSVHTRSPPLSVVVGLGHGGPGAADPDPEHEGEGRVVTVELEGLFLVNVYVP  376
AT2G41460.1|A.thaliana            VSKLGYSGTAIISRIKPLSVRYGTGLSG---------HDTEGRIVTAEFDSFYLINTYVP  391
                                  .:******.:: :*  ****  * * .*         *: ***:**.*::.::*:*.***

Cre03.g175850.t1.1|C.reinhardtii  NSGEGLKRLDYRVGRWDGAFAAFLQGLQARGKPVVVTGDLNCAHKEIDIHAPKTNLKSAG  436
AT2G41460.1|A.thaliana            NSGDGLKRLSYRIEEWDRTLSNHIKELE-KSKPVVLTGDLNCAHEEIDIFNPAGNKRSAG  450
                                  ***:*****.**: .** ::: .:: *: :.****:********:****. *  * :***

Cre03.g175850.t1.1|C.reinhardtii  FTPEERESFGRLLLAEAGLADTFRRLYPDTVAYTYFTRRFNCREKNKGWRLDYFLTSESM  496
AT2G41460.1|A.thaliana            FTIEERQSFGANLL-DKGFVDTFRKQHPGVVGYTYWGYRHGGRKTNKGWRLDYFLVSQSI  509
                                  ** ***:***  ** : *:.****: :*..*.***:  *.. *:.**********.*:*:

Cre03.g175850.t1.1|C.reinhardtii  MPPELQQGGEGAAAAAGPASAWAVYDTWIMQDVYGSDHLPLGLTCVRKAAA*   547
AT2G41460.1|A.thaliana            AA--------------------NVHDSYILPDINGSDHCPIGLILKL*----   536
```

1276

1277

K

Figure S3. Amino acid alignment of conserved Chlamydomonas proteins with their homologs in land plants.

Related to Figure 2-4

The alignment was performed using the Clustal Omega. The colors indicate amino acids with different biochemical properties. (A) Cre07.g344550 and AT4G34200; (B) Cre01.g050950 and AT1G74470; (C) Cre06.g278195 and AT1G42960; (D) Cre24.g755197 and AT5G51010; (E) Cre16.g672300 and Eruve.1973s006; (F) Cre07.g356350 and AT4G15560; (G) Cre03.g177350 and AT5G12470; (H) Cre03.g175800 and AT1G50000; (I) Cre09.g394550 and AT1G10700; (J) Cre03.g175850 and AT2G41460; (K) Cre12.g495951 and AT5G13120.

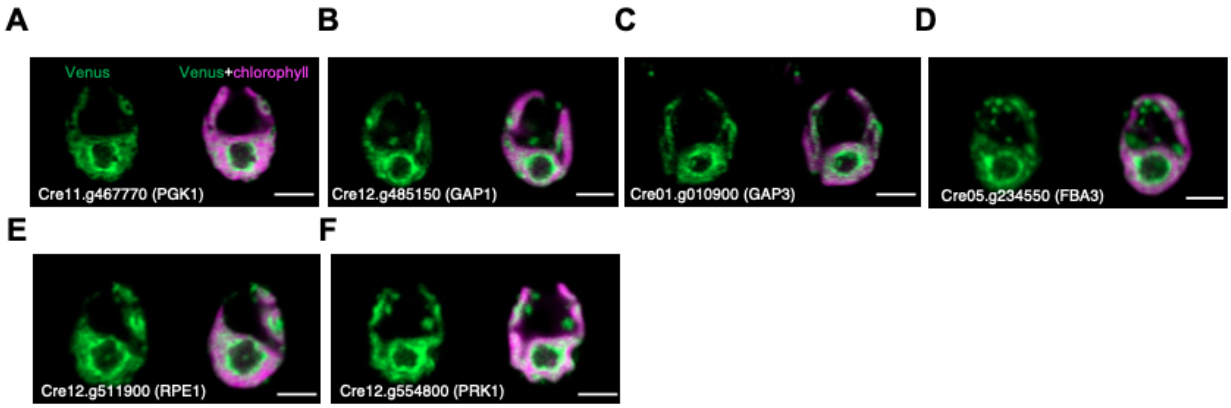

Figure S4. The Calvin-Benson cycle enzymes showed enrichment around pyrenoid.

Related to Figure 4

(A-F) Representative images of Cre11.g467770 (PGK1), Cre12.g485150 (GAP1), Cre01.g010900 (GAP3), Cre05.g234550 (FBA3), Cre12.g511900 (RPE1), and Cre12.g554800 (PRK1) showing enrichment in the stroma around pyrenoid. All scale bars are 5 μm.

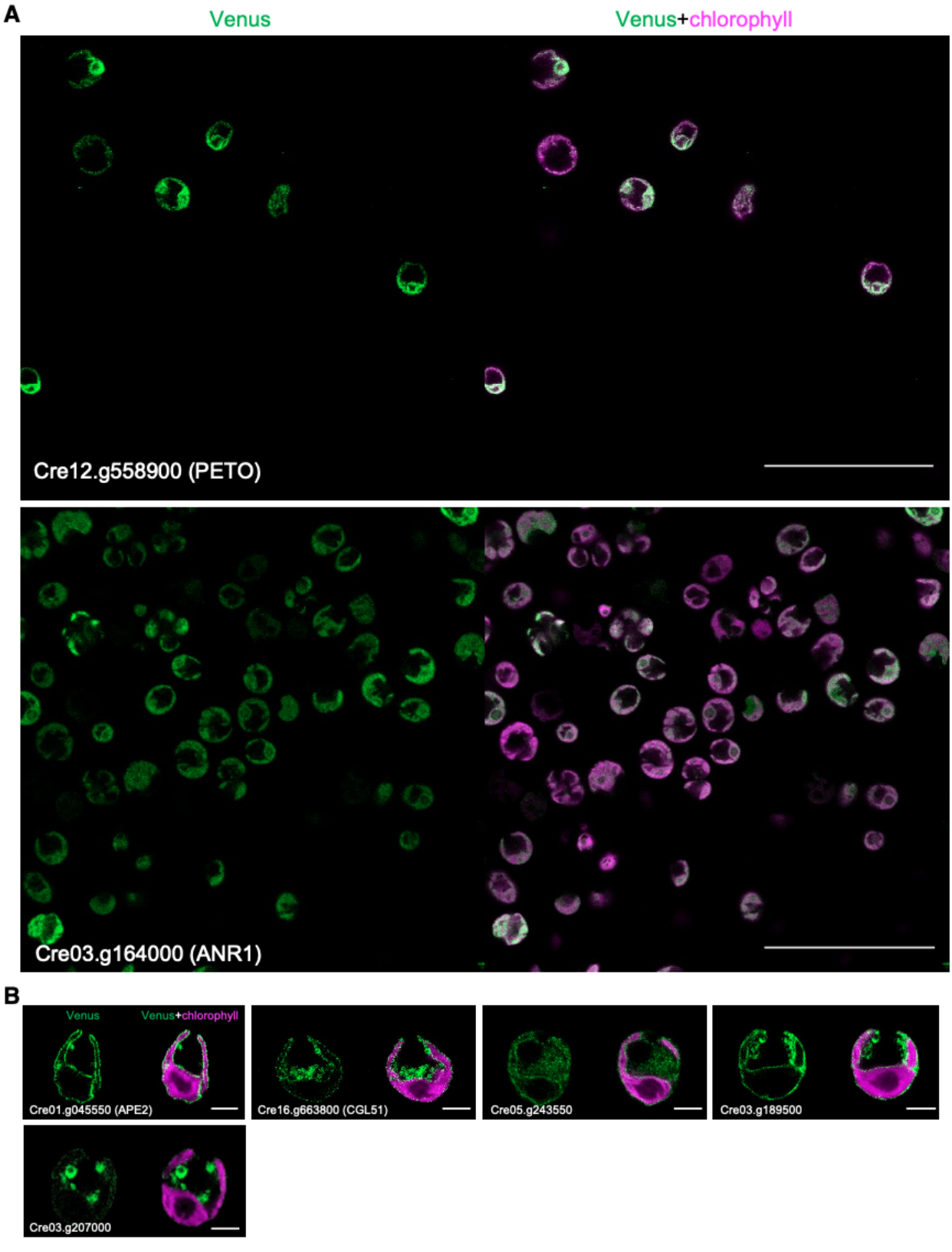

1296

1297

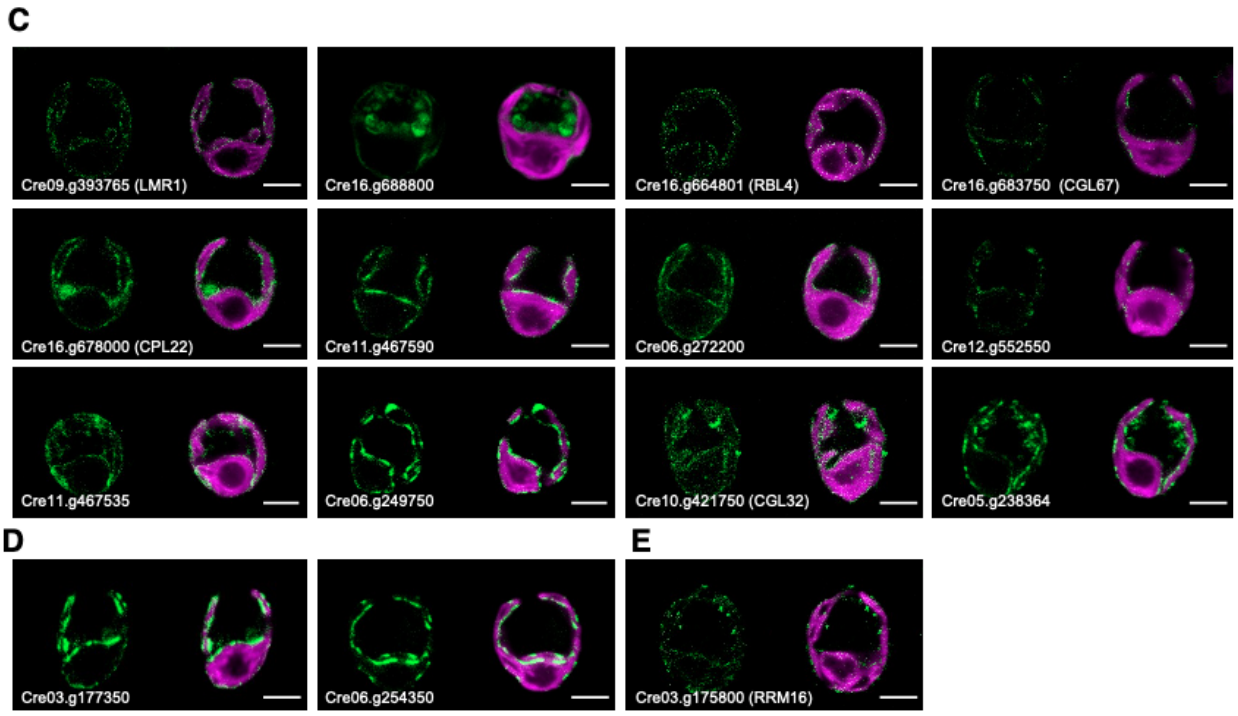

Figure S5. PETO showed different localization patterns from ANR1 and the diverse localizations of proteins localized to chloroplast envelope.

Related to Figure 5

(A) Representative localization images of PETO and ANR1. Scale bars, 50 μm.

(B) Representative images of proteins homogeneously localized throughout the chloroplast envelope. Scale bars, 5 μm.

(C) Representative images of proteins localized to patches along the chloroplast envelope. Scale bars, 5 μm.

(D) Representative images of proteins localized to nucleus-facing portion of the chloroplast envelope. Scale bars, 5 μm.

(E) Representative images of protein localized as punctate dots along the chloroplast envelope. Scale bars, 5 μm.

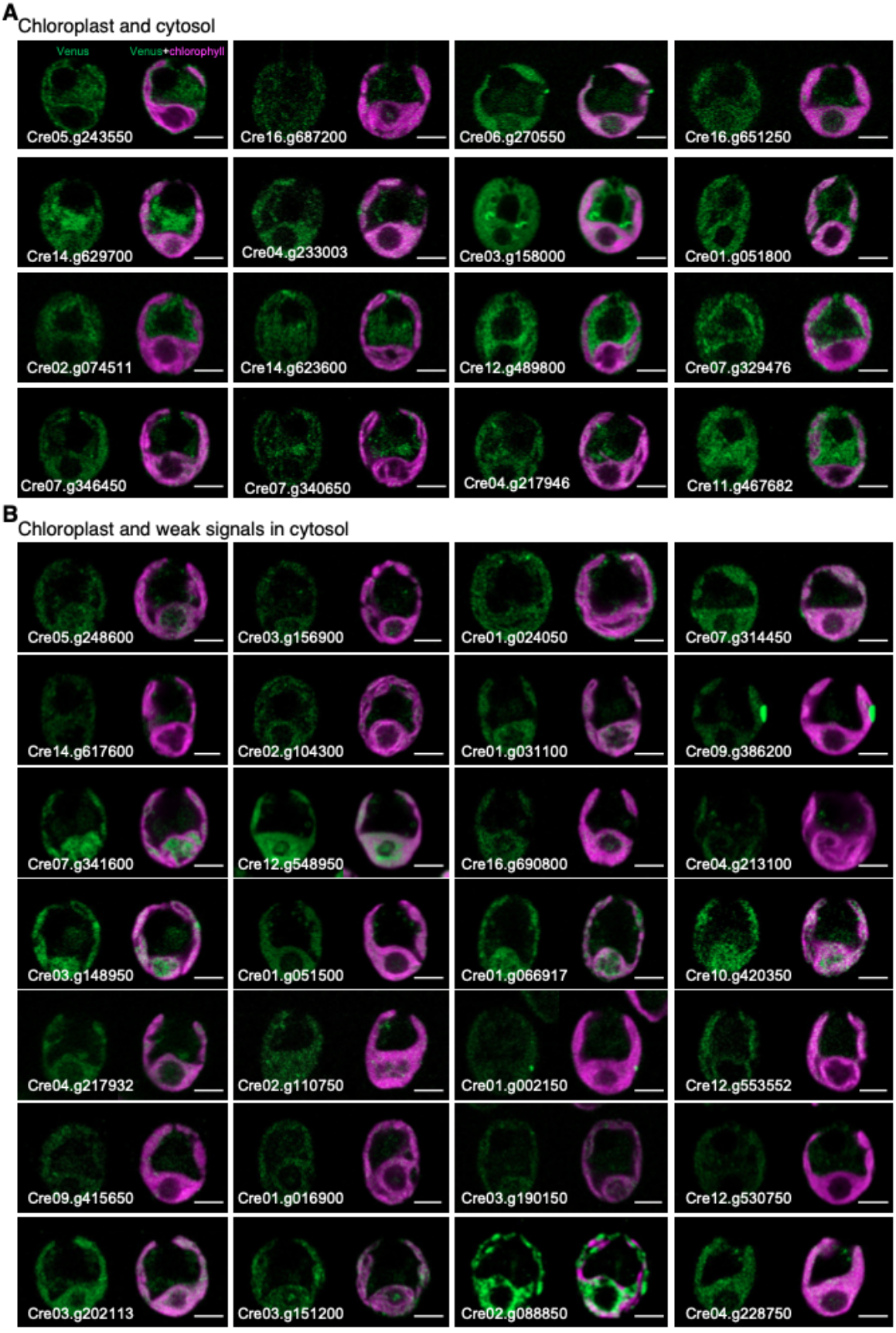

1313

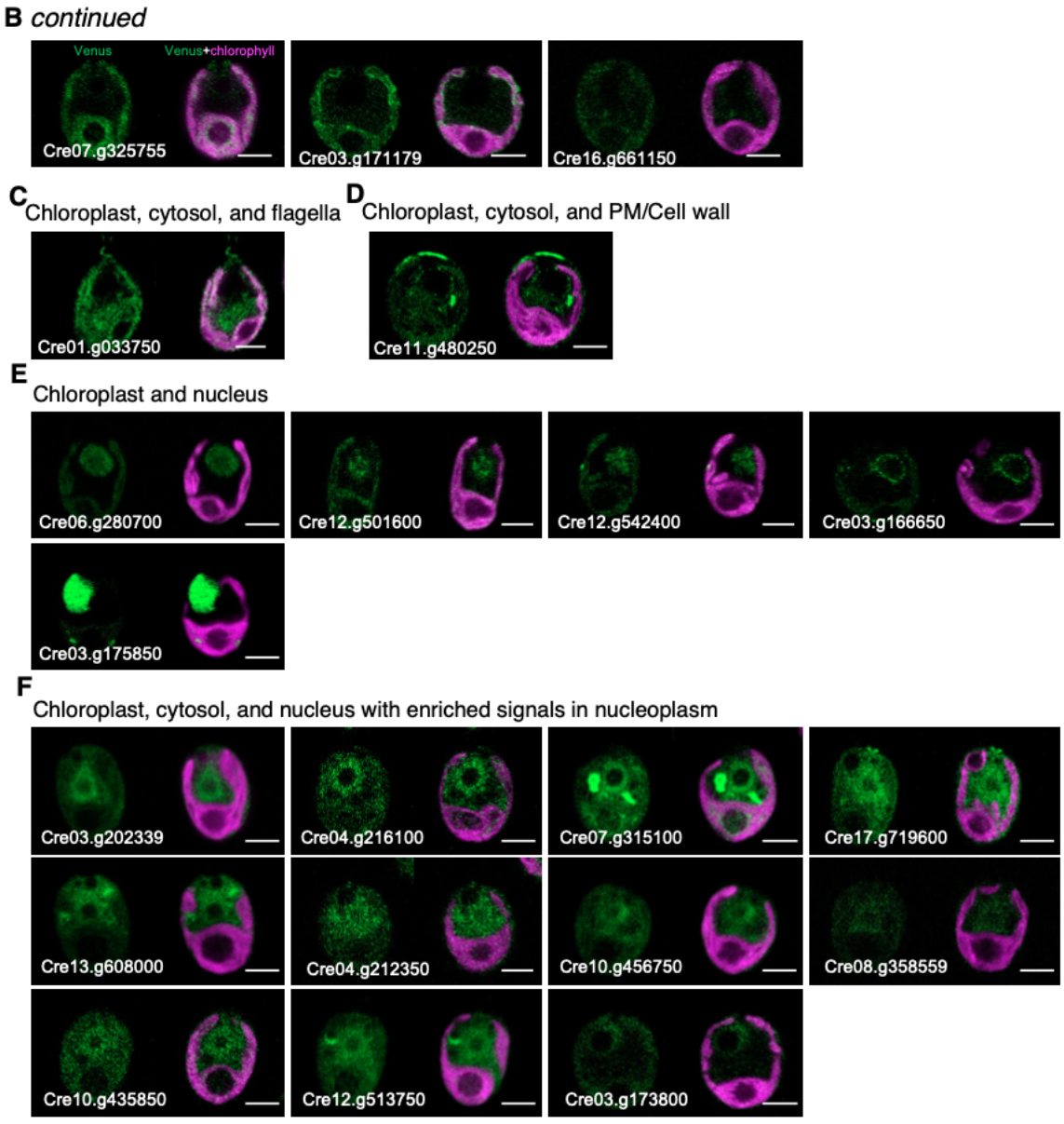

1314

1315

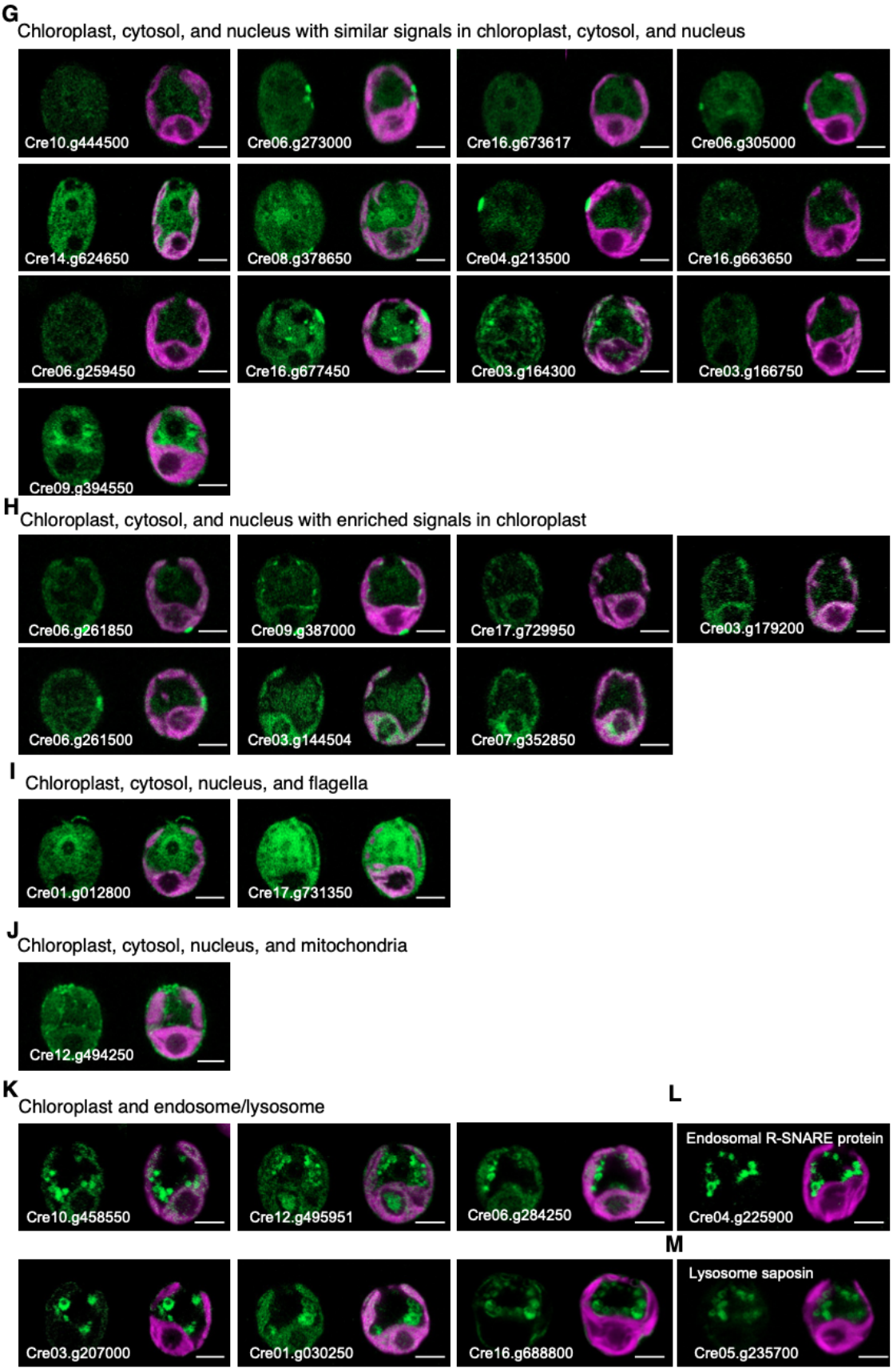

1316

N

Chloroplast and crescent structures in cytoplasm

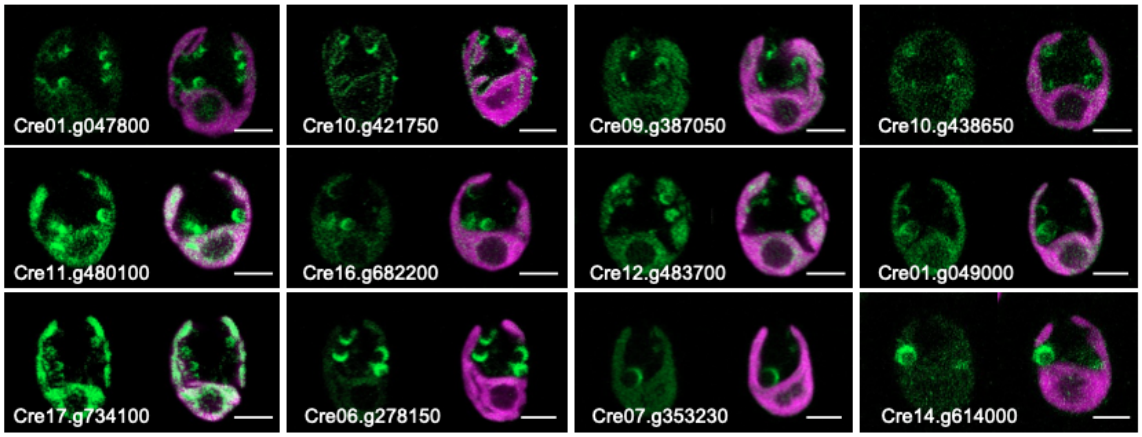

O

Chloroplast and one or two small puncta in cytoplasm

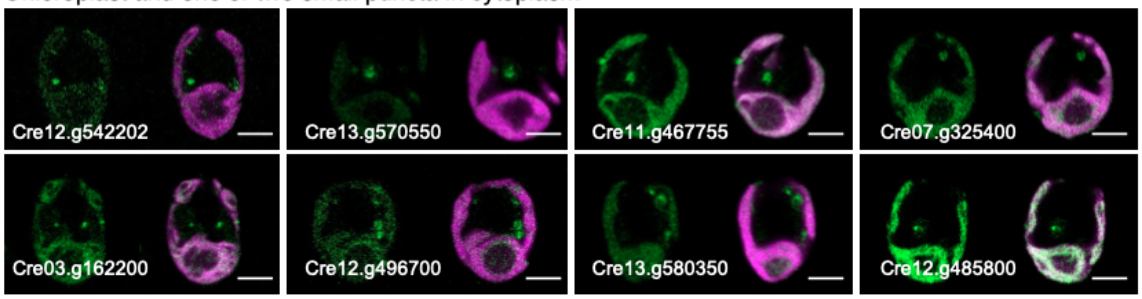

P

Chloroplast and a few medium puncta in cytoplasm

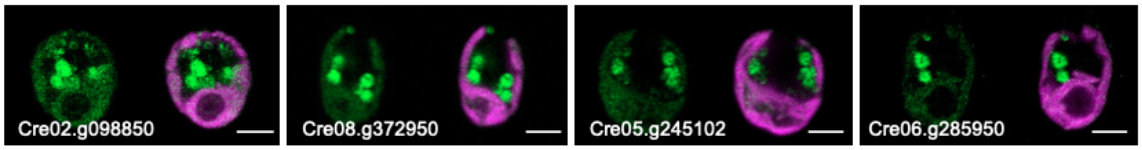

Q

Chloroplast and a few large puncta/vesicles in cytoplasm

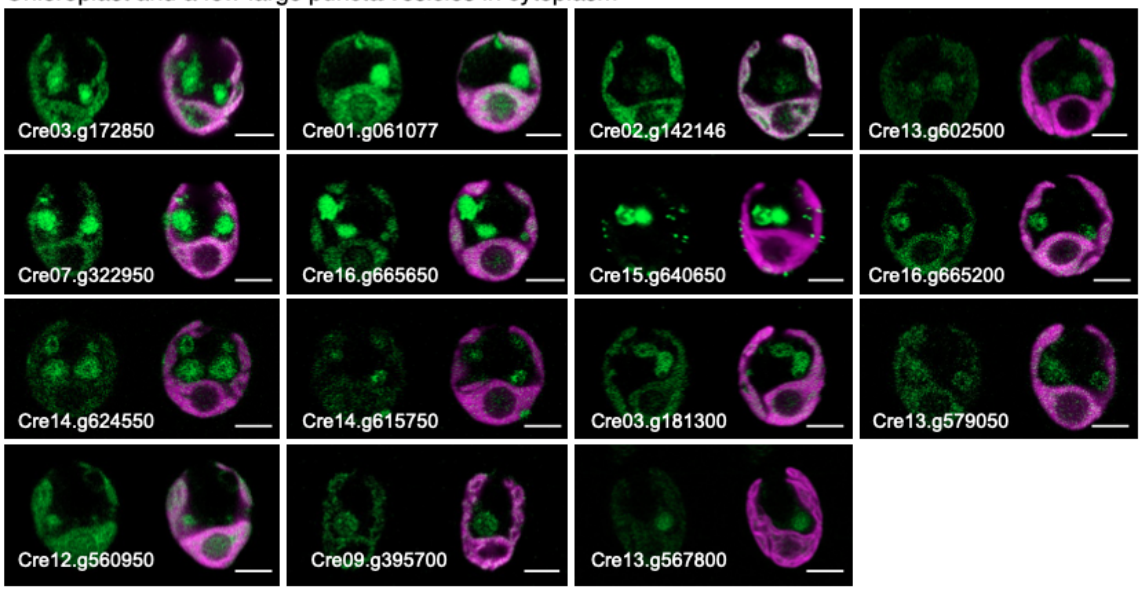

1317

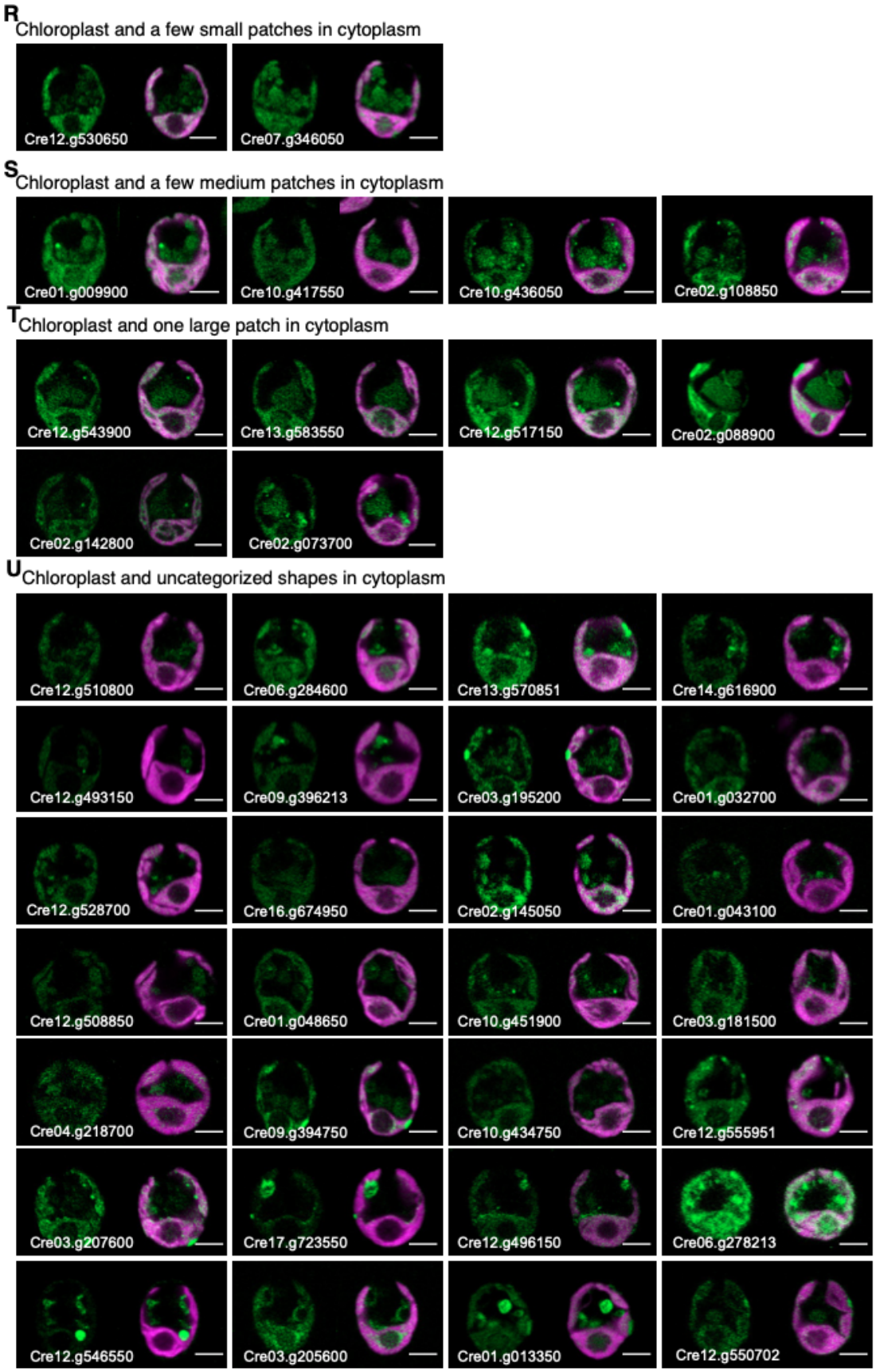

1318

U *continued*

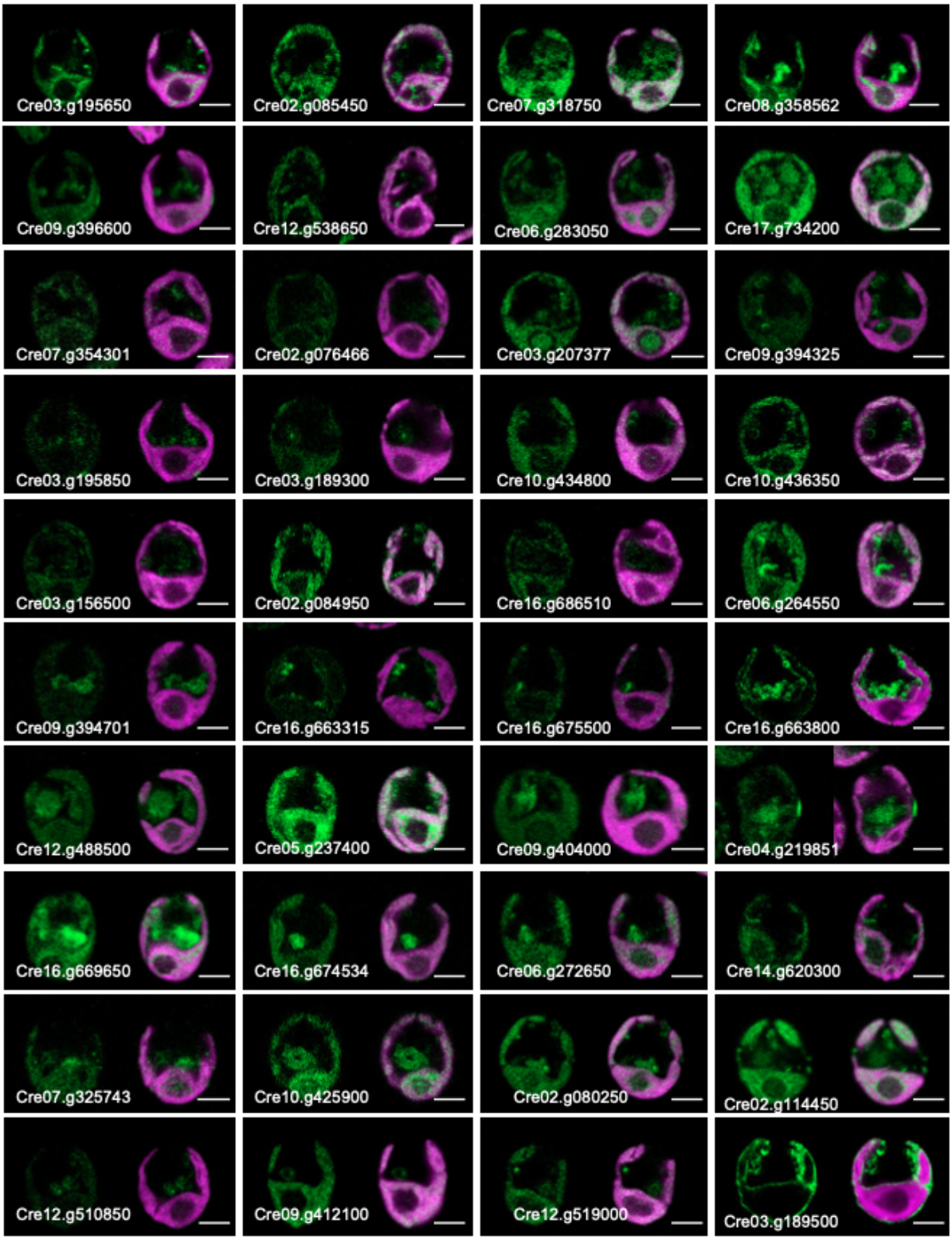

1319

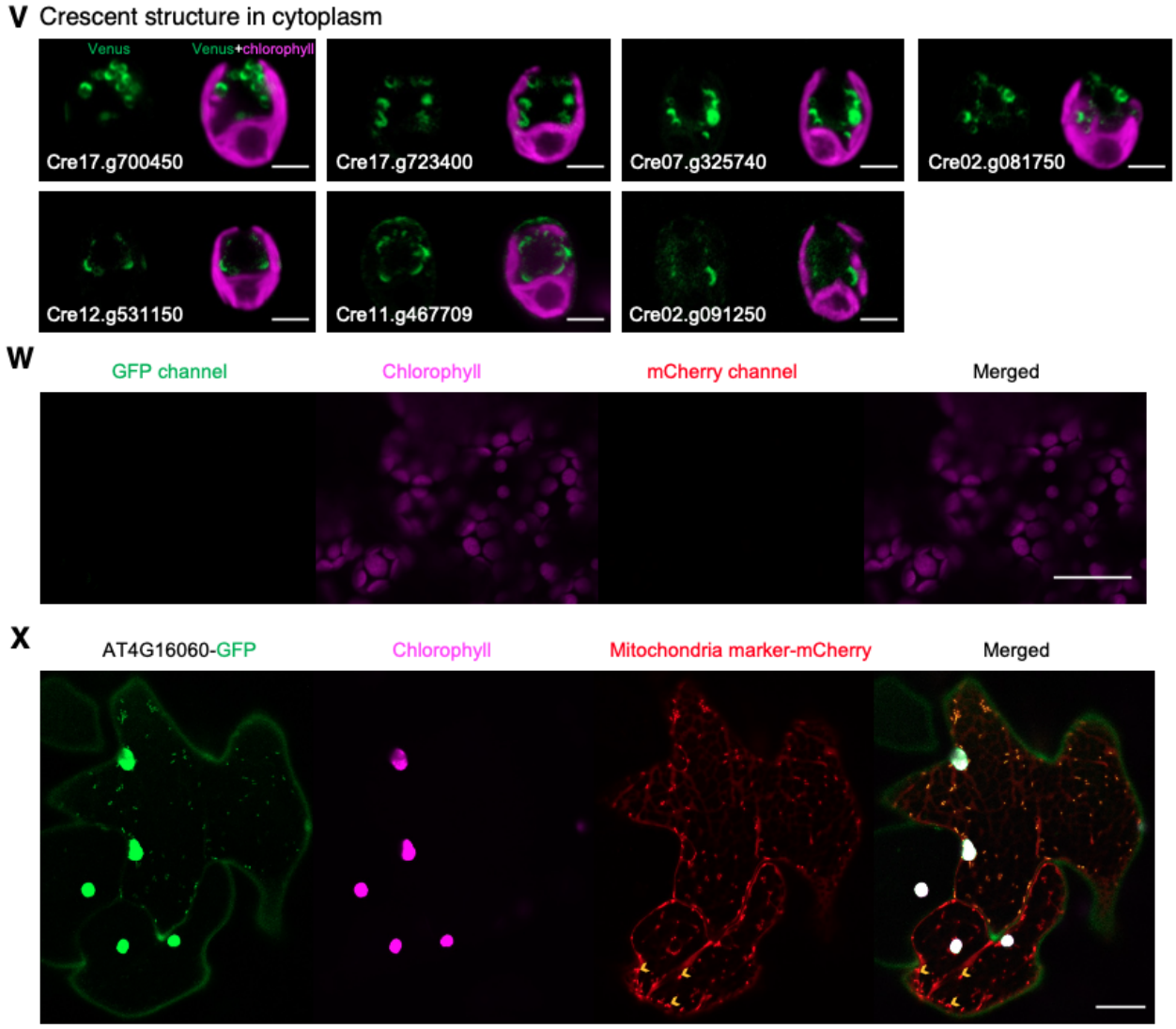

Figure S6. Diverse localizations of proteins localized to chloroplast and other organelles.

Related to Figure 6

(A) Representative images of proteins dual-localized to chloroplast and cytosol.

(B) Representative images of proteins dual-localized to chloroplast and weak signals in cytosol.

(C) Representative images of protein localized to chloroplast, cytosol, and flagella.

(D) Representative images of protein localized to chloroplast, cytosol, and PM/Cell wall.

(E) Representative images of proteins dual-localized to chloroplast and nucleus.

(F) Representative images of proteins localized to chloroplast, nucleus, and cytosol with enriched fluorescence signals in nucleoplasm.

(G) Representative images of proteins localized to chloroplast, nucleus, and cytosol with similar fluorescence signals between chloroplast and nucleus.

(H) Representative images of proteins localized to chloroplast, nucleus, and cytosol with enriched fluorescence signals in chloroplast.

(I) Representative images of proteins localized to chloroplast, nucleus, cytosol, and flagella.

(J) Representative images of proteins localized to chloroplast, nucleus, cytosol, and mitochondria.

(K) Representative images of proteins dual-localized to chloroplast and endosomes/lysosomes (many small puncta or vesicles in cytoplasm).

(L) Representative images of endosomal R-SNARE protein localized to endosomes.

(M) Representative images of lysosome saposin localized to lysosomes.

(N) Representative images of proteins dual-localized to chloroplast and crescent structures in the cytoplasm.

(O) Representative images of proteins dual-localized to chloroplast and one or two small puncta in the cytoplasm.

(P) Representative images of proteins dual-localized to chloroplast and a few medium puncta in the cytoplasm.

(Q) Representative images of proteins dual-localized to chloroplast and a few large puncta/vesicles in the cytoplasm.

(R) Representative images of proteins dual-localized to chloroplast and a few small patches in the cytoplasm.

(S) Representative images of proteins dual-localized to chloroplast and a few medium patches in the cytoplasm.

(T) Representative images of proteins dual-localized to chloroplast and one large patch in the cytoplasm.

(U) Representative images of proteins dual-localized to chloroplast and uncategorized shapes in the cytoplasm.

(V) Representative images of proteins exclusively to the crescent structures in the cytoplasm. All scale bars in (A)-(V) are 5 μm.

(W) Representative images of chloroplast in the tobacco leaf cells without infiltration with Agrobacterium tumefaciens.

(X) Representative images of mitochondria mCherry marker (CD3-991) in the tobacco leaf cell without GFP expression. The yellow arrows indicate mitochondria. All scale bars in (W) and (X) are 20 μm.

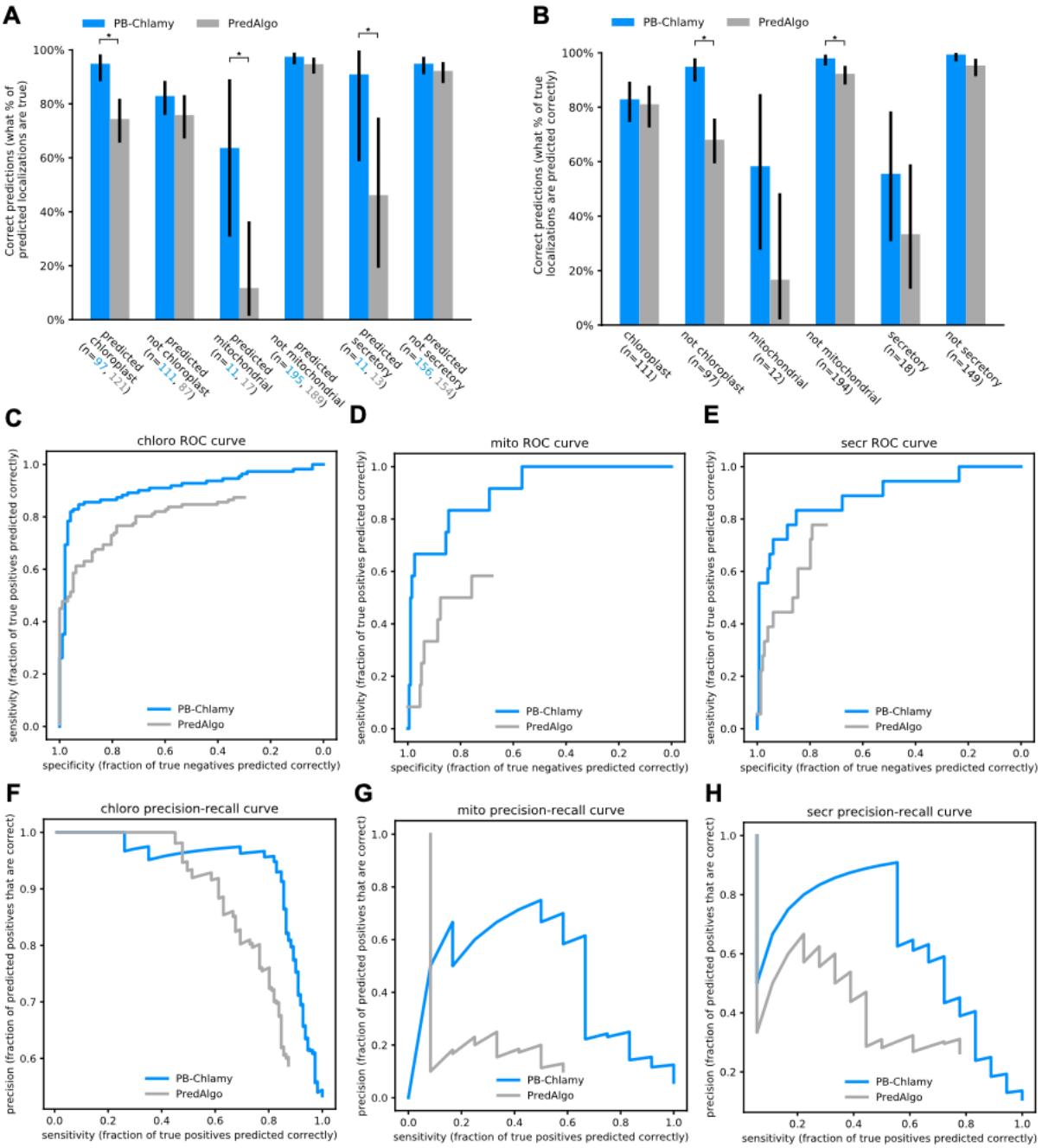

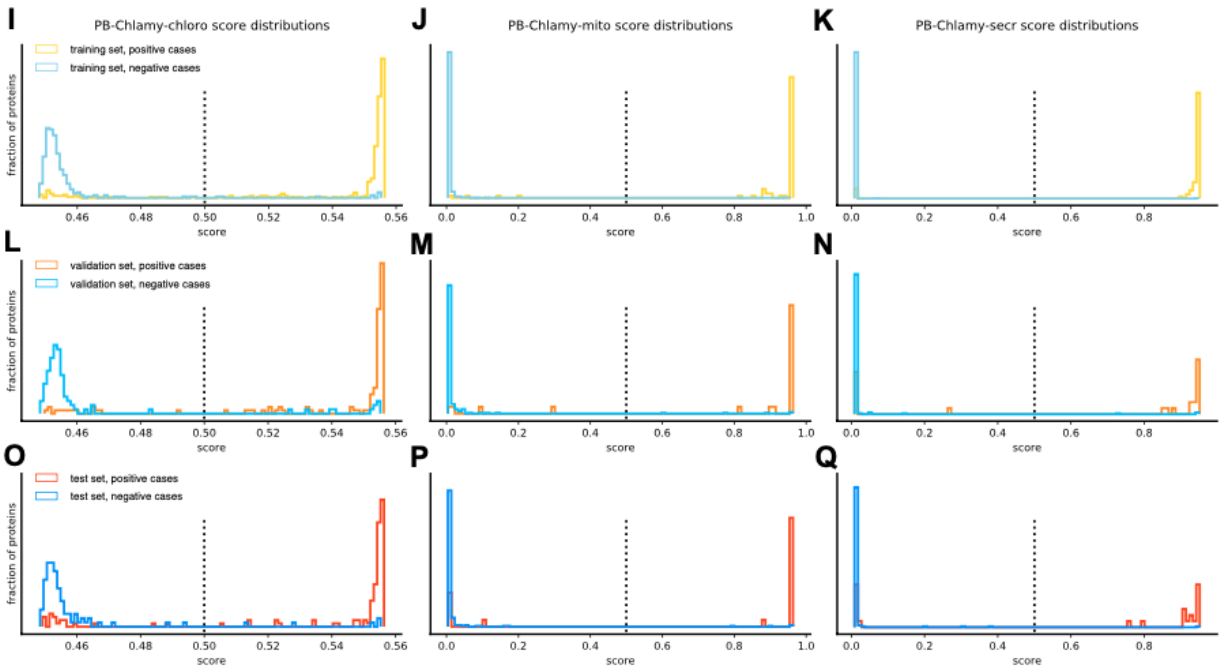

Figure S7. PB-Chlamy reliably predicts Chlamydomonas protein localizations.

Related to Figure 7

(A) The percent of predicted positive and negative protein localizations that are correct, for PB-Chlamy and PredAlgo. Error bars represent binomial 90% confidence intervals. The number of proteins varies between PB-Chlamy and PredAlgo, as the two programs predict different numbers of positive and negative proteins. The p-values comparing PB-Chlamy and PredAlgo (using Fisher's exact test) are: chloroplast 0.000036, non-chloroplast 0.28, mitochondrial 0.010, non-mitochondrial 0.20, secretory 0.033, non-secretory 0.36. The asterisk * indicates $p<0.05$.

(B) The percent of true positive and negative protein localizations that were correctly classified by PB-Chlamy and PredAlgo. Error bars represent binomial 90% confidence intervals. The p-values comparing PB-Chlamy and PredAlgo using Fisher's exact test are: chloroplast 0.86, non-chloroplast 0.0000016, mitochondrial 0.089, non-mitochondrial 0.016, secretory 0.31, non-secretory 0.067. The asterisk * indicates $p<0.05$.

(C-E) ROC curves comparing PB-Chlamy and PredAlgo for each localization category. PredAlgo uses a static score cutoff for predictions, therefore ROC curves terminate at this cutoff and do not reach a sensitivity of 1.

(F-H) Precision-recall curves comparing PB-Chlamy and PredAlgo for each localization category.

(I-Q) The raw PB-Chlamy prediction score distributions, normalized, for each chloroplast (I, L, O), mitochondrial (J, M, P) and secretory (K, N, Q), showing the training (I, J, K), validation (L, M, N) and test (O, P, Q) sets, with true positives and true negatives overlaid. The dotted bar at 0.5 is the cutoff for positive vs negative predictions.

Table S1. List of the 5,784 target genes that we attempted to clone and localize in this study. Related to Figure 1 and Star Methods.

Table S2. Localizations of 1,032 proteins localized in this study. Related to Figure 1.

Table S3. Number of proteins exhibiting each of the 141 distinct localization patterns. Related to Figure 1.

Table S4. Our localizations match previously-published localizations for 27 of the 28 previously-localized Chlamydomonas proteins represented in our study. Related to Figure 1.

Table S5. Whole list of protein-protein interactions identified in this study. Related to Figure 1-6.

Table S6. Links for viewing the data on Chlamylibrary.org and information for ordering plasmids and strains from the Chlamydomonas Resource Center. Related to Star Methods.

Table S7. Predicted localizations of Chlamydomonas proteins (genome v5.6) by PB-Chlamy. Related to Figure 7.

(All tables in the attached excel spreadsheet)

Movie S1. The puncta of Cre15.g640650 show rapid movement. Related to Figure 2.

REFERENCES

Aksoy, M., Pootakham, W., and Grossman, A.R. (2014). Critical Function of a *Chlamydomonas reinhardtii* Putative Polyphosphate Polymerase Subunit during Nutrient Deprivation. Plant Cell *26*, 4214–4229. https://doi.org/10.1105/tpc.114.129270.

Allmer, J., Naumann, B., Markert, C., Zhang, M., and Hippler, M. (2006). Mass spectrometric genomic data mining: Novel insights into bioenergetic pathways in *Chlamydomonas reinhardtii*. Proteomics *6*, 6207–6220. https://doi.org/10.1002/pmic.200600208.

Armbrust, E.V., Ferris, P.J., and Goodenough, U.W. (1993). A mating type-linked gene cluster expressed in Chlamydomonas zygotes participates in the uniparental inheritance of the chloroplast genome. Cell *74*, 801–811. https://doi.org/10.1016/0092-8674(93)90460-8.

Atteia, A., Adrait, A., Brugiere, S., Tardif, M., van Lis, R., Deusch, O., Dagan, T., Kuhn, L., Gontero, B., Martin, W., et al. (2009). A proteomic survey of *Chlamydomonas reinhardtii* mitochondria sheds new light on the metabolic plasticity of the organelle and on the nature of the -proteobacterial mitochondrial ancestor. Mol. Biol. Evol. *26*, 1533–1548. https://doi.org/10.1093/molbev/msp068.

Behrenfeld, M.J., Randerson, J.T., McClain, C.R., Feldman, G.C., Los, S.O., Tucker, C.J., Falkowski, P.G., Field, C.B., Frouin, R., Esaias, W.E., et al. (2001). Biospheric primary production during an ENSO transition. Science *291*, 2594–2597. https://doi.org/10.1126/science.1055071.

Bottomley, M.J., Collard, M.W., Huggenvik, J.I., Liu, Z., Gibson, T.J., and Sattler, M. (2001). The SAND domain structure defines a novel DNA-binding fold in transcriptional regulation. Nat. Struct. Biol. *8*, 626–633. doi: 10.1038/89675.

Carrie, C., and Whelan, J. (2013). Widespread dual targeting of proteins in land plants: When, where, how and why. Plant Signal. Behav. *8*, e25034. https://doi.org/10.4161/psb.25034.

Carrie, C., Giraud, E., and Whelan, J. (2009). Protein transport in organelles: Dual targeting of proteins to mitochondria and chloroplasts: Dual targeting of proteins. FEBS J. *276*, 1187–1195. https://doi.org/10.1111/j.1742-4658.2009.06876.x.

Castellana, M., Wilson, M.Z., Xu, Y., Joshi, P., Cristea, I.M., Rabinowitz, J.D., Gitai, Z., and Wingreen, N.S. (2014). Enzyme clustering accelerates processing of intermediates through metabolic channeling. Nat. Biotechnol. *32*, 1011–1018. https://doi.org/10.1038/nbt.3018.

Cross, F.R. (2016). Tying down loose ends in the Chlamydomonas genome: functional significance of abundant upstream open reading frames. G3 (Bethesda) *6*, 435–446. https://doi.org/10.1534/g3.115.023119.

Depège, N., Bellafiore, S., and Rochaix, J.-D. (2003). Role of chloroplast protein kinase Stt7 in LHCII phosphorylation and state transition in Chlamydomonas. Science *299*, 1572–1575. https://doi.org/10.1126/science.1081397.

Deruere, J., Romer, S., d'Harlingue, A., Backhaus, R.A., Kuntz, M., and Camara, B. (1994). Fibril assembly and carotenoid overaccumulation in chromoplasts: a model for supramolecular lipoprotein structures. Plant Cell *6*, 119–133. doi: 10.1105/tpc.6.1.119.

1453 Docampo, R., de Souza, W., Miranda, K., Rohloff, P., and Moreno, S.N.J. (2005).
1454 Acidocalcisomes conserved from bacteria to man. Nat. Rev. Microbiol. *3*, 251–261.
1455 https://doi.org/10.1038/nrmicro1097.

1456 Dorfer, V., Strobl, M., Winkler, S., and Mechtler, K. (2021). MS Amanda 2.0: Advancements in
1457 the standalone implementation. Rapid Commun. Mass Spectrom. *35*: e9088
1458 https://doi.org/10.1002/rcm.9088.

1459 Elias, B.A., and Givan, C.V. (1977). Alpha-ketoglutarate supply for amino acid synthesis in
1460 higher plant chloroplasts: intrachloroplastic localization of NADP-specific isocitrate
1461 dehydrogenase. Plant Physiol. *59*, 738–740. https://doi.org/10.1104/pp.59.4.738.

1462 Elnaggar, A., Heinzinger, M., Dallago, C., Rehawi, G., Wang, Y., Jones, L., Gibbs, T., Feher, T.,
1463 Angerer, C., Steinegger, M., et al. (2021). ProtTrans: Towards cracking the language of lifes
1464 code through self-supervised deep learning and high performance computing. IEEE Trans.
1465 Pattern Anal. Mach. Intell. *14*. https://doi.org/10.1109/TPAMI.2021.3095381.

1466 Emanuelsson, O., Nielsen, H., and Heijne, G.V. (1999). ChloroP, a neural network-based
1467 method for predicting chloroplast transit peptides and their cleavage sites. Protein Sci. *8*, 978–
1468 984. https://doi.org/10.1110/ps.8.5.978.

1469 Eng, J.K., McCormack, A.L., and Yates, J.R. (1994). An approach to correlate tandem mass
1470 spectral data of peptides with amino acid sequences in a protein database. J. Am. Soc. Mass
1471 Spectrom. *5*, 976–989. https://doi.org/10.1016/1044-0305(94)80016-2.

1472 Engel, B.D., Schaffer, M., Kuhn Cuellar, L., Villa, E., Plitzko, J.M., and Baumeister, W. (2015).
1473 Native architecture of the Chlamydomonas chloroplast revealed by in situ cryo-electron
1474 tomography. eLife *4*, e04889. https://doi.org/10.7554/eLife.04889.

1475 Ferro, M., Brugiere, S., Salvi, D., Seigneurin-Berny, D., Court, M., Moyet, L., Ramus, C., Miras,
1476 S., Mellal, M., Le Gall, S., et al. (2010). AT_CHLORO, a comprehensive chloroplast proteome
1477 database with subplastidial localization and curated information on envelope proteins. Mol. Cell
1478 Proteomics *9*, 1063–1084. doi: 10.1074/mcp.M900325-MCP200.

1479 Flügel, F., Timm, S., Arrivault, S., Florian, A., Stitt, M., Fernie, A.R., and Bauwe, H. (2017). The
1480 photorespiratory metabolite 2-phosphoglycolate regulates photosynthesis and starch
1481 accumulation in Arabidopsis. Plant Cell *29*, 2537–2551. https://doi.org/10.1105/tpc.17.00256.

1482 Freeman Rosenzweig, E.S., Xu, B., Kuhn Cuellar, L., Martinez-Sanchez, A., Schaffer, M.,
1483 Strauss, M., Cartwright, H.N., Ronceray, P., Plitzko, J.M., Förster, F., et al. (2017). The
1484 eukaryotic CO_2-concentrating organelle is liquid-like and exhibits dynamic reorganization. Cell
1485 *171*, 148-162. https://doi.org/10.1016/j.cell.2017.08.008.

1486 Fujiwara, M.T., Yasuzawa, M., Sasaki, S., Nakano, T., Niwa, Y., Yoshida, S., Abe, T., and Itoh,
1487 R.D. (2017). The Arabidopsis minD mutation causes aberrant FtsZ1 ring placement and
1488 moderate heterogeneity of chloroplasts in the leaf epidermis. Plant Signal. Behav. *12*, e1343776.
1489 https://doi.org/10.1080/15592324.2017.1343776.

1490 Gross, J., Cho, W.K., Lezhneva, L., Falk, J., Krupinska, K., Shinozaki, K., Seki, M., Herrmann,
1491 R.G., and Meurer, J. (2006). A plant locus essential for phylloquinone (Vitamin K1) biosynthesis

originated from a fusion of four eubacterial genes. J. Biol. Chem. *281*, 17189–17196. https://doi.org/10.1074/jbc.M601754200.

Gutman, B.L., and Niyogi, K.K. (2004). Chlamydomonas and Arabidopsis. A dynamic duo. Plant Physiol. *135*, 607–610. https://doi.org/10.1104/pp.104.041491.

Hildebrandt, T.M., Nunes Nesi, A., Araújo, W.L., and Braun, H.-P. (2015). Amino acid catabolism in plants. Mol. Plant *8*, 1563–1579. https://doi.org/10.1016/j.molp.2015.09.005.

Hirano, T., Tanidokoro, K., Shimizu, Y., Kawarabayasi, Y., Ohshima, T., Sato, M., Tadano, S., Ishikawa, H., Takio, S., Takechi, K., et al. (2016). Moss chloroplasts are surrounded by a peptidoglycan wall containing D-amino acids. Plant Cell *28*, 1521–1532. https://doi.org/10.1105/tpc.16.00104.

Hölzl, G., and Dörmann, P. (2019). Chloroplast lipids and their biosynthesis. Annu. Rev. Plant Biol. *70*, 51–81. https://doi.org/10.1146/annurev-arplant-050718-100202.

Hooper, C.M., Castleden, I.R., Tanz, S.K., Aryamanesh, N., and Millar, A.H. (2017). SUBA4: the interactive data analysis centre for Arabidopsis subcellular protein locations. Nucleic Acids Res. *45*, D1064–D1074. https://doi.org/10.1093/nar/gkw1041.

Hopp, T.P., Prickett, K.S., Price, V.L., Libby, R.T., March, C.J., Cerretti, D.P., Urdal, D.L., and Conlon, P.J. (1988). A short polypeptide marker sequence useful for recombinant protein identification and purification. Nat. Biotehnol. *6*, 1204–1210. https://doi.org/10.1038/nbt1088-1204

Huang, G., Ulrich, P.N., Storey, M., Johnson, D., Tischer, J., Tovar, J.A., Moreno, S.N.J., Orlando, R., and Docampo, R. (2014). Proteomic analysis of the acidocalcisome, an organelle conserved from bacteria to human cells. PLoS Pathog. *10*, e1004555. https://doi.org/10.1371/journal.ppat.1004555.

Huh, W.-K., Falvo, J.V., Gerke, L.C., Carroll, A.S., Howson, R.W., Weissman, J.S., and O'Shea, E.K. (2003). Global analysis of protein localization in budding yeast. Nature *425*, 686–691. https://doi.org/10.1038/nature02026.

Isemer, R., Krause, K., Grabe, N., Kitahata, N., Asami, T., and Krupinska, K. (2012a). Plastid located WHIRLY1 enhances the responsiveness of Arabidopsis seedlings toward abscisic acid. Front. Plant Sci. *3*. https://doi.org/10.3389/fpls.2012.00283.

Isemer, R., Mulisch, M., Schäfer, A., Kirchner, S., Koop, H.-U., and Krupinska, K. (2012b). Recombinant Whirly1 translocates from transplastomic chloroplasts to the nucleus. FEBS Lett. *586*, 85–88. https://doi.org/10.1016/j.febslet.2011.11.029.

Ishida, H., Yoshimoto, K., Izumi, M., Reisen, D., Yano, Y., Makino, A., Ohsumi, Y., Hanson, M.R., and Mae, T. (2008). Mobilization of Rubisco and stroma-localized fluorescent proteins of chloroplasts to the vacuole by an ATG gene-dependent autophagic process. Plant Physiol. *148*, 142–155. https://doi.org/10.1104/pp.108.122770.

Iwai, M., Takizawa, K., Tokutsu, R., Okamuro, A., Takahashi, Y., and Minagawa, J. (2010). Isolation of the elusive supercomplex that drives cyclic electron flow in photosynthesis. Nature *464*, 1210–1213. https://doi.org/10.1038/nature08885.

Jarvis, P., and Robinson, C. (2004). Mechanisms of protein import and routing in chloroplasts. Cur. Biol. *14*, R1064–R1077. https://doi.org/10.1016/j.cub.2004.11.049.

Jumper, J., Evans, R., Pritzel, A., Green, T., Figurnov, M., Ronneberger, O., Tunyasuvunakool, K., Bates, R., Žídek, A., Potapenko, A., et al. (2021). Highly accurate protein structure prediction with AlphaFold. Nature *596*, 583–589. https://doi.org/10.1038/s41586-021-03819-2.

Karcher, D., Köster, D., Schadach, A., Klevesath, A., and Bock, R. (2009). The Chlamydomonas chloroplast HLP protein is required for nucleoid organization and genome maintenance. Mol. Plant *2*, 1223–1232. https://doi.org/10.1093/mp/ssp083.

Karpowicz, S.J., Prochnik, S.E., Grossman, A.R., and Merchant, S.S. (2011). The GreenCut2 resource, a phylogenomically derived inventory of proteins specific to the plant lineage. J. Biol. Chem. *286*, 21427–21439. https://doi.org/10.1074/jbc.M111.233734.

Keeling, P.J. (2010). The endosymbiotic origin, diversification and fate of plastids. Phil. Trans. R. Soc. B *365*, 729–748. https://doi.org/10.1098/rstb.2009.0103.

Kobayashi, Y., Misumi, O., Odahara, M., Ishibashi, K., Hirono, M., Hidaka, K., Endo, M., Sugiyama, H., Iwasaki, H., Kuroiwa, T., et al. (2017). Holliday junction resolvases mediate chloroplast nucleoid segregation. Science *356*, 631–634. https://doi.org/10.1126/science.aan0038.

Komine, Y., Eggink, L.L., Park, H., and Hoober, J.K. (2000). Vacuolar granules in *Chlamydomonas reinhardtii*: polyphosphate and a 70-kDa polypeptide as major components. Planta *210*, 897–905. https://doi.org/10.1007/s004250050695.

Kong, F., Liang, Y., Légeret, B., Beyly-Adriano, A., Blangy, S., Haslam, R.P., Napier, J.A., Beisson, F., Peltier, G., and Li-Beisson, Y. (2017). Chlamydomonas carries out fatty acid β-oxidation in ancestral peroxisomes using a bona fide acyl-CoA oxidase. Plant J. *90*, 358–371. https://doi.org/10.1111/tpj.13498.

Krath, B.N., and Hove-Jensen, B. (1999). Organellar and Cytosolic Localization of Four Phosphoribosyl Diphosphate Synthase Isozymes in Spinach. Plant Physiol. *119*, 497–506. https://doi.org/10.1104/pp.119.2.497.

Kropat, J., Hong-Hermesdorf, A., Casero, D., Ent, P., Castruita, M., Pellegrini, M., Merchant, S.S., and Malasarn, D. (2011). A revised mineral nutrient supplement increases biomass and growth rate in *Chlamydomonas reinhardtii*. Plant J. *66*, 770–780. https://doi.org/10.1111/j.1365-313X.2011.04537.x.

Krupinska, K., Blanco, N.E., Oetke, S., and Zottini, M. (2020). Genome communication in plants mediated by organelle–nucleus-located proteins. Phil. Trans. R. Soc. B *375*, 20190397. https://doi.org/10.1098/rstb.2019.0397.

Küken, A., Sommer, F., Yaneva-Roder, L., Mackinder, L.C.M., Höhne, M., Geimer, S., Jonikas, M.C., Schroda, M., Stitt, M., Nikoloski, Z., et al. (2018). Effects of microcompartmentation on

flux distribution and metabolic pools in *Chlamydomonas reinhardtii* chloroplasts. eLife *7*, e37960. https://doi.org/10.7554/eLife.37960.

Lange, B.M., Rujan, T., Martin, W., and Croteau, R. (2000). Isoprenoid biosynthesis: The evolution of two ancient and distinct pathways across genomes. Proc. Natl. Acad. Sci. USA *97*, 13172–13177. https://doi.org/10.1073/pnas.240454797.

Lee, P.T., Hsu, A.Y., Ha, H.T., and Clarke, C.F. (1997). A C-methyltransferase involved in both ubiquinone and menaquinone biosynthesis: isolation and identification of the *Escherichia coli* ubiE gene. J. Bacteriol. *179*, 1748–1754. https://doi.org/10.1128/jb.179.5.1748-1754.1997.

Leister, D. (2003). Chloroplast research in the genomic age. Trends Genet. *19*, 47–56. https://doi.org/10.1016/S0168-9525(02)00003-3.

Leister, D., and Kleine, T. (2008). Towards a comprehensive catalog of chloroplast proteins and their interactions. Cell Res. *18*, 1081–1083. https://doi.org/10.1038/cr.2008.297.

Li, X., Patena, W., Fauser, F., Jinkerson, R.E., Saroussi, S., Meyer, M.T., Ivanova, N., Robertson, J.M., Yue, R., Zhang, R., et al. (2019). A genome-wide algal mutant library and functional screen identifies genes required for eukaryotic photosynthesis. Nat. Genet. *51*, 627–635. https://doi.org/10.1038/s41588-019-0370-6.

Lois, L.M., Campos, N., Putra, S.R., Danielsen, K., Rohmer, M., and Boronat, A. (1998). Cloning and characterization of a gene from *Escherichia coli* encoding a transketolase-like enzyme that catalyzes the synthesis of D-1-deoxyxylulose 5-phosphate, a common precursor for isoprenoid, thiamin, and pyridoxol biosynthesis. Proc. Natl. Acad. Sci. USA *95*, 2105–2110. https://doi.org/10.1073/pnas.95.5.2105.

Lundquist, P.K., Poliakov, A., Bhuiyan, N.H., Zybailov, B., Sun, Q., and van Wijk, K.J. (2012). The functional network of the Arabidopsis plastoglobule proteome based on quantitative proteomics and genome-wide coexpression analysis. Plant Physiol. *158*, 1172–1192. https://doi.org/10.1104/pp.111.193144.

Mackinder, L.C.M., Meyer, M.T., Mettler-Altmann, T., Chen, V.K., Mitchell, M.C., Caspari, O., Freeman Rosenzweig, E.S., Pallesen, L., Reeves, G., Itakura, A., et al. (2016). A repeat protein links Rubisco to form the eukaryotic carbon-concentrating organelle. Proc. Natl. Acad. Sci. USA *113*, 5958–5963. https://doi.org/10.1073/pnas.1522866113.

Mackinder, L.C.M., Chen, C., Leib, R.D., Patena, W., Blum, S.R., Rodman, M., Ramundo, S., Adams, C.M., and Jonikas, M.C. (2017). A spatial interactome reveals the protein organization of the algal CO_2-concentrating mechanism. Cell *171*, 133-147.e14. https://doi.org/10.1016/j.cell.2017.08.044.

Major, L.L., Wolucka, B.A., and Naismith, J.H. (2005). Structure and function of GDP-mannose-3',5'-epimerase: an enzyme which performs three chemical reactions at the same active site. J. Am. Chem. Soc. *127*, 18309–18320. https://doi.org/10.1021/ja056490i.

Mallik, R., Kundu, A., and Chaudhuri, S. (2018). High mobility group proteins: the multifaceted regulators of chromatin dynamics. Nucleus *61*, 213–226. https://doi.org/10.1007/s13237-018-0257-4.

1606 Merchant, S.S., Prochnik, S.E., Vallon, O., Harris, E.H., Karpowicz, S.J., Witman, G.B., Terry, A.,
1607 Salamov, A., Fritz-Laylin, L.K., Maréchal-Drouard, L., et al. (2007). The Chlamydomonas
1608 genome reveals the evolution of key animal and plant functions. Science *318*, 245–250.
1609 https://doi.org/10.1126/science.1143609.

1610 Mesnage, S., Dellarole, M., Baxter, N.J., Rouget, J.-B., Dimitrov, J.D., Wang, N., Fujimoto, Y.,
1611 Hounslow, A.M., Lacroix-Desmazes, S., Fukase, K., et al. (2014). Molecular basis for bacterial
1612 peptidoglycan recognition by LysM domains. Nat. Commun. *5*, 4269.
1613 https://doi.org/10.1038/ncomms5269.

1614 Meyer, M.T., Itakura, A.K., Patena, W., Wang, L., He, S., Emrich-Mills, T., Lau, C.S., Yates, G.,
1615 Mackinder, L.C.M., and Jonikas, M.C. (2020). Assembly of the algal CO_2-fixing organelle, the
1616 pyrenoid, is guided by a Rubisco-binding motif. Sci. Adv. *6*, eabd2408. DOI:
1617 10.1126/sciadv.abd2408

1618 Minai, L., Wostrikoff, K., Wollman, F.-A., and Choquet, Y. (2006). Chloroplast biogenesis of
1619 photosystem II cores involves a series of assembly-controlled steps that regulate translation.
1620 Plant Cell *18*, 159–175. https://doi.org/10.1105/tpc.105.037705.

1621 Moriwaki, Y. (@Ag_smith). Twitter post: AlphaFold2 can also predict heterocomplexes. all you
1622 have to do is input the two sequences you want to predict and connect them with a long linker.
1623 https://twitter.com/Ag_smith/status/1417063635000598528. 2021-07-19.
1624
1625 Nagai, T., Ibata, K., Park, E.S., Kubota, M., Mikoshiba, K., and Miyawaki, A. (2002). A variant of
1626 yellow fluorescent protein with fast and efficient maturation for cell-biological applications. Nat.
1627 Biotehnol. *20*, 87–90. doi: 10.1038/nbt0102-87.

1628 Nesvizhskii, A.I., Keller, A., Kolker, E., and Aebersold, R. (2003). A statistical model for
1629 identifying proteins by tandem mass spectrometry. Anal. Chem. *75*, 4646–4658.
1630 https://doi.org/10.1021/ac0341261.

1631 Neupert, J., Karcher, D., and Bock, R. (2009). Generation of Chlamydomonas strains that
1632 efficiently express nuclear transgenes. Plant J. *57*, 1140–1150.
1633 https://doi.org/10.1111/j.1365-313X.2008.03746.x.

1634 Nomura, H., Komori, T., Uemura, S., Kanda, Y., Shimotani, K., Nakai, K., Furuichi, T.,
1635 Takebayashi, K., Sugimoto, T., Sano, S., et al. (2012). Chloroplast-mediated activation of plant
1636 immune signalling in Arabidopsis. Nat. Commun. *3*, 926.
1637 https://doi.org/10.1038/ncomms1926.

1638 O'Connell, J.D., Zhao, A., Ellington, A.D., and Marcotte, E.M. (2012). Dynamic reorganization of
1639 metabolic enzymes into intracellular bodies. Annu. Rev. Cell Dev. Biol. *28*, 89–111.
1640 https://doi.org/10.1146/annurev-cellbio-101011-155841.

1641 Osafune, T., Yokota, A., Sumida, S., and Hase, E. (1990). Immunogold localization of ribulose-
1642 1,5-bisphosphate carboxylase with reference to pyrenoid morphology in chloroplasts of
1643 synchronized *Euglena gracilis* cells. Plant Physiol. *92*, 802–808.
1644 https://doi.org/10.1104/pp.92.3.802.

1645 Pareek, V., Sha, Z., He, J., Wingreen, N.S., and Benkovic, S.J. (2021). Metabolic channeling:
1646 predictions, deductions, and evidence. Mol. Cell *81*, 3775–3785.
1647 https://doi.org/10.1016/j.molcel.2021.08.030.

1648 Pazour, G.J., Agrin, N., Leszyk, J., and Witman, G.B. (2005). Proteomic analysis of a eukaryotic
1649 cilium. J. Cell Biol. *170*, 103–113. https://doi.org/10.1083/jcb.200504008.

1650 Pérez-Amador, M.A., Abler, M.L., De Rocher, E.J., Thompson, D.M., van Hoof, A., LeBrasseur,
1651 N.D., Lers, A., and Green, P.J. (2000). Identification of BFN1, a bifunctional nuclease induced
1652 during leaf and stem senescence in Arabidopsis. Plant Physiol. *122*, 169–180.
1653 https://doi.org/10.1104/pp.122.1.169.

1654 Pettersen, E.F., Goddard, T.D., Huang, C.C., Meng, E.C., Couch, G.S., Croll, T.I., Morris, J.H.,
1655 and Ferrin, T.E. (2021). UCSF ChimeraX□: Structure visualization for researchers, educators,
1656 and developers. Protein Sci. *30*, 70–82. https://doi.org/10.1002/pro.3943.

1657 Pfister, B., and Zeeman, S.C. (2016). Formation of starch in plant cells. Cell Mol. Life Sci. *73*,
1658 2781–2807. https://doi.org/10.1007/s00018-016-2250-x.

1659 Pronina, N.A., and Semenenko, V.E. (1990). Membrane-bound carbonic anhydrase takes part
1660 in CO_2 concentration in algal cells. Curr. Res. Photosynth. *4*, 489–492. DOI: 10.1007/978-94-
1661 009-0511-5_739

1662 Raven, J.A. (1997). CO_2-concentrating mechanisms: a direct role for thylakoid lumen
1663 acidification? Plant Cell Environ. *20*, 147–154. https://doi.org/10.1046/j.1365-
1664 3040.1997.d01-67.x.

1665 Rousseaux, C., and Gregg, W. (2013). Interannual variation in phytoplankton primary production
1666 at a global scale. Remote Sens. *6*, 1–19. https://doi.org/10.3390/rs6010001.

1667 Ruiz, F.A., Marchesini, N., Seufferheld, M., Govindjee, and Docampo, R. (2001). The
1668 polyphosphate bodies of *Chlamydomonas reinhardtii* possess a proton-pumping
1669 pyrophosphatase and are similar to acidocalcisomes. J. Biol. Chem. *276*, 46196–46203.
1670 https://doi.org/10.1074/jbc.M105268200.

1671 Sainsbury, F., Thuenemann, E.C., and Lomonossoff, G.P. (2009). pEAQ: versatile expression
1672 vectors for easy and quick transient expression of heterologous proteins in plants. Plant
1673 Biotechnol. J. *7*, 682–693. https://doi.org/10.1111/j.1467-7652.2009.00434.x.

1674 Sasaki, Y., and Nagano, Y. (2004). Plant acetyl-CoA carboxylase: structure, biosynthesis,
1675 regulation, and gene manipulation for plant breeding. Biosci. Biotechnol. Biochem. *68*, 1175–
1676 1184. https://doi.org/10.1271/bbb.68.1175.

1677 Scebba, F., De Bastiani, M., Bernacchia, G., Andreucci, A., Galli, A., and Pitto, L. (2007).
1678 PRMT11: a new Arabidopsis MBD7 protein partner with arginine methyltransferase activity.
1679 Plant J. *52*, 210–222. https://doi.org/10.1111/j.1365-313X.2007.03238.x.

1680 Schindelin, J., Arganda-Carreras, I., Frise, E., Kaynig, V., Longair, M., Pietzsch, T., Preibisch, S.,
1681 Rueden, C., Saalfeld, S., Schmid, B., et al. (2012). Fiji: an open-source platform for biological-
1682 image analysis. Nat. Methods *9*, 676–682. https://doi.org/10.1038/nmeth.2019.

1683 Schwarte, S., and Bauwe, H. (2007). Identification of the photorespiratory 2-phosphoglycolate
1684 phosphatase, PGLP1, in Arabidopsis. Plant Physiol. *144*, 1580–1586.
1685 https://doi.org/10.1104/pp.107.099192.

1686 Shanmugabalaji, V., Grimm, B., and Kessler, F. (2020). Characterization of a plastoglobule-
1687 localized SOUL4 heme-binding protein in *Arabidopsis thaliana*. Front. Plant Sci. *11*, 2.
1688 https://doi.org/10.3389/fpls.2020.00002.

1689 Shevchenko, A., Tomas, H., Havli, J., Olsen, J.V., and Mann, M. (2006). In-gel digestion for
1690 mass spectrometric characterization of proteins and proteomes. Nat. Protoc. *1*, 2856–2860.
1691 https://doi.org/10.1038/nprot.2006.468.

1692 Sowa, M.E., Bennett, E.J., Gygi, S.P., and Harper, J.W. (2009). Defining the human
1693 deubiquitinating enzyme interaction landscape. Cell *138*, 389–403.
1694 https://doi.org/10.1016/j.cell.2009.04.042.

1695 Steinegger, M., Mirdita, M., and Söding, J. (2019). Protein-level assembly increases protein
1696 sequence recovery from metagenomic samples manyfold. Nat. Methods *16*, 603–606.
1697 https://doi.org/10.1038/s41592-019-0437-4.

1698 Suzuki, K., Nakanishi, H., Bower, J., Yoder, D.W., Osteryoung, K.W., and Miyagishima, S.
1699 (2009). Plastid chaperonin proteins Cpn60α and Cpn60β are required for plastid division in
1700 *Arabidopsis thaliana*. BMC Plant Biol. *9*, 38. https://doi.org/10.1186/1471-2229-9-38.
1701 https://doi.org/10.1186/1471-2229-9-38.

1702 Takahashi, H., Schmollinger, S., Lee, J.-H., Schroda, M., Rappaport, F., Wollman, F.-A., and
1703 Vallon, O. (2016). PETO Interacts with other effectors of cyclic electron flow in Chlamydomonas.
1704 Mol. Plant *9*, 558–568. https://doi.org/10.1016/j.molp.2015.12.017.

1705 Tanaka, R., Oster, U., Kruse, E., Rüdiger, W., and Grimm, B. (1999). Reduced activity of
1706 geranylgeranyl reductase leads to loss of chlorophyll and tocopherol and to partially
1707 geranylgeranylated chlorophyll in transgenic Tobacco plants expressing antisense RNA for
1708 geranylgeranyl reductase. Plant Physiol. *120*, 695–704. https://doi.org/10.1104/pp.120.3.695.

1709 Tanaka, R., Rothbart, M., Oka, S., Takabayashi, A., Takahashi, K., Shibata, M., Myouga, F.,
1710 Motohashi, R., Shinozaki, K., Grimm, B., et al. (2010). LIL3, a light-harvesting-like protein, plays
1711 an essential role in chlorophyll and tocopherol biosynthesis. Proc. Natl. Acad. Sci. USA *107*,
1712 16721–16725. https://doi.org/10.1073/pnas.1004699107.

1713 Tardif, M., Atteia, A., Specht, M., Cogne, G., Rolland, N., Brugière, S., Hippler, M., Ferro, M.,
1714 Bruley, C., Peltier, G., et al. (2012). PredAlgo: A new subcellular localization prediction tool
1715 dedicated to green algae. Mol. Biol. Evol. *29*, 3625–3639.
1716 https://doi.org/10.1093/molbev/mss178.

1717 Terashima, M., Specht, M., Naumann, B., and Hippler, M. (2010). Characterizing the anaerobic
1718 response of *Chlamydomonas reinhardtii* by quantitative proteomics. Mol. Cell Proteomics *9*,
1719 1514–1532. doi: 10.1074/mcp.M900421-MCP200.

1720 Terashima, M., Petroutsos, D., Hudig, M., Tolstygina, I., Trompelt, K., Gabelein, P., Fufezan, C.,
1721 Kudla, J., Weinl, S., Finazzi, G., et al. (2012). Calcium-dependent regulation of cyclic

photosynthetic electron transfer by a CAS, ANR1, and PGRL1 complex. Proc. Natl. Acad. Sci. USA *109*, 17717–17722. https://doi.org/10.1073/pnas.1207118109.

Thul, P.J., Åkesson, L., Wiking, M., Mahdessian, D., Geladaki, A., Ait Blal, H., Alm, T., Asplund, A., Björk, L., Breckels, L.M., et al. (2017). A subcellular map of the human proteome. Science *356*, eaal3321. https://doi.org/10.1126/science.aal3321.

Tsibris, J.C., McCormick, D.B., and Wright, L.D. (1966). Studies on the binding and function of flavin phosphates with flavin mononucleotide-dependent enzymes. J. Biol. Chem. *241*, 1138–1143. https://doi.org/10.1016/S0021-9258(18)96813-4.

Fauser, F., Vilarrasa-Blasi, J., Onishi, M., Ramundo, S., Patena, W., Millican, M., Osaki, J., Philp, C., Nemeth, M., Salomé, P.A., et al. (2022). Systematic characterization of gene function in a photosynthetic organism alga *Chlamydomonas reinhardtii*. Nat. Genet. https://doi.org/10.1038/s41588-022-01052-9.

Walker, K.A., and Harwood, J.L. (1985). Localization of chloroplastic fatty acid synthesis *de novo* in the stroma. Biochem. J. *226*, 551–556. https://doi.org/10.1042/bj2260551

Wang, L., Yamano, T., Takane, S., Niikawa, Y., Toyokawa, C., Ozawa, S., Tokutsu, R., Takahashi, Y., Minagawa, J., Kanesaki, Y., et al. (2016). Chloroplast-mediated regulation of CO_2-concentrating mechanism by Ca^{2+}-binding protein CAS in the green alga *Chlamydomonas reinhardtii*. Proc. Natl. Acad. Sci. USA *113*, 12586–12591. https://doi.org/10.1073/pnas.1606519113.

Wang, Y., Ries, A., Wu, K., Yang, A., and Crawford, N.M. (2010). The Arabidopsis prohibitin gene *PHB3* functions in nitric oxide–mediated responses and in hydrogen peroxide–induced nitric oxide accumulation. Plant Cell *22*, 249–259. https://doi.org/10.1105/tpc.109.072066.

Willeford, K.O., Gombos, Z., and Gibbs, M. (1989). Evidence for chloroplastic succinate dehydrogenase participating in the chloroplastic respiratory and photosynthetic electron transport Chains of *Chlamydomonas reinhardtii*. Plant Physiol. *90*, 1084–1087. https://doi.org/10.1104/pp.90.3.1084.

Wise, R.R., and Hoober, J.K. (2006). The Structure and Function of Plastids. Dordrecht: Springer 3–21.

Wolf, T., Debut, L., Sanh, V., Chaumond, J., Delangue, C., Moi, A., Cistac, P., Rault, T., Louf, R., Funtowicz, M., et al. (2020). HuggingFace's transformers: State-of-the-art natural language processing. arXiv:1910.03771 [cs.CL]. https://doi.org/10.48550/arXiv.1910.03771.

Wolfe, G.R., Park, H., Sharp, W.P., and Hoober, J.K. (1997). Light-harvesting complex apoproteins in cytoplasmic vacuoles in *Chlamydomonas reinhardtii* (Chlorophyta). J. Phycol. *33*, 377–386. doi: 10.1111/j.0022-3646.1997.00377.x

Wolfenden, R. (1969). Transition state analogues for enzyme catalysis. Nature *223*, 704–705. https://doi.org/10.1038/223704a0.

Wunder, T., Oh, Z.G., and Mueller-Cajar, O. (2019). CO_2-fixing liquid droplets: Towards a dissection of the microalgal pyrenoid. Traffic *20*, 380–389. https://doi.org/10.1111/tra.12650.

1760 Yamano, T., Iguchi, H., and Fukuzawa, H. (2013). Rapid transformation of *Chlamydomonas*
1761 *reinhardtii* without cell-wall removal. J. Biosci. Bioeng. *115*, 691–694.
1762 https://doi.org/10.1016/j.jbiosc.2012.12.020.

1763 Ytterberg, A.J., Peltier, J.-B., and van Wijk, K.J. (2006). Protein profiling of plastoglobules in
1764 chloroplasts and chromoplasts. A surprising site for differential accumulation of metabolic
1765 enzymes. Plant Physiol. *140*, 984–997. https://doi.org/10.1104/pp.105.076083.

1766 Zhan, Y., Dhaliwal, J., Adjibade, P., Uniacke, J., Mazroui, R., and Zerges, W. (2015). Localized
1767 control of oxidized RNA. J. Cell Sci *128*, 4210–4219. https://doi.org/10.1242/jcs.175232.

1768 Zhan, Y., Marchand, C.H., Maes, A., Mauries, A., Sun, Y., Dhaliwal, J.S., Uniacke, J., Arragain,
1769 S., Jiang, H., Gold, N.D., et al. (2018). Pyrenoid functions revealed by proteomics in
1770 *Chlamydomonas reinhardtii*. PLoS ONE *13*, e0185039.
1771 https://doi.org/10.1371/journal.pone.0185039.

1772 Zhang, R., Patena, W., Armbruster, U., Gang, S.S., Blum, S.R., and Jonikas, M.C. (2014). High-
1773 throughput genotyping of green algal mutants reveals random distribution of mutagenic insertion
1774 sites and endonucleolytic cleavage of transforming DNA. Plant Cell *26*, 1398–1409.
1775 https://doi.org/10.1105/tpc.114.124099.

1776 Zrenner, R., Stitt, M., Sonnewald, U., and Boldt, R. (2006). Pyrimidine and purine biosynthesis
1777 and degradation in plants. Annu. Rev. Plant Biol. *57*, 805–836.
1778 https://doi.org/10.1146/annurev.arplant.57.032905.105421.

1779